The Bioenergetics of Walking and Running in Space Suits

by

Christopher Edward Carr

Submitted to the Harvard-MIT Division of Health Sciences and Technology
in partial fulfillment of the requirements for the degree of

Doctorate of Science in Medical Physics

at the

MASSACHUSETTS INSTITUTE OF TECHNOLOGY

May 2005 [June 2005]

Author .....
Harvard-MIT Division of Health Sciences and Technology
May 16, 2005

Certified by .....
Dava J. Newman, Ph.D.
Professor, MacVicar Faculty Fellow, HST Affiliate
MIT Department of Aeronautics & Astronautics and Engineering Systems Division
Thesis Supervisor

Accepted by .....
Martha L. Gray, Ph.D.
Edward Hood Taplin Professor of Medical and Electrical Engineering
Director, Harvard-MIT Division of Health Sciences and Technology

The Bioenergetics of Walking and Running in Space Suits

by

Christopher Edward Carr

Submitted to the Harvard-MIT Division of Health Sciences and Technology
on May 16, 2005, in partial fulfillment of the
requirements for the degree of
Doctorate of Science in Medical Physics

Abstract

Space-suited activity is critical for human spaceflight, and is synonymous with human planetary exploration. Space suits impose kinematic and kinetic boundary conditions that affect movement and locomotion, and in doing so modify the metabolic cost of physical activity. Metabolic requirements, found to be significantly elevated in space-suited activity, are a major driver of the allowable duration and intensity of extravehicular activity.

To investigate how space suited locomotion impacts the energetics of walking and running, I developed a framework for analyzing energetics data, derived from basic thermodynamics, that clearly differentiates between *muscle efficiency* and *energy recovery*. The framework, when applied to unsuited locomotion, revealed that the human run-walk transition in Earth gravity occurs when energy recovery for walking and running are approximately equal. The dependence of muscle efficiency on gravity –during locomotion and under a particular set of assumptions– was derived as part of the framework.

Next, I collected and transformed data from prior studies of suited and unsuited locomotion into a common format, and performed regression analysis. This analysis revealed that in reduced gravity environments, running in space suits is likely to be more efficient, per unit mass and per unit distance, than walking in space suits. Second, the results suggested that space suits may behave like springs during running.

To investigate the spring-like nature of space suit legs, I built a lower-body exoskeleton to simulate aspects of the current NASA spacesuit, the Extravehicular Mobility Unit (EMU). Evaluation of the exoskeleton legs revealed that they produce knee torques similar to the EMU in both form and magnitude. Therefore, space suit joints such as the EMU knee joint behave like non-linear springs, with the effect of these springs most pronounced when locomotion requires large changes in knee flexion such as during running.

To characterize the impact of space suit legs on the energetics of walking and running, I measured the energetic cost of locomotion with and without the lower-body exoskeleton in a variety of simulated gravitational environments at specific and self-

selected Froude numbers, non-dimensional parameters used to characterize the run-walk transition. Exoskeleton locomotion increased energy recovery and significantly improved the efficiency of locomotion, per unit mass and per unit distance, in reduced gravity but not in Earth gravity. The framework was used to predict, based on Earth-gravity data, the metabolic cost of unsuited locomotion in reduced gravity; there were no statistical differences between the predictions and the observed values. The results suggest that the optimal space-suit knee-joint torque may be non-zero: it may be possible to build a 'tuned space suit' that minimizes the energy cost of locomotion. Furthermore, the observed lowering of the self-selected run-walk transition Froude number during exoskeleton locomotion is consistent with the hypothesis that the run-walk transition is mediated by energy recovery.

The major contributions of the dissertation include:

1. A model that predicts metabolic cost in non-dimensional form for unsuited locomotion across running and walking and across gravity levels,
2. An assessment of historical data that reveals the effect of pressure suits on work output and the metabolic cost of locomotion,
3. A method of simulating a space suit using a lower-body exoskeleton, and methods for designing and characterizing the exoskeleton,
4. An explanation for the differences in the energetic costs of walking and running in space suits,
5. Evidence that there is an optimal space suit leg stiffness, perhaps an optimal space suit leg stiffness for a given gravity environment,
6. Evidence, mostly indirect, that energy recovery plays a role in gait switching.

Thesis Supervisor: Dava J. Newman, Ph.D.
Title: Professor, MacVicar Faculty Fellow, HST Affiliate
MIT Department of Aeronautics & Astronautics and Engineering Systems Division

Acknowledgments

It has been a pleasure to be able to get up in the morning and be excited about going to MIT - not just because of the work, but largely because of the people with whom I have had the opportunity to work these last several years. To any of these individuals whose name is not mentioned below, I thank you.

I am grateful to my advisor, **Dava J. Newman**, for giving me the freedom to pursue my own path. Dava, a truly wonderful individual, has not only been my advisor, but has also been a great source of inspiration through her dedication to teaching, research, adventure, and last but definitely not least, friends and family. An email that could have been entitled "Saved by olive oil!", sent from a sailboat in the middle of the Pacific Ocean, comes to mind...

Professor Farish Jenkins, Jr. impressed me from the moment he called me by name on the first day of Anatomy at Harvard Medical School. I have fond memories of the multicolor anatomically correct drawings he produced from chalk, his demonstrations of human gait (including his recitation of a key scene from Moby Dick, complete with a peg leg), the apples from his orchard, and his guided tours of that fascinatingly delicate and robust machine, the human body. Farish has a style that brings out the best in others, and his commitment to strength of character and purpose amid the frenzy of modern academic life is a pleasure to behold.

I have been very fortunate to get to know **Professor Kip Hodges** here at MIT, and while learning the basics of field geology in the Bird Spring Mountains of Nevada. When I was in second grade, I ran a club of rock-hounds. When the grade-school teachers asked all the students to choose the titles of our future jobs, I decided upon *geological astrophysicist.* I am forever indebted to Kip, **Professor Clark Burchfiel**, and the graduate geology students, for helping me to reconnect with the geology of my youth. Do people actually get paid to walk around and look at rocks, I wondered!?

It has been a pleasure to interact with **Professor Maria Zuber** during my graduate years. Early in graduate school I took her Introduction to Planetary Science course; during one session, I was the only student to show up for class. The personal lecture Maria gave me for most of that class period, seemingly out of principle, left a deep impression on me. Further meetings only deepened my respect for Maria as a scientist and as a person, and I was very happy that she was able to attend my defense.

Dr. Fred Bowman, whom I met in an 'Engineering and Medicine' seminar my Freshman year at MIT, was the first person to introduce me to this thing called HST. When the time came for graduate school, I didn't think twice. Later, Fred helped me navigate the murky waters of HST finance, making it possible for me to attend the IMBP Space Biology and Medicine course and complete one of my clinical rotations in a Russian hospital. I finally felt like a true HST student at the end of that trip when, upon returning to my Cambridge apartment late on a Wednesday night,

I realized that I had assisted with a coronary artery bypass graft surgery that morning in Moscow.

Amy Smith, **Sally Susnowitz**, **Kim Vandiver**, and the rest of the MIT International Development Initiative (IDI) team gave me the opportunity to feel that I was making a difference *in the now*, even while I confronted seemingly impassible challenges in my research life. Amy's unbridled creativity never ceases to amaze, and it is a pleasure to have the opportunity to see her journey firsthand. Sally, with her attention to detail and fantastic sense of humour, manages to keep us on track. Kim has served as a role model ever since I came to know him during my undergrad solar-car days. Whenever I didn't know how to build something, needed a mysterious tool, or just wanted to unwind or reminisce about those solar-car days, a talk with **Dick Perdichizzi** was the perfect solution.

Sally Chapman, **Marie Stuppard**, **Jennie Leith**, **Ping Lee**, and many others have worked wonders behind the scenes to make sure that the research equipment arrived or that the undergraduate researcher (or the graduate student) received a check. Like the friendly and helpful janitorial staff, including **Phyllis** and **Joe**, MIT wouldn't run without them.

I am deeply indebted to many current and former members of the Man-Vehicle Lab, only some of whom I have the space to thank here.

I learned a great deal from my past office-mates; in particular, **Joe Saleh** has been a constant mentor and friend, and it has been a delight to see the smiles and self-confidence that has emerged in my current office-mates as a result of Joe's mentoring.

My evolving friendship with **Joaquin Blaya** has been a great source of strength - no doubt his courage to embark on a journey of volunteering and self-discovery in Chile helped to encourage me to strengthen my work with IDI.

A chance encounter in an elevator led to sharing an office with **Phil Ferguson**, our go-to man for dynamics, our pro at Latex, our star bag-pipe player, and one of our representatives from the 51st state in the North. Phil has an amazing ability to balance work and the rest of his life, and has helped to make our lab both more effective and more fun.

My office-mates over this past year, **Julie Arnold** and **Nicole Jordan**, have made many days brighter, and have allowed me the liberty of feeling valued (one of the great gifts one human being can bestoy upon another).

Kristen Bethke, with her positive outlook, cheerful disposition, and ability to empathize with others, has been a source of joy and also productivity, not just for me but also for many others.

I am grateful to **Jessica Marquez** for many things. A partial list: making me laugh, providing an occational opportunity to practice my Spanish, taking on and going beyond the traverse-planning work I began in my Master's, making sure I took time out to eat in the final days, and being persistent in tracking down the infamous Stone (1964) reference. For this latter task I thank our department librarian, **Eileen Dorschner**, for multiple emails, calls, and faxes to NASA Ames that eventually

led to a fax of a fax of a copy of a paper, partially in Russian, which included a key figure I used to answer the first question at my defense!

In addition to revealing his creativity in the lab, **Liang Simm** has made a huge difference in our lab social atmosphere: teaching us about Australia, facilitating the occational lab trip to the pub, or bringing us together at a master receital at the New England Conservatory. Who will ever forget the scientific proof that Tim Tams are better than Oreos?

A proper description of the contributions of **Alan Natapoff** should involve superlative adjectives, a bit of Latin and Greek, a reference to Tolstoy and Voltaire, perhaps imagery from a historic battle, a tale of political intrigue set in another century, a famous scientific experiment, a bit of perspective, and a firm handshake. Alan, officially our lab statistician, has been for me what I suspect he has been for so many others: a shepard, a mentor, and a friend.

Many friends outside MIT have helped make this dissertation possible. A few are: Christy, Jason, Derek, Dingli, Aditya, Ryan L., Ryan H., Andy, Peter, Adam, Carl, Barbara and of course my family, Dean, Kathy, and Jonathan. You all have provided the rock upon which I have laid my foundation.

Dean, Kathy, and Jonathan: This dissertation is for you.

Biographical Note

Christopher Carr was born in 1976 in Helsinki, Finland, as a citizen of the United States. He was raised in Seattle, Washington, and attended the Massachusetts Institute of Technology from 1995-1999, earning bachelors of science degrees in Aeronautics and Astronautics, and Electrical Science and Engineering. He spent the summers of 1999 and 2000 working on a Mars Sample Return mission design study at the Caltech/NASA Jet Propulsion Laboratory in Pasadena, California. He returned to MIT in the fall of 1999 as a graduate student in the MIT Man-Vehicle Laboratory and the MIT Department of Aeronautics and Astronautics. After completing a Masters of Science in Aeronautics and Astronautics in 2001, he continued as a graduate student in the Harvard-MIT Division of Health Sciences and Technology doctoral program in Medical Engineering and Medical Physics.

Contents

List of Figures

List of Tables

Chapter 1

Introduction

1.1 Motivation

Space-suited activity is critical for human spaceflight, and is synonymous with human planetary exploration. Space-suited activity, absolutely essential for Apollo lunar surface exploration, was not planned for the Shuttle program until it was realized that contingencies such as a payload bay door failure would require astronauts to venture outside their shirt-sleeve environment to conduct a contingency extravehicular activity (EVA), or space-walk. The value of space-suited activity was later demonstrated through satellite captures and repairs, including multiple repairs or upgrades of the Hubble space telescope, and construction of the International Space Station.

A high fraction of the EVAs conducted to date (154 unique space-walks, some with more than one space-walker, from March 1965 to April 1997 [Portree and Treviño, 1997]) have been in conducted in weightlessness; it is likely that during a single future Mars mission, over four times as many EVAs would be conducted as in the entire history of human spaceflight (Figure 1-1).

1.2 Problem Statement

Space suits impose kinematic and kinetic boundary conditions that affect movement and locomotion, and in doing so modify the metabolic cost of physical activity.

Figure 1-1: The number of extravehicular activities in the US and Russian space programs from 1965-2000 are compared to the number of extravehicular activities for a single human mission to Mars. Planned extravehicular activities due to construction of the International Space Station are shown for the time period 2001-2006. Number of extravehicular activities for a human Mars mission are based on a 600 day surface stay by four to six crew members, each conducting approximately two extravehicular activities per week, a conservatively low estimate. Figure from [Carr, 2001].

Metabolic requirements, found to be significantly elevated in suited (as compared to unsuited) movement [Roth, 1966], are a major driver of the allowable duration and intensity of extravehicular activity.

The principle question I address in this dissertation is *How do space suits affect the energetics of walking and running, and can this information be used to improve space suit design and to learn something fundamental about locomotion?*

1.3 Hypotheses and Research Objectives

Three principle hypotheses were developed and tested as part of this work:

1. Dominant factors exist that can explain the metabolic cost of locomotion in space suits.
2. Space suit legs act like springs.
3. Energy recovery plays a role in the run-walk transition, and explains the effect of space-suited locomotion on walking and running.

To test the first hypthesis and to lay the groundwork for subsequent work, I sought to develop a framework for consistent analysis of energetics data, (Objective 1) and to review what is known about suited and unsuited locomotion through quantitative case-study analysis, and a meta-analysis based on regression modeling (Objective 2).

To test the second hypothesis, I sought to understand how and why the energetics of running and walking in space suits differs by examining past data and simulating aspects of space suited locomotion (Objective 3).

To test the third hypothesis, I examined or calculated, based on the energetics framework, how energy recovery changes under various conditions of unsuited and suited locomotion (Objective 4).

Two additional research objectives included making recommendations that will guide designers of space suits and extravehicular activity systems (Objective 5), and exploring what space-suited locomotion has to tell us about unsuited locomotion (Objective 6).

1.4 Thesis Outline

Chapter contents, very briefly described in this section, are described in more detail in the next section, the Executive Summary.

Chapter 2, Literature Analysis, defines a framework for making consistent comparisons of metabolic cost across studies, and applies this framework to the analysis of unsuited and suited locomotion (Objectives 1-3). Results of applying the framework to unsuited locomotion suggest a possible role for energy recovery during gait in the run-walk transition (Objectives 4,6).

Chapter 3, Regression Analysis, describes a meta-analysis of data from prior studies of unsuited and suited locomotion. The results demonstrate that running tends to be more efficient per unit distance than walking in space suits, and suggests that space suit legs may act as springs during running (Objectives 2-3).

Chapter 4, Exoskeleton Characterization, describes the characterization of a lower-body exoskeleton intented for simulation of some aspects of space-suited locomotion. The lower-body exoskeleton legs are shown to induce similar knee joint-torques as does the current NASA space suit, the Extravehicular Mobility Unit (EMU). Because a physical spring has a joint-torque relationship similar in form and magnitude to the EMU, space suit joints like the EMU knee joints act like springs (Objective 3).

Chapter 5, Exoskeleton Energetics, describes a locomotion experiment with the lower body exoskeleton. The experiment is used to validate the model developed in Chapter 2, and understand the specific effects of space suit legs on the energetics of locomotion (Objectives 3-6). The results suggest that spring-like space suit legs improve efficiency per unit distance during locomotion, although the impact of the rest of the space suit impairs performance relative to unsuited locomotion. The results also suggest that there may be an optimal, non-zero joint-torque for space suit knee joints (Objective 5). Finally, the effects of the exoskeleton on the run-walk transition suggest a role for recovery in the run-walk transition (Objective 6).

1.5 Executive Summary

1.5.1 Chapter 2 - Literature Analysis

In Chapter 2 I review the biological and biomechanical determinants of metabolic cost during muscular exercise and locomotion, unsuited and suited.

A framework, derived from basic thermodynamics, is developed to enable comparison of metabolic cost across and between studies. This framework, when applied to locomotion, is used to define and differentiate between *muscle efficiency* and *energy recovery*, two concepts often confused in the existing running energetics literature. Calculations based on data reported in the literature reveal that the human run-walk transition in Earth gravity occurs at the point for which energy recovery is approximately the same for walking and running, suggesting a possible role for recovery in gait switching.

Muscle physiology limits the overall efficiency by which chemical energy is converted through metabolism to work. Walking and running utilize different methods of energy storage and release, and consequently differ in their relative recovery of energy. These differences contribute to the relative changes in the metabolic cost of walking and running as gravity is varied, with the metabolic cost of locomoting *at a given velocity* dropping in proportion to the reduction in gravity for running and less

than in proportion for walking.

Application of the framework to space suits demonstrates that suit pressurization has a significant impact on mechanical efficiency, mobility, and the metabolic cost of locomotion relative to unsuited conditions. Metabolic data from the Apollo lunar surface missions, not previously published, is presented and demonstrates that low metabolic rates were an important and beneficial consequence of performing traverses on the Moon using the Lunar Rover. The results of modeling work by Carr et al. [2003] hint that space suits may affect walking and running differently, and that the impact during running may be less severe.

1.5.2 Chapter 3 - Regression Analysis

I performed a cross-study analysis of past suited and unsuited locomotion energetics studies to try to understand how space suits affect cost of transport. I hypothesized that space suit legs act as springs during running, thereby maintaining or lowering cost of transport relative to space-suited walking.

I transformed data from past studies into a common format, and developed a regression equation for the specific resistance, a non-dimensional form of metabolic cost, based on the Froude number (a non-dimensional velocity), surface slope, earth-relative gravitational acceleration, and space-suit pressure. Acceptance criteria for regression factors included significance and a reduction in the residual variance. I divided suited data into fast running and walking or slow running groups and performed a group means hypothesis test and categorical regression of metabolic cost per unit weight (efficiency per unit time) and specific resistance (efficiency per unit distance).

The specific resistance regression achieved a DOF-corrected multiple R^2 of 0.83; all factors were significant ($p < 0.0005$). No additional evaluated factors met the acceptance criteria. The categorical regression, but not the hypothesis test, suggested that the fast running group had reduced efficiency per unit time; both tests suggested that the fast running group had increased efficiency per unit distance. Variations in specific resistance across studies were largely explained by a simple regression model.

Several findings suggest that gas-pressure suit legs function as springs during running, including the finding of higher efficiency per unit distance during fast running, despite the increased work against space suit joint torques at higher velocities.

1.5.3 Chapter 4 - Exoskeleton Characterization

In the historical analysis of suited and unsuited locomotion energetics (Chapter 3), I found evidence that space suits act as springs during running. Video images from the lunar surface suggest that knee torques create, in large part, this spring effect. I hypothesized that a lower-body exoskeleton, properly constructed, could be used to simulate the knee torques of a range of space suits.

In Chapter 4 I report characterization of a lower body exoskeleton. Equivalent spring stiffness of each exoskeleton leg varies as a function of exoskeleton knee angle and load, and the exoskeleton joint torque relationship closely matches Extravehicular Mobility Unit knee torques in form and in magnitude. I have built a physical nonlinear spring, and demonstrated that this spring achieves space-suit like joint torques; therefore space suit legs act as springs, with this effect most pronounced when locomotion requires large changes in knee flexion such as during running.

1.5.4 Chapter 5 - Exoskeleton Energetics

I hypothesized that locomotion with the exoskeleton would improve net energy recovery, reduce the cost of transport, and lower the Froude number of the run-walk transition relative to unsuited locomotion.

I measured the energetic cost and other variables during treadmill locomotion, with and without a lower body exoskeleton, in simulated reduced gravity ($G = 0.165, 0.379$) and in Earth gravity ($G = 1$). Subjects walked or ran at constant Froude numbers of 0.25 or 0.60, respectively, and walked and ran at a self-selected run-walk transition. Using the framework developed in Chapter 2, $1g$ measurements of specific resistance[1] during unsuited locomotion were used to estimate the specific resistance

[1] A non-dimensional measure of efficiency per unit distance: energy per unit of force supported per unit distance traveled.

of unsuited locomotion in the reduced gravity conditions. Net energy recovery was estimated for all exoskeleton conditions, based on metabolic cost measurements from the exoskeleton and unsuited conditions.

Six subjects completed the experiment after giving informed consent. Exoskeleton locomotion significantly lowered the cost of transport[2] $[J/(kg \cdot m)]$ and specific resistance $[J/(N \cdot m)]$ relative to the unsuited condition, increased the estimated net energy recovery, and lowered the Froude number of the run-walk transition relative to the unsuited condition. Theoretical and actual values for the unsuited specific resistance in reduced gravity conditions showed no statistically significant differences. The exoskeleton control condition (an exoskeleton leg with 1/8th the stiffness of the primary exoskeleton leg with space-suit-knee-like stiffness) had the lowest cost of transport of the three conditions tested.

Although order effects cannot be ruled out, it appears that the high energy recovery of the exoskeleton legs led to the observed reduction in the cost of transport and specific resistance during exoskeleton locomotion. The lower costs of transport of the exoskeleton control condition suggests the possibility of a tuned space suit: a exoskeleton or space suit leg stiffness that results in minimum metabolic cost during locomotion. The findings explain the previously observed effect of space suits on running: exoskeleton locomotion improved recovery during both walking and running, but because space suits impair walking recovery, the benefit of spring-like legs is most prominent during space-suited running. The results of the experiment and the success of the theoretical model also point to a potential role for recovery in the run-walk transition, although more data is needed to evaluate the linkage between recovery and gait transitions.

[2]Energy per unit mass carried a unit distance.

1.5.5 Overall Contributions

The major contributions of the dissertation include:

1. A model that predicts metabolic cost in non-dimensional form for unsuited locomotion across running and walking and across gravity levels (Chapters 2 and 5),
2. An assessment of historical data that reveals the effect of pressure suits on work output and the metabolic cost of locomotion (Chapters 2 and 3),
3. A method of simulating a space suit using a lower-body exoskeleton, and methods for designing and characterizing the exoskeleton (Chapter 4),
4. An explanation for the differences in the energetic costs of walking and running in space suits (Chapters 2-5),
5. Evidence that there is an optimal space suit leg stiffness, perhaps an optimal space suit leg stiffness for a given gravity environment (Chapter 5),
6. Evidence, mostly indirect, that energy recovery plays a role in gait switching (Chapters 2 and 5).

Chapter 2

Literature Analysis: The Metabolic Cost of Space Suits

Abstract

In this chapter I review the biological and biomechanical determinants of metabolic cost during muscular exercise and locomotion, unsuited and suited.

A framework, derived from basic thermodynamics, is developed to enable comparison of metabolic cost across and between studies. This framework, when applied to locomotion, is used to define and differentiate between *muscle efficiency* and *energy recovery*, two concepts often confused in the existing running energetics literature. Calculations based on data reported in the literature reveal that the human run-walk transition in Earth gravity occurs at the point for which energy recovery is approximately the same for walking and running, suggesting a possible role for recovery in gait switching.

Muscle physiology limits the overall efficiency by which chemical energy is converted through metabolism to work. Walking and running utilize different methods of energy storage and release, and consequently differ in their relative recovery of energy. These differences contribute to the relative changes in the metabolic cost of walking and running as gravity is varied, with the metabolic cost of locomoting *at a given velocity* dropping in proportion to the reduction in gravity for running and less

than in proportion for walking.

Application of the framework to space suits demonstrates that suit pressurization has a significant impact on mechanical efficiency, mobility, and the metabolic cost of locomotion relative to unsuited conditions. Metabolic data from the Apollo lunar surface missions, not previously published, is presented and demonstrates that low metabolic rates were an important and beneficial consequence of performing traverses on the Moon using the Lunar Rover. The results of modeling work by Carr et al. [2003] hint that space suits may affect walking and running differently, and that the impact during running may be less severe.

2.1 Introduction

Metabolism is the mechanism by which chemical processes occur in living organisms in order to maintain life and sustain energy production in support of human activities [OED, 2004]. Space suits support basic physiological functions in the space environment and permit humans to affect physical change in the environment, or to acquire information. Space suits impose kinematic and kinetic boundary conditions that affect movement and locomotion, and in doing so modify the metabolic cost of physical activity. Human metabolism is a primary determinant of the duration and intensity of activity by astronauts in space suits during extravehicular activity (EVA); EVA consumables such as oxygen and water set the total allowable metabolic cost, the integral of the metabolic rate over the duration of the EVA. To carry out NASA's new exploration vision to return humans to the moon by 2020 and later to send humans to Mars [Bush, 2004], significant changes in today's space suits are required to improve the efficiency of locomotion and improve interaction with the external environment.

This review focuses primarily on the sources of metabolic cost during extravehicular activity operations and factors that modify those sources; life-support system considerations are essentially excluded from this discussion, whereas locomotion is emphasized. After reviewing what is known about unsuited locomotion I review and analyze the interactions of space suits with mass carried, traverse velocity, surface

slope, and (perhaps of most interest) gravity. Because the mechanical counter pressure spacesuit concept [Annis and Webb, 1971], is now being explored once again [Tanaka et al., 2002, 2003, Frazer et al., 2002, Bethke et al., 2004, Danaher et al., 2005], potential metabolic consequences of using an MCP suit during planetary exploration are also discussed based on results from past studies with gas-pressure and MCP suits.

2.2 A Framework for Energetics Analysis

In this section, a basic framework is developed that clearly defines metabolic cost and muscular efficiency. This framework can be applied to generic activities involving external work, or to locomotion, in which it facilitates a clear differentiation between muscle *efficiency* and energy *recovery*, terms often given inconsistent meanings in the literature.

2.2.1 Enthalpy, Heat, and Work

The 1st law of thermodynamics expressed in terms of a differential change in enthalpy can be written as

$$dH = dW + dQ \tag{2.1}$$

where dH is the differential change in enthalpy of breathing gases, food, and waste products, dW is the differential work done by the system, and dQ is the differential change in heat added to the system. The sources of metabolic cost during human movement can be represented in an equivalent form (modified from [Wortz, 1968])[1]:

[1]Wortz [1968] originally wrote the work terms using Q_i instead of W_i, and defined these terms as amounts of energy, not work. His definition could lead to an overestimate of the sum of terms on the right-hand side of Equation 2.2, because, for example, waste heat generated during a muscular task to perform external work W_w is accounted in the Wortz model by the heat storage term Q_s, but might also incorrectly be included as part of the term representing "energy utilized in performing useful work" [Wortz, 1968] term, Q_w. The notation used here avoids this confusion, and adds a explicit term for the space suit,W_{ws}.

$$Q_m = W_w + W_{wc} + W_{wr} + W_{ws} + Q_n + Q_s, \tag{2.2}$$

where Q_m is the metabolic cost, W_w is the external (useful) work (done by the system), W_{wc} is the work done by the counterforce, W_{wr} is the work done to restore the body and limb position and orientation, W_{ws} is the work done deforming the space suit, Q_n is net heat lost, and Q_s is body heat storage.

Equation 2.2 illustrates the sources of metabolic cost based on measurable (as opposed to physiological) quantities: Q_m can be estimated from measurements of oxygen consumption and carbon dioxide production. W_w can be estimated based on force and position measurements or the mechanics of the particular task (for example, potential energy change achieved while raising or lowering a weight, as in Prescott and Wortz [1966]). Likewise, W_{wc} and W_{wr} can be estimated from force and position measurements or mechanics calculations (for example, measurements from an instrumented foot-restraint used by an astronaut who generates a counterforce against the foot restraint to permit upper-body work while maintaining body position). W_{ws} can be predicted from static and dynamic torque measurements of space suits [Dionne., 1991, Barer et al., 1994, Menendez et al., 1994, Morgan et al., 1996, Newman et al., 2000, Schmidt et al., 2001, Gonzalez et al., 2002, Yang and Yuan, 2002, Du et al., 2003]. During a cyclical movement $W_{ws} = 0$ since no net work is performed in deforming the space suit; unless the energy stored from deforming the space suit is used to do some form of external work (or work on the center of mass, such as during locomotion), the work done in deforming the space suit is converted to heat and accounted for by $Q_n + Q_s$. Q_n can be estimated through heat flux measurements: One common method, used during the Apollo missions [Waligora, 1976], relies on the use of a liquid cooling garment (LCG) and estimation of enthalpy changes between outlet and inlet water (or another fluid) with corrections for radiative cooling, any non-LCG conductive and convective cooling, and evaporative heat losses associated with sweating or respiration. Q_s can be estimated from deviations in body temperature relative to normal, or computed as

$$Q_s = Q_m - Q_n - W_w - W_{wc} - W_{wr} - W_{ws}. \tag{2.3}$$

A physiological breakdown of the sources of metabolic cost can be represented as

$$Q_m = Q_b + Q_w + Q_{wc} + Q_{wr} + Q_{ws}, \tag{2.4}$$

where Q_b is basal metabolism, Q_w is the energy associated with the external (useful) work, Q_{wc} is energy associated with generating the counterforce, Q_{wr} is the energy associated with restoration of the body position, and Q_{ws} is the energy associated with deformation of the space suit.

The Equation 2.4 terms are harder to measure but can be estimated from the Equation 2.2 terms or from differences in Q_m between different conditions. The W_i work terms from Equation 2.2 are related to the Q_i terms of Equation 2.4 through marginal efficiencies E_i such that, for example, $W_{wc} = E_{wc} \cdot Q_{wc}$. Q_b can be estimated as Q_m in a minimum external force condition such that $Q_w + Q_{wc} + Q_{wr} + Q_{ws} \approx 0$ (a subject at rest). Q_{ws} can be estimated as the ΔQ_m between conditions with and without a space suit.

2.2.2 Overall Mechanical Efficiency

A space suit may limit (or in very particular circumstances, enhance) the ability to perform external work, can transmit loads that affect the energy cost of generating the counterforce Q_{wc}, and may hinder or help the maintenance or restoration of body position. Therefore, it is clear that Q_w, Q_{wc}, Q_{wr}, and Q_{ws} are coupled terms, and it is often useful or necessary to lump them together. Q_{wc} can be estimated as the ΔQ_m between conditions with 'normal' and 'reduced' traction. Depending upon the experimental design, some sources of metabolic cost in Equations 2.2 and 2.4 cannot be disambiguated; however, when external work is performed, the overall mechanical efficiency E can be defined by the ratio of the external (useful) work to the total metabolic cost [Wortz, 1968]:

$$E = \frac{W_w}{Q_m}. \tag{2.5}$$

By expressing the metabolic cost from Equation 2.4 in terms of work and efficiency,

$$Q_m = \frac{W_w}{E_w} + \frac{W_{wc}}{E_{wc}} + \frac{W_{wr}}{E_{wr}} + \frac{W_{ws}}{E_{ws}} + Q_b, \tag{2.6}$$

one can see that the metabolic cost (as intuition would suggest) is minimized by minimizing each work term, maximizing each efficiency term, and minimizing basal metabolism (for example, staying calm).

Designers of current EVA systems have improved the value of EVA operations by minimizing the metabolic cost required to achieve a particular outcome through all of these methods. EVA tools provide biomechanical advantage to match the rate of work done to the ability to supply that work, or to improve the efficiency at which the work is done. Foot restraints help to reduce the energy cost of providing the counteractive force, and to reduce the energy spent restoring the body position. Work envelopes, if appropriately defined, reduce the work done on the space suit by ensuring that suit torques are not excessive in the work area Schmidt et al. [2001].

2.2.3 Total Metabolic Cost and Energy Supplied to do External Work

Assuming a (conservatively high) overall efficiency of 0.30 and a maximum sustainable metabolic rate of a human of about 750W, the maximum sustainable rate of external work is roughly 225W. Consequences of this result for EVA operations include a requirement that a space suit need only support sustained work rates below 750W, and a requirement that all tasks to be performed require an energy delivery rate Q_w less than 225W. In practice, the energy delivery rate for a given task is much lower because of space suit forces and the biomechanical nature of the task, including considerations of local muscle fatigue.

Adequate cooling was provided during Apollo lunar surface EVA using a maximum

heat removal capability of about 590W (2000 BTU/hr, or 1900 kJ/hr) [Johnston et al., 1975], the same heat removal capacity of early ventilation and cooling systems such as the 1959 system developed by Webb [Webb, 1959]. A similar system has proved more than adequate for cooling during subsequent low earth orbit operations (personal communication, Dr. Jeffrey Hoffman).

2.2.4 Energy Required to Generate Counterforce

Newton's third law requires forces to be equal and opposite: any force associated with energy delivered to do external (useful) work (Q_w) must be balanced by a counter-force, associated with Q_{wc}.

Springer et al. [1963] simulated a loss of traction in a one-degree-of-freedom task, and measured a 12% ($N = 10$, $p < 0.01$) and 29% ($N = 14$, $p < 0.001$) increase in oxygen consumption for raising and lowering weights of seven and 15.5 pounds, respectively, with no difference in work rates. These increases correspond to decreases in E of 11% and 22%. The maximum efficiency of 1.5% occurred in the tractive condition with the 15.5 weight. Prescott and Wortz [1966] demonstrated that metabolic rates during an upper body task increased as simulated reduced gravity levels were reduced ($N = 7$, $p < 0.01$) but that no such increase occurred during several types of exercises that involved no external work ($N = 7$); this finding is consistent with increases in the muscular power required to generate a given counter-force.

If the counter-force cannot be produced, then the astronaut cannot generate the force required to do the desired external work. This well-understood principle formed the basis for a variety of load-transmission devices (such as foot restraints) used during microgravity EVA. For example, upper body activity often results in torques that must be 'removed' by the ankles (the muscles and tendons that cross the ankle joint must produce counter-torques); the stiff space suit ankle reduces the magnitude of the torque that must be produced by the ankles, lowering Q_{wc}.

2.3 Biological and biomechanical determinants of metabolic cost

The energy required for maintenance of life, or homeostasis, and movement, or locomotion, is derived from a reduction in enthalpy through aerobic and (in the short-term) anaerobic metabolism. Both the usage of energy released by basal metabolism (Q_b) and the work done by muscles ($W_w + W_{wc} + W_{wr} + W_{ws}$) are limited in efficiency by thermodynamics and biomechanics. When chemical energy is released, only part of that energy is available for 'basal' processes (such as cellular repair, communication, digestion, pumping of blood, and cognition) and muscular contraction; the rest is converted directly to heat ($Q_s + Q_n$), and contributes to an increase in entropy [van Ingen Schenau and Cavanagh, 1990].

The efficiency of human movement and physical interaction with the world (E_w, E_{wc}, E_{wr}, E_{ws}, and therefore E), to the extent determined by biological factors, is determined by cellular energetics, musculoskeletal structure and function, supply of substrates to and removal of wastes from the relevant tissues, and integration of the result via coordination and control. These factors may be modified during extravehicular activity due to the impact of the space suit or due to short- or long-term physiological adaptation to an altered gravity environment.

At the cellular level, muscle contraction results from the repetitive load-dependent displacement of the protein myosin along actin filaments [Reconditi et al., 2004]; the load-dependence of the myosin stroke is the primary molecular determinant of the mechanical performance and efficiency of skeletal muscle [Reconditi et al., 2004], and explains the high relative efficiency of muscle at high loads and slow shortening velocities, originally characterized by A.V. Hill [Hill, 1922]. Adenosine tri-phosphate (ATP) consumption due to muscular contraction is driven by the rate of myosin and actin cross-bridge cycling (70-85%) and contraction regulation via calcium regulation (15-30%) [Conley, 1994].

Endogenous ATP sustains maximum metabolism rates, related to the maximal shortening velocity of the muscle fiber, for only four seconds; between four seconds

and about 30 seconds, maximal ATP use relies on ATP synthesis by creatine kinase (CK) from endogenous creatine phosphate (PCr) [Hochachka, 1994]. Beyond a few minutes of maximal work, glycolysis provides the dominant source of energy for regeneration of PCr and thus ATP. Glycolysis without aerobic metabolism leads to fermentation and the buildup of lactic acid; in the short-run, an oxygen debt is occurred that must be paid back through future increased aerobic metabolism. The volume fraction of skeletal muscle fiber occupied by mitochondria is a good measure of skeletal muscle oxidative capacity because skeletal muscle mitochondria consume an approximately equal volume of oxygen per volume of mitochondria at $\dot{V}O_{2,max}$ (the maximum volume flow rate of total organism oxygen consumption), even across different mammalian species [Billeter et al., 1994]. The structure of skeletal muscle is optimized for delivery of oxygen to mitochondria, and shows a linear relationship between capillary length density and mitochondrial volume density and an increased volume density of mitochondria near capillaries [Billeter et al., 1994]. The maximum transfer rate of non-oxygen metabolic substrates (carbohydrates, triglycerides, lactate) limits the maximum sustainable work rate over time scales longer than a few minutes [Billeter et al., 1994]. Margaria calculated that the efficiency of oxidative synthesis of PCr from glucose is 0.64 (versus 0.76 for synthesis from glycolysis); in experimental studies he observed a maximum mechanical efficiency in aerobic muscular exercise of about 0.25, which suggests an efficiency of production of mechanical work from PCr of about 0.40 [Margaria, 1976].

The value found by Margaria for the peak mechanical efficiency agrees well with the Hill muscle model as implemented by Alexander [2003], shown in Figure 2-1 and described in detail in Appendix A.

Muscles achieve a wide range of power outputs at relatively high efficiencies through the selective recruitment of different fiber types characterized by their different myosin isoforms [Billeter et al., 1994]. 'Slow' or type I fibers have higher oxidative capacities resulting from a higher mitochondrial volume fraction in comparison to 'fast' or type II fibers; type I fibers are optimized for support and low shortening velocity contractions whereas type II fibers are most efficient for fast shortening ve-

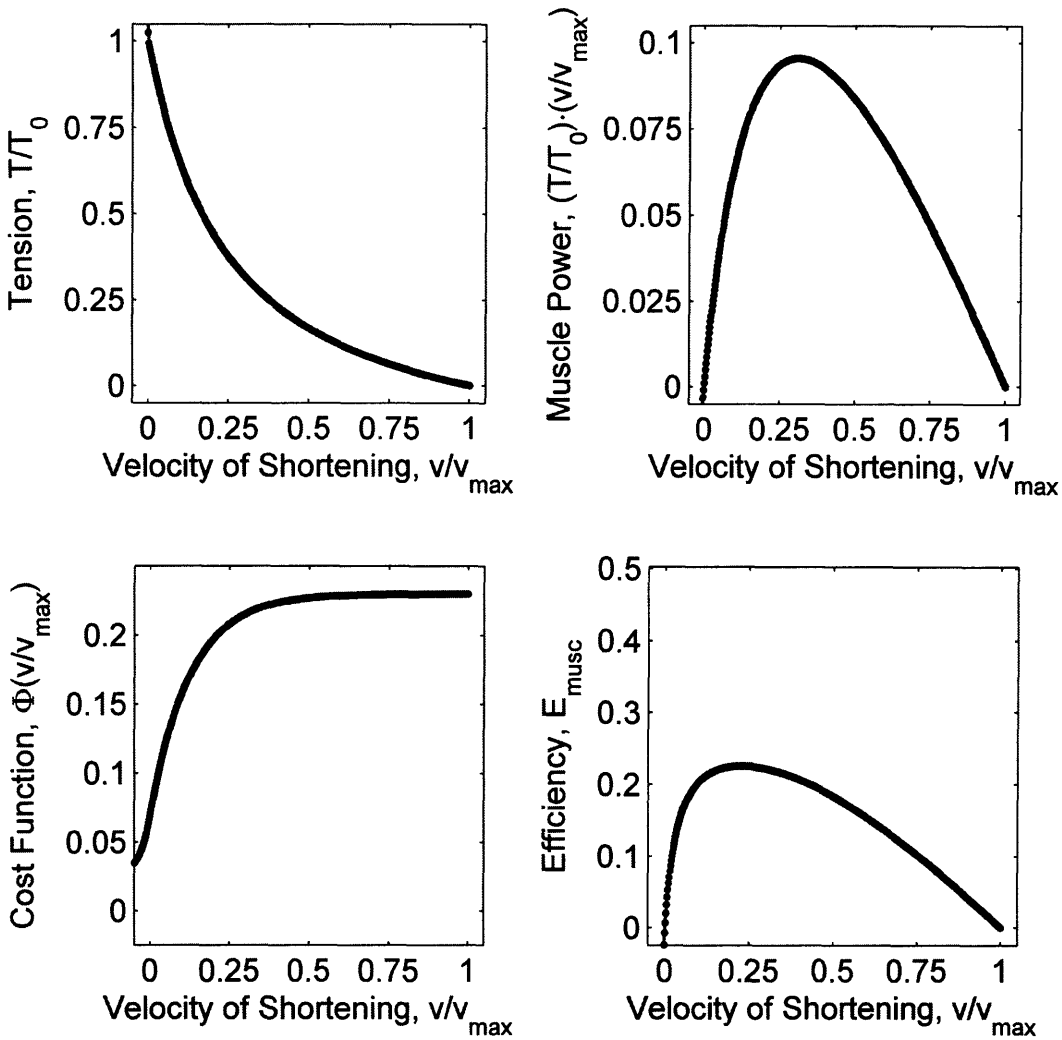

Figure 2-1: Hill muscle model for positive muscle contraction velocities. In the model, v/v_{max} is the ratio of muscle contraction velocity to maximum muscle contraction velocity, T/T_0 is the ratio of muscle tension to isometric tension, Φ is a cost function describing cellular energetics (see Appendix A for details), and E_{musc} is the muscle efficiency. Appendix A describes how the model can be tuned for different muscles; the above model uses parameter values typical for vertebrate muscles. Peak efficiency, above, is 0.23 for $v/v_{max} = 0.23$. The peak power condition occurs at $v/v_{max} = 0.31$, for which the efficiency is 0.22.

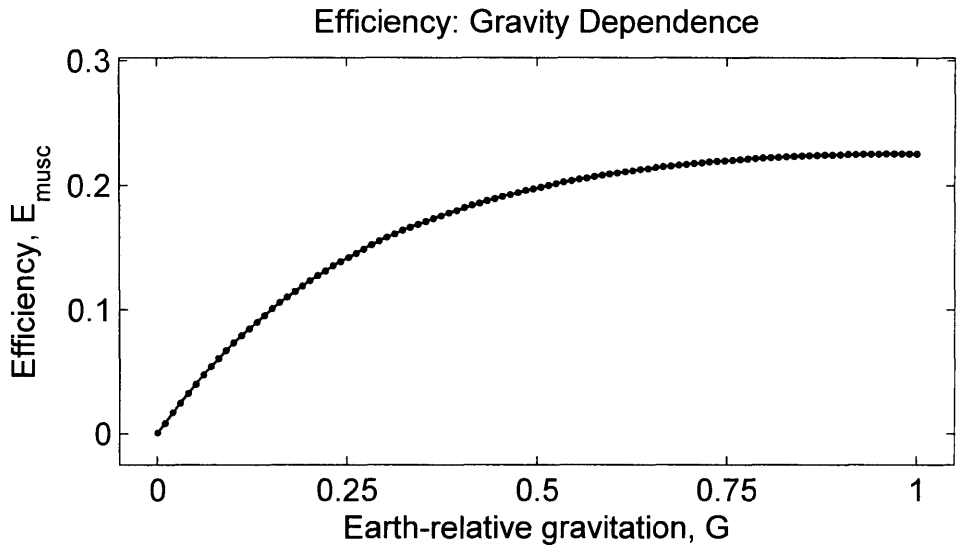

Figure 2-2: Approximate gravitational dependency of muscle efficiency derived from the Hill Model. See Appendix A for derivation.

locities. Humans exposed to weightlessness experience muscle atrophy and selective loss of contractile proteins that lead to increases in the highest-efficiency shortening velocity in both fiber types [Fitts et al., 2001]. This may be an appropriate adaptation to reduced gravity, in which locomotion muscles, contracting against reduced weight, would contract at higher velocities.

For an isolated muscle contracting against a fixed mass one can compute, using the Hill model, how the muscle efficiency would vary with gravity (Figure 2-2). This result, derived in detail in Appendix A, is based on the assumption that the muscle is optimized for Earth gravity, so that at $G = 1$ the muscle would have a contraction velocity that achieves peak muscle efficiency. In this model, muscle efficiency would decline from 0.23 to 0.18 on Mars (a 22% drop), or to 0.11 on the Moon (a 52% drop). Because humans can adjust muscle activation patterns (for example, producing lower forces by recruiting a smaller muscle volume), these values are likely to represent a lower bound for the achievable peak muscle efficiency.

Muscles are not merely devices for producing force, but are also elastic energy storage devices, dampers, struts, and sensors that allow movement and interaction through integrated and multilevel feedback control [Dickinson et al., 2000]. Muscu-

loskeletal system dynamics and control impacts the overall achievable efficiency by modulating the transformation of energy within an organism and between an organism and the environment. During running, for example, mass-specific mechanical work increases in a curvilinear manner with speed, but metabolic cost is observed to increase linearly with speed [Roberts, 1998]. Therefore the mechanical work rate of the body does not determine the metabolic energetics of running, and energy storage and recovery play an important role in locomotion.

2.4 Unsuited Locomotion: A brief review

Humans on land in earth gravity show three characteristics forms of locomotion [Minetti, 1998]: In walking, at least one foot maintains ground contact at all times, whereas in running there is no double support phase. Skipping is characterized by a stance phase involving an exchange of the support foot, and an extended aerial phase between two stance periods with the same supporting foot. Loping, a type of one- or two-footed hopping observed in reduced gravity environments, is biomechanically similar to skipping without the support foot exchange, or to running, with an extended aerial phase. Figure 2-3 illustrates these four forms of locomotion.

At its most basic approximation, the compass gait of walking can be modeled as an inverted pendulum [McMahon, 1984]. Stance-leg knee flexion, a second determinant of gait, can also be incorporated, leading to an improved model of ballistic walking [Mochon and McMahon, 1980]. Other major components of gait include pelvic rotation, pelvic tilt, plantar flexion of the stance ankle, and lateral displacement of the pelvis. These components of gait generally act to reduce oscillations of the center of mass, and thus limit the mechanical work done by the muscles during locomotion [Lee and Farley, 1998]. The metabolic cost of walking is largely explained by the cost of generating muscular force during the stance phase [Griffin et al., 2003]; the required muscular force is dictated by the time of contact and the load carried. Energy expenditures during the swing phase are harder to assess, but have recently been shown to account for up to 30% of the metabolic rate, at least in guinea fowl [Marsh et al.,

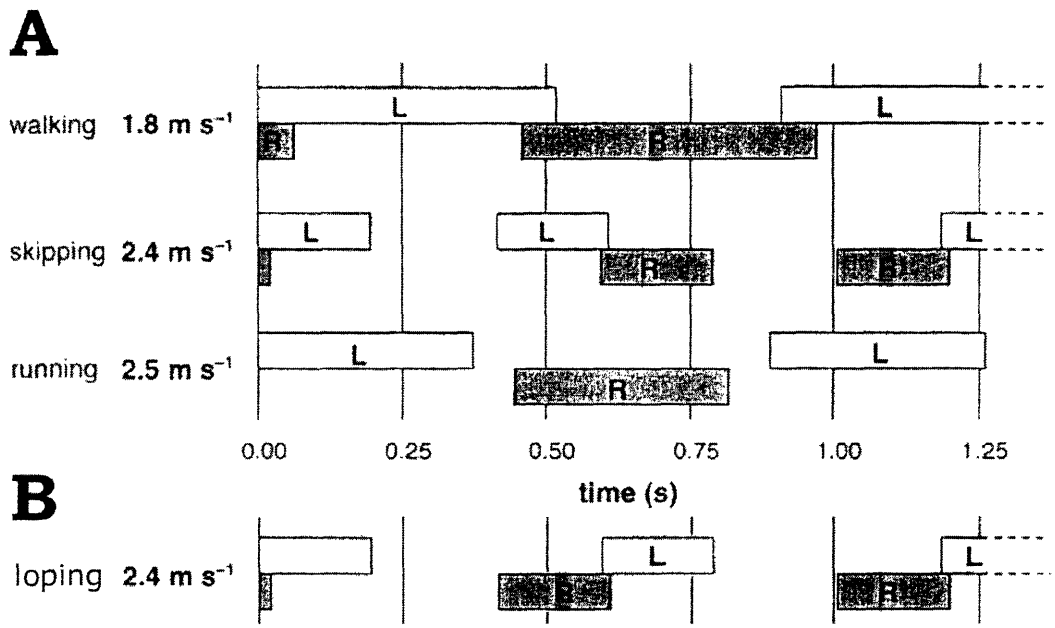

Figure 2-3: Forms of Gait in Humans: **A**. Three forms of locomotion in humans in earth gravity on land. R and L indicate contact periods for right and left feet, respectively. From Minetti [1998]. **B**. A hypothetical reconstruction of loping meant to illustrate the biomechanical similarities of loping and skipping.

2004].

Load-carrying studies have found a linear relationship between load carried and metabolic cost [Santee et al., 2001]. Hill-climbing studies have found a similar relationship between slope gradient and metabolic cost for positive slopes [Margaria, 1976]. Minimum metabolic cost is achieved for slightly negative slopes (8-10 degrees) [Margaria, 1976, Santee et al., 2001].

McMahon developed another simple model of locomotion that treated the body as an inverted pendulum with a single spring representing leg stiffness [McMahon and Cheng, 1990]. Humans (and other animals) modify leg stiffness [Farley et al., 1998] and there is a change in leg stiffness in response to changes in surface compliance [McMahon, 1984, Ferris and Farley, 1997]. Metabolic cost is also affected by changes in surface compliance: Kerdok et al. [2002] found that a 12.5-fold reduction in surface stiffness[2] resulted in a 12% reduction in metabolic cost with unchanged support

[2]The surface had high energy recovery.

mechanics.

2.4.1 Locomoting in Reduced Gravity

As gravity is reduced[3], the metabolic cost of walking at a given velocity declines [Wortz, 1968, Fox et al., 1975, Newman et al., 1994]. Fox et al. [1975] found that the mass specific volume rate of oxygen consumption, $\dot{V}O_2$ per unit mass, was reduced in simulated $0.25g$ and $0.5g$ treadmill walking at 3.2, 4.8, and 6.4 km/hr; net $\dot{V}O_2$ per unit weight carried was nearly uniform with a slight elevation for simulated reduced gravity conditions (not statistically significant) relative to $1g$ controls. Wortz [1968] maintained a subject's 165 lb weight during simulated reduced gravity locomotion at 4 mph by addition of weights in reduced gravity conditions, and demonstrated a progressive elevation in the metabolic cost per unit weight of reduced gravity locomotion at 0.5g, 0.25g and 0.17g compared to 1g controls Wortz [1968].

The findings of Wortz [1968] and Fox et al. [1975] both suggest that the reduced metabolic cost of locomotion in partial gravity results largely from the reduction in body weight carried but do not specify the source of the decrease in mechanical efficiency during partial gravity locomotion. Several factors are likely at work: Increased inertial forces in Wortz experiment; decreased recovery during walking at moderately reduced gravities $< 0.5\ G$ [Griffin et al., 1999], and higher muscle contraction velocities.

While smaller fluctuations in horizontal forces are observed in moderately reduced gravity, the ratio of vertical forces to horizontal forces stays nearly the same [Griffin et al., 1999], suggesting a reduced cost of stability at least under some reduced gravity conditions. Non-propulsive lateral forces benefit stability and maneuverability [Dickinson et al., 2000], suggesting that there may be a reduced cost of maintaining stability in moderately reduced gravity conditions.

Metabolic rates during running are determined by the volume of muscle activated and the rate of ground force application [Wright and Weyand, 2001], which is directly related to the velocity of shortening of the muscle and the reciprocal of the contact

[3]See Davis and Cavanagh [1993] for a review of reduced gravity simulation methods.

time. A recent study by Pontzer [2005] links anatomical variables such as leg length to force production requirements to predict the metabolic cost of locomotion.

Farley and McMahon [1992] had subjects walk at 1 m/s and run at 3 m/s in $1g$ and in simulated reduced gravity (Figure 2-4). They found that a 75% drop in gravity produced a 72% drop in the rate of energy consumption $((\dot{Q}_m - \dot{Q}_b)/(BodyMass))$ during running, but only a 33% decline during walking. The mass-specific oxygen uptake findings of Newman et al. [1994] are very similar in form to the metabolic rate changes observed by Farley and McMahon [1992], with large percent decreases in metabolic cost during locomotion at 2.3 m/s but much smaller percent decreases at 0.5 m/s (Figure 2-5). These finding demonstrate that running and walking energetics are different in nature; these differences derive in large part from the different mechanisms of energy storage and recovery, discussed in the next section.

Studies of walking and running [Newman et al., 1994, Ivanenko et al., 2002, Davis and Cavanagh, 1993] have found that contact time is relatively constant and peak ground reaction forces decreased as the simulated gravity level is reduced, suggesting that humans maintain similar kinematics but not kinetics across gravity levels from 100% to as little as 10% of Earth gravity.

In terms of the Hill model, this suggests that humans are able to maintain contraction velocities by reducing the volume of muscle recruited in reduced gravity. This provides direct evidence that the gravitational dependence of E illustrated in Figure 2-2 is likely to represent a lower bound for peak muscle efficiency in reduced gravity conditions.

2.4.2 Recovery during Walking and Running

In level locomotion on a flat non deformable surface there is no true external work, so that $Q_w = 0$ ('external' work as referred to by many locomotion researchers is the work done while accelerating the center of mass). In locomotion without a space suit $Q_{ws} = 0$. In this condition, Equation 2.4 can be written as

$$Q_m - Q_b = Q_{loco}, \tag{2.7}$$

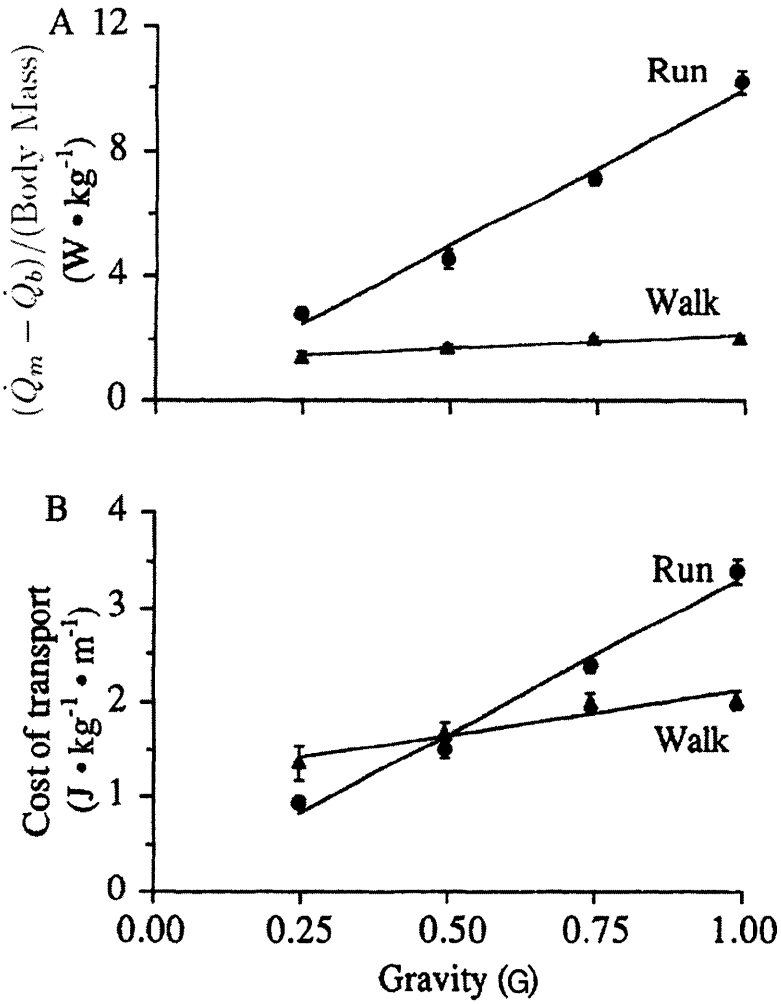

Figure 2-4: **A**. Metabolic rate during running decreased in direct proportion to gravity. By contrast, metabolic rate during walking decreased only slightly when gravity was reduced. Values are means±SE for 4 subjects. **B**. Walking a unit distance was not cheaper than running at all levels of gravity because reducing gravity had a much larger effect on energy consumption during running at 3 m/s than during walking at 1 m/s. Abridged caption and figure from Farley and McMahon [1992]; the plot has been relabeled with the notation used in this chapter.

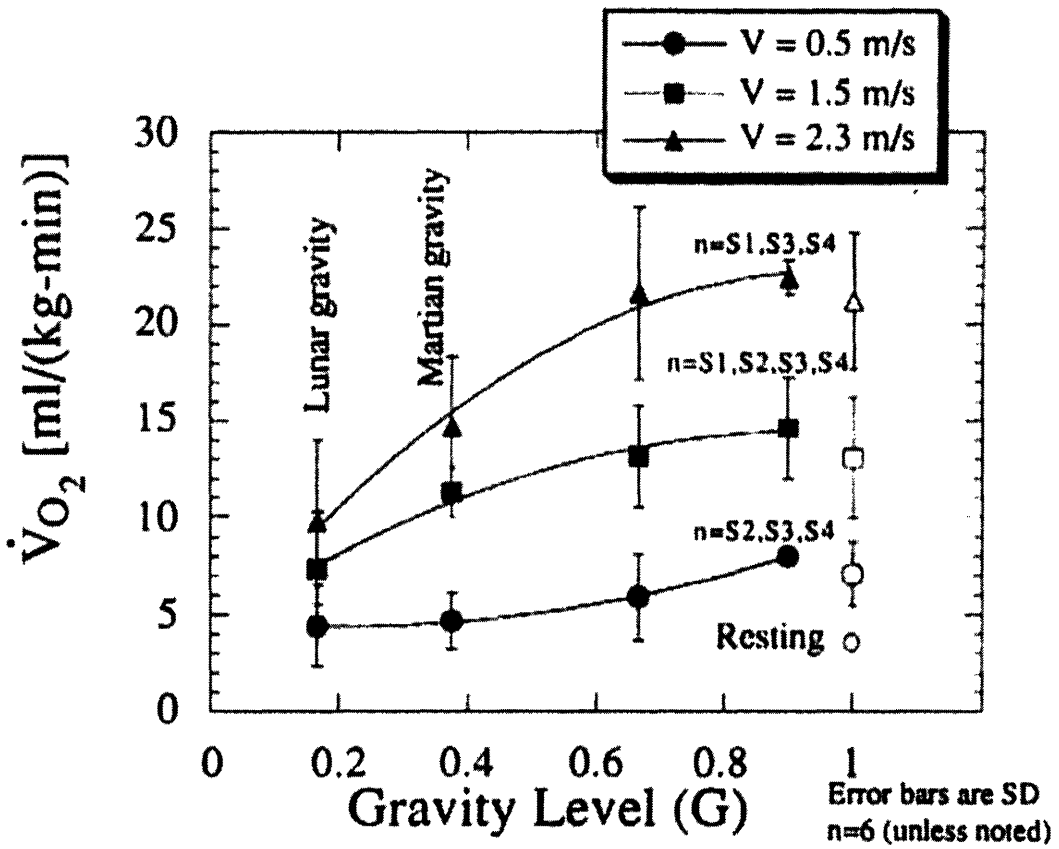

Figure 2-5: Oxygen uptake $\dot{V}_{O_2}$, versus gravity level. Each point is the mean and the error bars are standard deviations of the means. Plot and caption from Newman et al. [1994]; the study was performed using an underwater treadmill, with subjects ballasted to achieve the indicated reduced gravity weight conditions.

where $Q_{loco} = Q_{wr} + Q_{wc}$ is the energy expended to maintain the required center of mass motion (e.g. to generate the required counter-forces and restore the body position). Q_{loco} can also be expressed as

$$Q_{loco} = \frac{W_{musc}}{E_{musc}}, \tag{2.8}$$

where W_{musc} is the net work done by the locomotion muscles on the center of mass, and E_{musc} is the net efficiency of that muscular effort. The net work done by the locomotion muscles on the center of mass, $W_{musc} = W_{in} - W_{out}$, is equal to the difference between the total work done on the center of mass W_{in}, and the work recovered through energy storage mechanisms such as inter-conversion of kinetic and potential energy, or storage and release of elastic strain energy, W_{out}. The ratio of recovered work to total work is the recovery, η:

$$\eta = \frac{W_{out}}{W_{in}}. \tag{2.9}$$

Equation 2.8 can be rewritten as

$$\frac{Q_{loco}}{W_{in}} = \frac{1-\eta}{E_{musc}} \tag{2.10}$$

or, alternatively as

$$Q_m - Q_b = W_{in} \cdot \frac{1-\eta}{E_{musc}}. \tag{2.11}$$

Equation 2.11 shows that the net metabolic cost of locomotion (e.g. excluding basal metabolism) is a function, in this model, of three factors: First, the kinematics and dynamics of the center of mass determine W_{in}. Second, muscle physiology and its interaction with the environment determines E_{musc}. Third, mechanisms of energy conversion, or energy storage and release determine the cycle-to-cycle energy recovery η. As previously mentioned, peak muscle efficiency E_{musc} during locomotion can reach $\sim 25\%$ [Margaria, 1976, Whitt and Wilson, 1982].

In walking, kinetic and potential energies are out of phase, and there is a high

percent recovery of potential energy (60-65%) [Griffin et al., 2004a], while in running, kinetic and potential energies are in phase and the contribution to recovery from interconversion of kinetic and potential energy is near zero. Percent recovery stays high in reduced gravity walking (0.5-0.75g) but is decreased at 0.25g [Griffin et al., 1999]. Griffin et al. [1999] determined recovery during reduced gravity walking as a function of velocity and gravity (Figure 2-6). Griffin et al. [2004a] also examined recovery as a function of a non-dimensional velocity called the Froude number, computed as

$$Fr = \frac{v^2}{gL}, \tag{2.12}$$

where Fr is the Froude number, v is the velocity, g is the gravitational acceleration, and L is the leg length. A consistent pattern emerges when recovery is plotted as a function of the Froude number (Figure 2-7), supporting the analogy of recovery as a pendular exchange of kinetic and potential energy. The run-walk transition in humans occurs near $Fr \approx 0.5$ Minetti [2001] across different G-levels, although increases in the Froude number are observed as gravity is reduced, at least in simulated reduced gravity experiments [Kram et al., 1997].

In reduced gravity walking, at least two factors act against a linear reduction in metabolic cost for a linear reduction in gravity: First, ground reaction forces in walking are much lower than during running so that muscle contraction velocities may be higher; this may cause muscle efficiency to decline more for reduced gravity walking than for reduced gravity running. Second, in environments with $G \leq 0.5$, energy recovery η is adversely affected in walking. In contrast, a reduction in G directly contributes to a reduction in W_{in} during running, consistent with the proportional drop in metabolic rate observed by Farley and McMahon [1992].

Recovery in running is determined by how effectively elastic strain energy, stored in tendons and muscles, can be released. Kaneko [1990] reported the efficiency of running, after noting the multiple inconsistent meanings applied to "running efficiency" in the literature, as the ratio of work done on the center of mass to the net metabolic cost W_{in}/Q_{loco}, so that

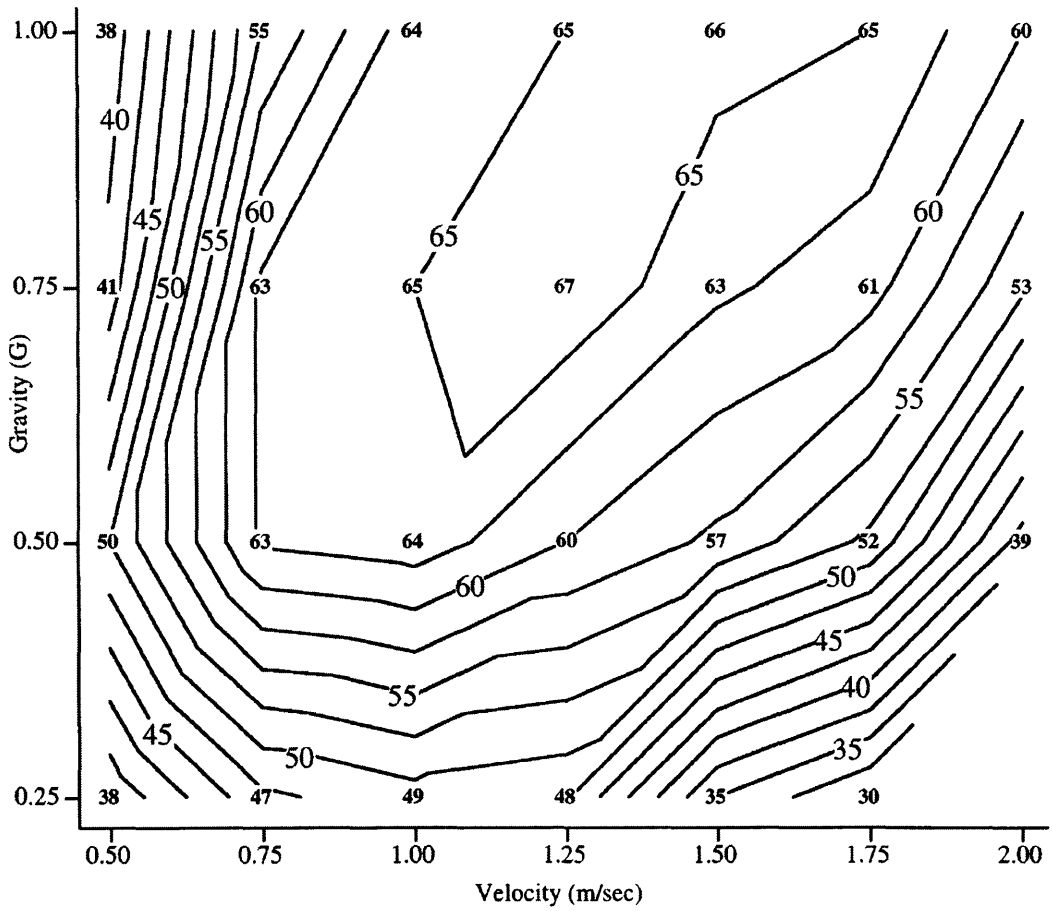

Figure 2-6: Energy recovery η in reduced gravity walking as a function of G and velocity. From Griffin et al. [1999].

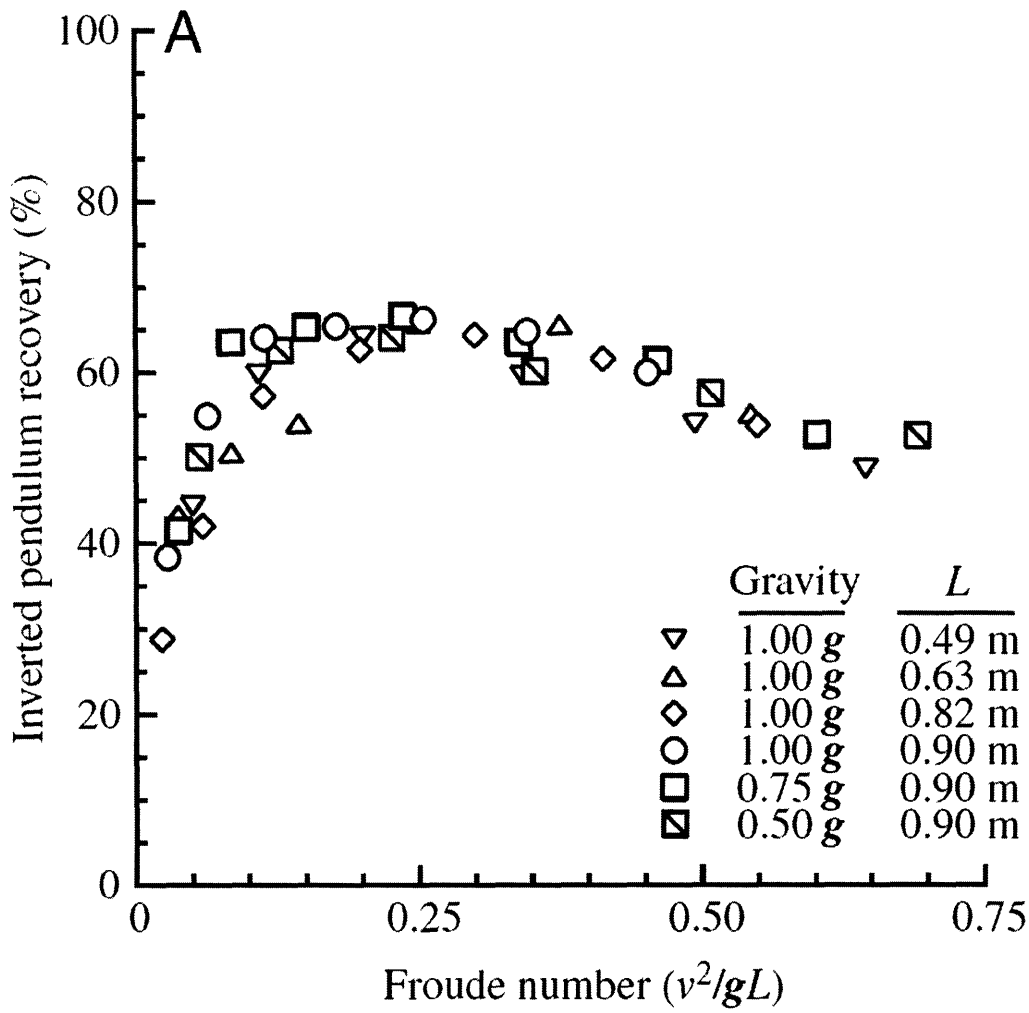

Figure 2-7: Percent recovery ($\eta \cdot 100$) of mechanical energy via the inverted pendulum-like mechanism in walking as a function of the dimensionless Froude number. Data from the literature are presented for children and adults walking at a range of speeds in normal gravity, and for adults walking at a range of speeds in simulated reduced gravity. Percent recovery is similar at equal Froude numbers, suggesting that at equal Froude numbers the inverted-pendulum dynamics are mechanically equivalent. Child data from Cavagna et al. [1983] for 3-4, 7-8 and 11-12-year olds. Adult and reduced gravity data from Griffin et al. [1999]. Caption and figure from Griffin et al. [2004a].

$$E_{Kaneko} = \frac{E_{musc}}{1-\eta}. \tag{2.13}$$

Kaneko [1990] demonstrated that running efficiency in 1g is around 50% at its peak, declines with increasing velocity (Figure 2-8) and declines as step frequency deviates from an optimal value of about 2.9 steps/sec (Figure 2-9). Why does the efficiency decrease with velocity? As the running speed increases, stride length increases dramatically while stride frequency elevates slightly [Cavanagh and Kram, 1989]. Furthermore, Weyand et al. [2000] have shown that faster top running speeds are achieved using greater ground reaction forces, not higher stride frequencies. As velocity increases, the elevation in stride length increases the relative proportion of Q_{loco} associated with the swing phase. Other irreversible factors such as losses to wind resistance also increase[4].

If E_{musc} is taken to be 0.225, the peak value for muscular work for $G = 1$ in the Hill muscle model implementation, then $E_{Kaneko} = 0.50$ represents a running recovery $\eta = 1 - E_{musc}/E_{Kaneko}$ of 0.55. Perhaps not coincidently, this value for running recovery is approximately equal to the recovery during human walking at $Fr = 0.5$; this finding strongly hints that recovery might play an important role in gait switching.

While much is known about unsuited locomotion, space suited locomotion is much less well understood.

2.5 Working in Space Suits

2.5.1 Energy Associated with Movements in a Space Suit

A.S. Iberall provided a theoretical basis for space suit design in 1951, and characterized the work done while deforming a space suit as the sum of the work done in

[4]Much more important than the losses due to wind resistance is the impact of wind on the maximum metabolic rate: in cycling, higher maximum metabolic rates are possible due to the increased cooling, and therefore reduced heat storage, associated with higher relative wind speeds for the same metabolic rate[Whitt and Wilson, 1982].

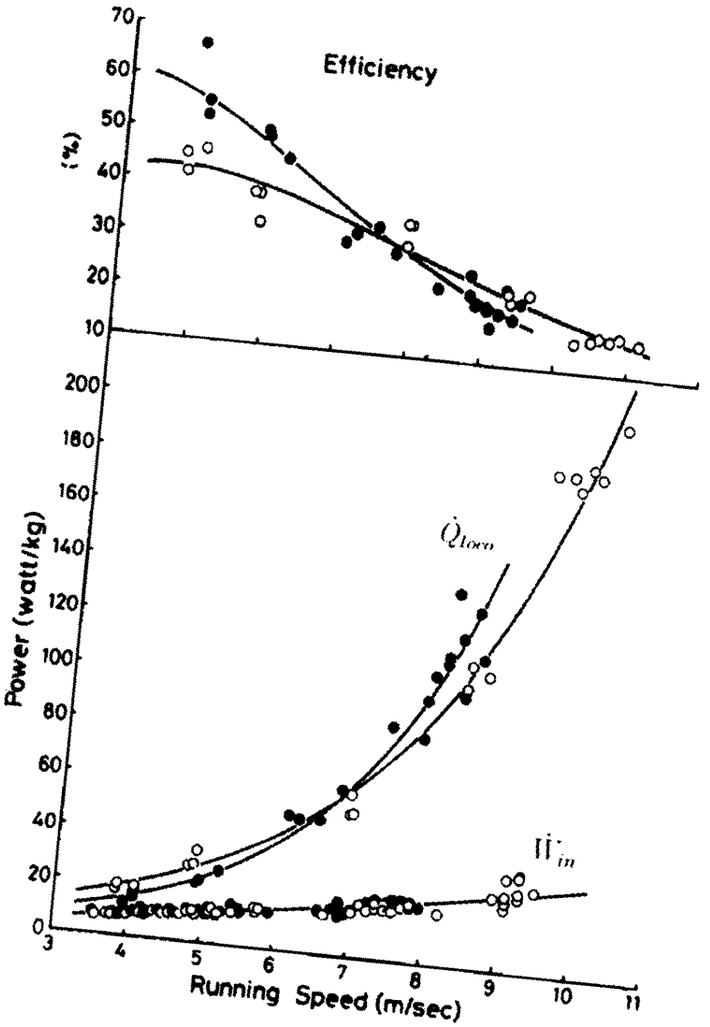

Figure 2-8: Efficiency of distance runners (•) and sprinters (○) in relation to running speed. Note that efficiency values are greater in distance runners than in sprinters at relatively low speeds ($< 7m/s$). Plot and caption from Kaneko [1990]; variables have been relabeled to match the notation used in this chapter.

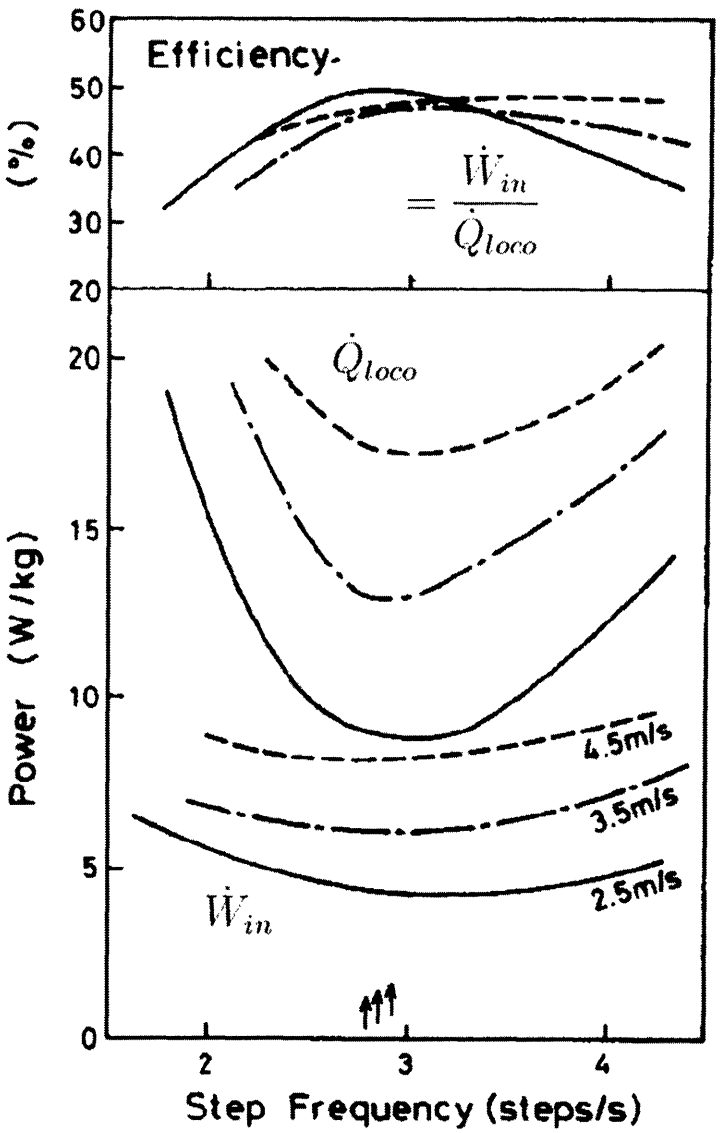

Figure 2-9: Total mechanical power ($\dot{W}_{in}$), net energy expenditure ($\dot{Q}_{loco}$), and efficiency ($\dot{W}_{in}/\dot{Q}_{loco}$) in relation to step frequency. Running speeds are indicated by different lines. Note that the most efficient step frequency is virtually the same as the freely chosen frequency indicated by the arrows. Plot and caption from Kaneko [1990]; variables have been relabeled to match the notation used in this chapter.

changing the gas volume, and the work done elastically deforming the suit [Iberall, 1951]. In a more complete articulation of his space suit design principles [Iberall, 1970], Iberall characterized the work done by the space suit occupant in an arbitrary deformation of the space suit as

$$\Delta W = \Delta W_p + \Delta W_b + \Delta W_s, \tag{2.14}$$

where ΔW is the total work done, ΔW_p is pressure-volume work, ΔW_b is bending work, and ΔW_s is stretching work. Bending and stretching work derive from deformation of the suit and redistribution of the stress distribution. Iberall argues that for arbitrary deformations, all right-hand terms in Equation 2.12 must vanish in order to minimize the work done by the spacesuit occupant.

To minimize pressure-volume work, space suit joints are designed to minimize the change in joint volume during bending [Harris, 2001]. Because the body is approximately incompressible over the small pressure increases incurred during suit joint movement, minimizing the volume change during bending of an isolated joint is, practically speaking, a sufficient condition for minimization of the joint-torque resulting from pressure-volume work.

Schmidt [2001] evaluated two physical models of space suit joint torques. One model, the beam model, assumes that joint-torques are due to deformation within the restraint layer of the space suit; work done against these joint-torques would account for ΔW_b and ΔW_s. The other model, the membrane model, assumes that joint-torques are due to gas compression; work done against these joint-torques would account for W_p. Data from the Extravehicular Mobility Unit (EMU) knee joint (Figure 2-10) demonstrates that space suit torques for joints like the EMU knee joint result largely from gas compression.

In a different type of space suit known as mechanical counter-pressure (MCP), body pressurization is provided by direct mechanical pressure applied to the skin by a fabric. Onle a single full prototype MCP suit has been built to date: the Space Activit Suit, or SAS [Annis and Webb, 1971]. Joint-torques in the SAS result from changes

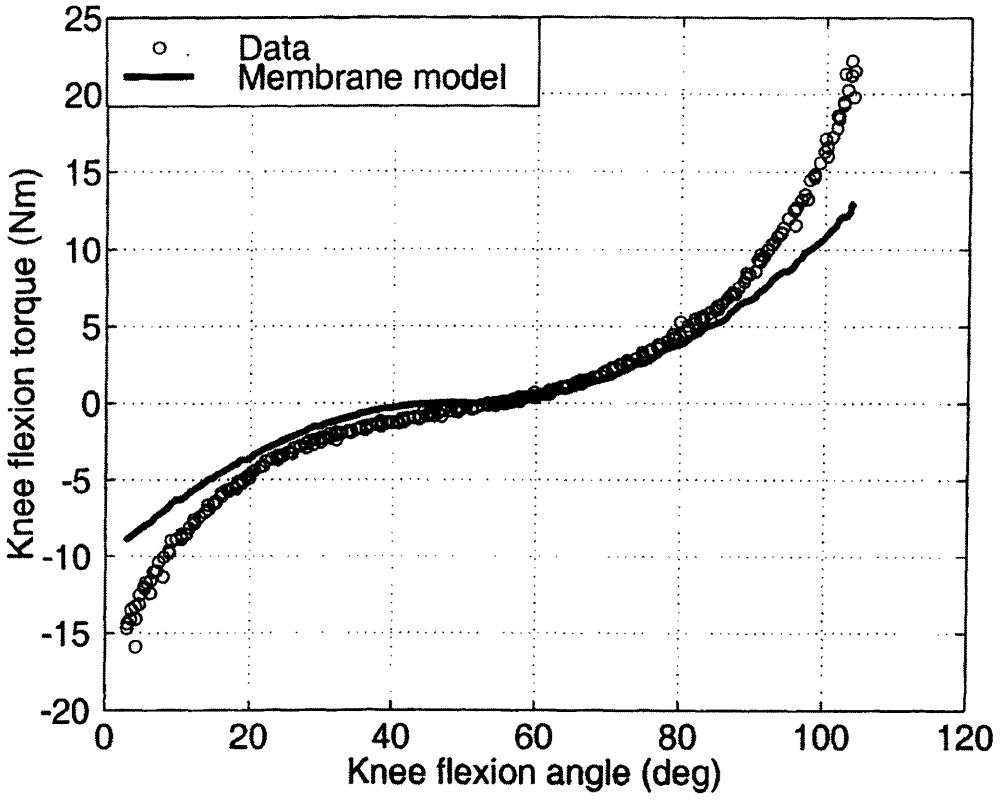

Figure 2-10: EMU Knee Torques agree in form and magnitude with torque predictions generated using the membrane model [Schmidt, 2001], which assumes that torques result from gas compression. At extreme knee flexion angles, actual torques are in excess of those predicted by the membrane model; this is indicative of unmodeled torques, such as those due to fabric bunching, which tend to be insignificant near the zero-torque flexion angle. Data and figure from [Schmidt, 2001].

in the stress-strain distribution of the fabric layer providing body pressurization, the $\Delta W_b + \Delta W_s$ components of Equation 2.14.

To the author's knowledge, no quantitative data exists on mechanical counter-pressure (MCP) joint-torques. However, it is clear that MCP joint-torques are low enough to vastly improve mobility in comparison to gas pressure space suits (Figure 2-11).

2.5.2 Suit Pressurization Effect

Streimer et al. [1964] investigated the effects of pressure suits on work output ($N = 5$ males, age 18-20, 50th-95th percentile stature) while in shirt-sleeves, or in one of three

Figure 2-11: Mobility of the only full prototype mechanical counter-pressure (MCP) space suit, the Space Activity Suit, was substantially better than all past and current space suits (Don't try doing this in a gas-pressure space suit). MCP joint-torques, unlike gas-pressure suits, result predominantly from changes in elastic strain energy ($\Delta W_s + \Delta W_b$). It is not known what are the minimum achievable joint-torques using MCP technology; current MCP efforts [Tanaka et al., 2002, 2003, Frazer et al., 2002, Bethke et al., 2004, Danaher et al., 2005] have focused on pressure production, and no joint-torque measurement of MCP garments have been reported to date. Image from Annis and Webb [1971].

different space suits. Subjects were evaluated in both unpressurized and pressurized conditions, and tractive and reduced traction conditions, for a total of 14 conditions. From the published metabolic data and work output means, the overall mechanical efficiency E was estimated for each condition. The overall mechanical efficiency E dropped from 6.4% in the shirt sleeve tractive condition, to as low as 2.4% in one of the reduced traction pressurized suit conditions. A two-factor ANOVA with replication (each space suit was considered a replication) of these E estimates demonstrated significant percent decreases in E resulting from suit pressurization (-31%, $p < 0.0001$), and reduction in traction (-12%, $p < 0.05$); the interaction effect was not significant.

To quantify the rate of energy expended in moving the space suit $\dot{Q}_{ws}$, the marginal efficiency of work $E_w = \dot{W}_w/\dot{Q}_w$ was computed from the shirt-sleeve tractive condition (with $\dot{Q}_{wc} + \dot{Q}_{wr} + \dot{Q}_{ws}$ set to 0, and $\dot{Q}_b = 80W$, a reasonable approximation of basal metabolic rate), and was assumed to be constant. For the reduced traction conditions, $\dot{Q}_{wc} + \dot{Q}_{wr}$ was estimated by assuming the same heat of work rate $\dot{Q}_w$ in tractive and reduced traction conditions. Q_{ws} was then estimated as $\dot{Q}_m - \dot{Q}_b - \dot{Q}_w - (\dot{Q}_{wc} + \dot{Q}_{wr})$.

Figure 2-12 shows the dual effects of reduced traction and suit pressurization for the work output study by Streimer et al. [1964], as compared to a cycle ergometry study by Annis and Webb [1971] in the only full prototype MCP space suit to date, the Space Activity Suit. The relatively low ratio of $\dot{Q}_{ws}/\dot{Q}_w$ observed in the MCP suit (at a metabolic cost of 560-730W) almost certainly results from the lower joint-torques and low mass of the MCP suit in comparison the gas pressure space suits.

2.5.3 Suited Locomotion

Webbon et al. [1981] used a Self Contained Atmospheric Protective Ensemble (SCAPE) suit pressurized to 1.8 kPa (0.26 PSI) to simulate a space suit while evaluating several liquid-ventilation cooling garments (LCVGs); the mean metabolic rate during treadmill walking at 0.9 m/s (2 mph) was 464W, 109% above the unsuited mean metabolic rate. This high metabolic rate illustrates the importance of minimizing change in volume during joint movement. Space suit joint designs achieve energetics

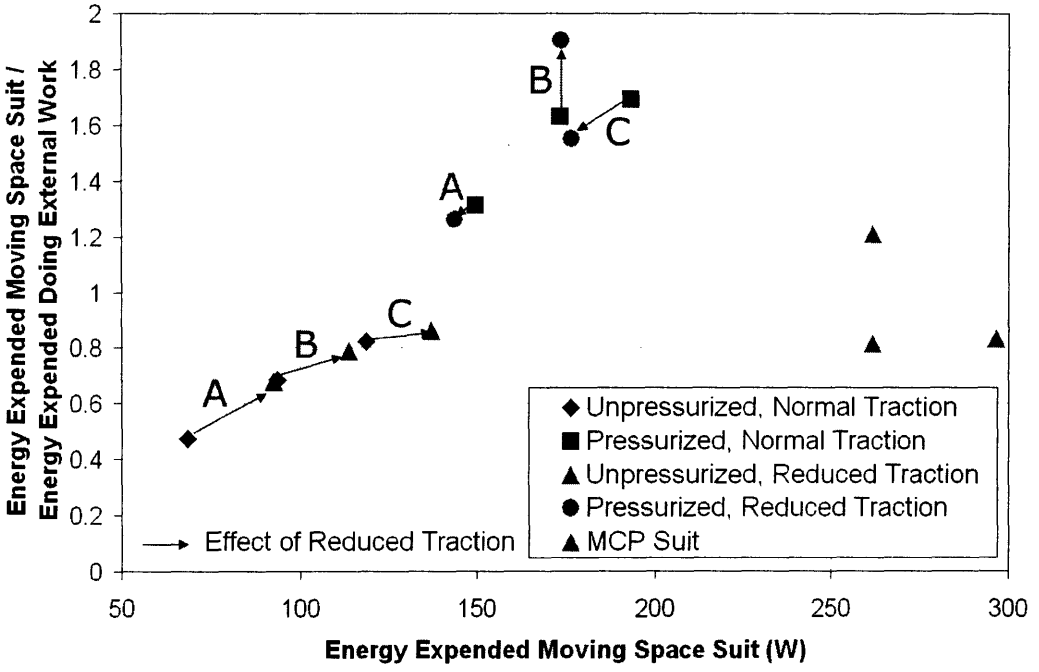

Figure 2-12: *Gas Pressure Suits*: The three space suits studied by Streimer et al. [1964] in a work output task are labeled A, B, and C. Using the framework, energy expended moving the space suit $\dot{Q}_{ws}$ was computed as described in the text, and plotted versus $\dot{Q}_{ws}/\dot{Q}_w$, which represents the factor by which overall mechanical efficiency is reduced by the space suit relative to the unsuited condition. The effect of reducing traction for unpressurized suits was consistent in sign: an elevation in $\dot{Q}_{ws}/\dot{Q}_w$. The effect of reducing traction for pressurized suits (24 kPa) was inconsistent, and may have even resulted in a reduction in $\dot{Q}_{ws}/\dot{Q}_w$. Loss of traction may have forced the suit occupant to use the suit as a load-carrying member in order to generate the required counterforce. *MCP Suit*: Annis and Webb [1971] had subjects wearing the Space Activity Suit (SAS) MCP suit pedal a bicycle ergometer. The data indicates that subjects in the MCP suit expended about as much energy moving the MCP suit as in doing external work, a substantial achievement at such a relatively high work rate.

comparable or closer to unsuited conditions than this SCAPE suit at $\approx$ 17 times the SCAPE suit operating pressure.

The framework was applied to the study of 0.45 m/s (1 mi/hr) walking in three space suits by Streimer et al. [1964]. $\dot{Q}_w$ was taken to be zero and $\dot{Q}_{wc} + \dot{Q}_{wr}$ was taken as $\dot{Q}_m - \dot{Q}_b = 131W$ in the unsuited condition. Locomotion data at slightly higher velocities (0.9-1.3 m/s) from Annis and Webb [1971] in the SAS is plotted with the Streimer et al. [1964] data for comparison (Figure 2-13). In the unpressurized condition, subjects used 75% more energy to maintain the movement of their body center of mass than energy moving the space suit. In the pressurized condition, subjects expended over 400% more energy moving the space suit than energy moving the body center of mass. This dramatic difference illustrates the extent to which limited mobility and increased joint-torques can dramatically increase the metabolic cost of locomotion. In comparison, subjects in the SAS, walking at higher velocities (more than twice as fast than the pressure suit subjects), achieved low $\dot{Q}_{ws}/\dot{Q}_w$ ratios comparable in magnitude to subjects in the unpressurized space suits evaluated by Streimer et al. [1964]. This indicates that the joint-torques and mobility limitations of the SAS lack the serious detrimental effect on the walking metabolic rate of the pressure suits tested by Streimer et al. [1964]. In other words, the SAS demonstrated significantly improved mobility relative to the gas pressure suits evaluated by Streimer et al. [1964].

Approximate recovery values can be estimated using Equation 2.11, if W_{in} can be estimated. One can assume a value for η based on the Froude number for walking (see Figure 2-7), and assume a reasonably high muscle efficiency (for example, $E_{musc} = 0.20$)[5]. W_{in} can then be estimated under the unsuited condition, with W_{in} in the suited condition given by

$$W_{in,suited} = \frac{m_{suited}}{m_{unsuited}} \cdot W_{in,unsuited}, \tag{2.15}$$

[5]Taking a constant value for muscle efficiency assumes that mechanical advantage is not modified by use of the suit (in which case muscle efficiency is likely to decline), an assumption probably not valid for most space suits.

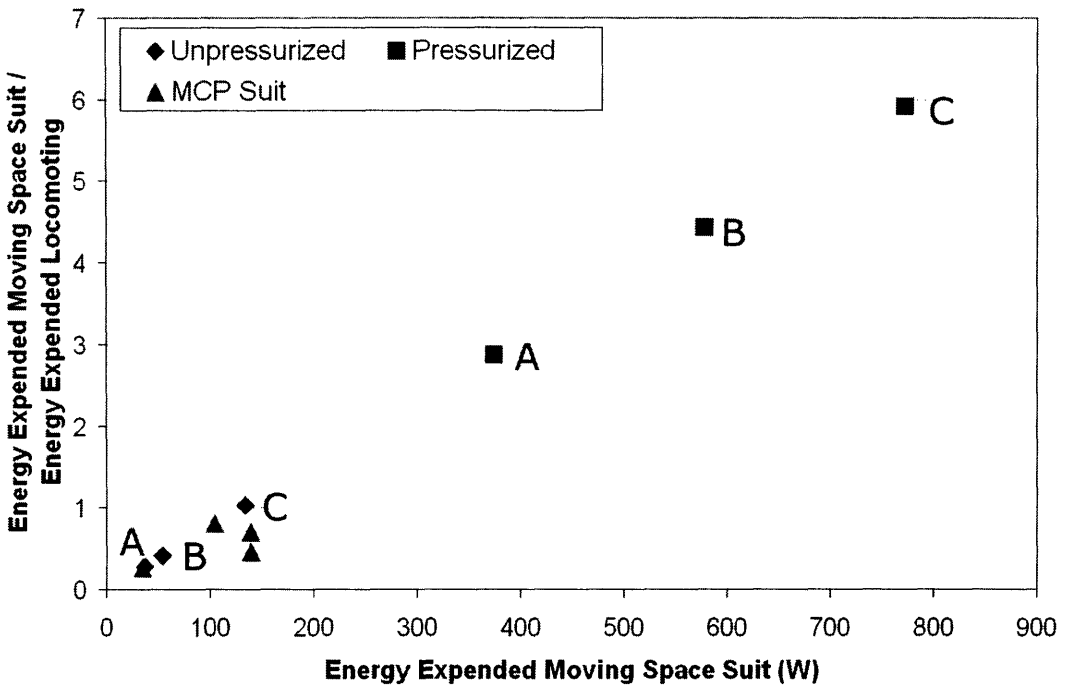

Figure 2-13: Streimer et al. [1964] measured metabolic cost during 0.45 m/s (1.0 mi/hr) locomotion in three space suits (labeled A, B, and C); locomotion data for 0.89-1.3 m/s from the SAS [Annis and Webb, 1971] is also plotted for comparison. Using the framework, energy expended moving the space suit $\dot{Q}_{ws}$ was computed as described in the text, and plotted versus $\dot{Q}_{ws}/\dot{Q}_w$. See text for interpretation.

Table 2.1: Recovery During Locomotion in the Space Activity Suit

Velocity $[m/s]$	Froude Number	$\dot{Q}_{wr} + \dot{Q}^a_{wc}$ $[W]$	$\dot{W}_{in}$ $[W]$	$\dot{Q}_{ws}$ $[W]$	$\eta_{unsuited}$	η_{suited}
0.89	0.09	199	94	140	0.55	0.28
0.89	0.09	129	61	35	0.55	0.46
1.11	0.13	129	79	104	0.65	0.41
1.33	0.19	304	185	140	0.65	0.52

SAS Suit mass taken as 4.7 kg, and muscle efficiency E_{musc} taken as 0.20.

[a] Energy associated with work done on the center of mass.

where m_{suited} and $m_{unsuited}$ are the total masses transported in the suited and unsuited conditions, respectively. For Equation 2.15 to be valid, the kinematics must not change in the suited condition as compared to the unsuited condition (so that the positive work done in moving the center of mass changes only by the mass ratio). Equation 2.15 is therefore a gross simplification.

Performing this procedure for the Streimer et al. [1964] data using $m_{unsuited} = 75$ kg and $m_{suited} = 125$ kg (an assumed 50 kg suit mass) kg yields an average recovery of 27% under unpressurized conditions and -150% under pressurized conditions. Clearly, the assumptions are invalid in this case, but one can safely conclude that recovery wass adversly affected. Performing a similar procedure with the locomotion data from Annis and Webb [1971] yields the results shown in Table 2.1: recovery values decline from the unsuited condition, but are still substantial.

As might be expected from studies of unsuited locomotion, surface condition also affects the metabolic cost of space-suited locomotion (Figure 2-14).

Similarly to unsuited locomotion, slope gradient has a significant effect on the metabolic cost of space-suited (Figure 2-15).

Some metabolic cost estimates, generated during Apollo Lunar-surface extravehicular activities using the estimation procedure described in [Waligora, 1976] have been published, but for later Apollo missions only broad averages for activity categories have been published. Stolwijk [1970] published limited metabolic data from Apollo 11, while the most complete treatment of data from the Apollo Missions, by Johnston et al. [1975], includes a relatively detailed assessment of components of Apollo 14 and

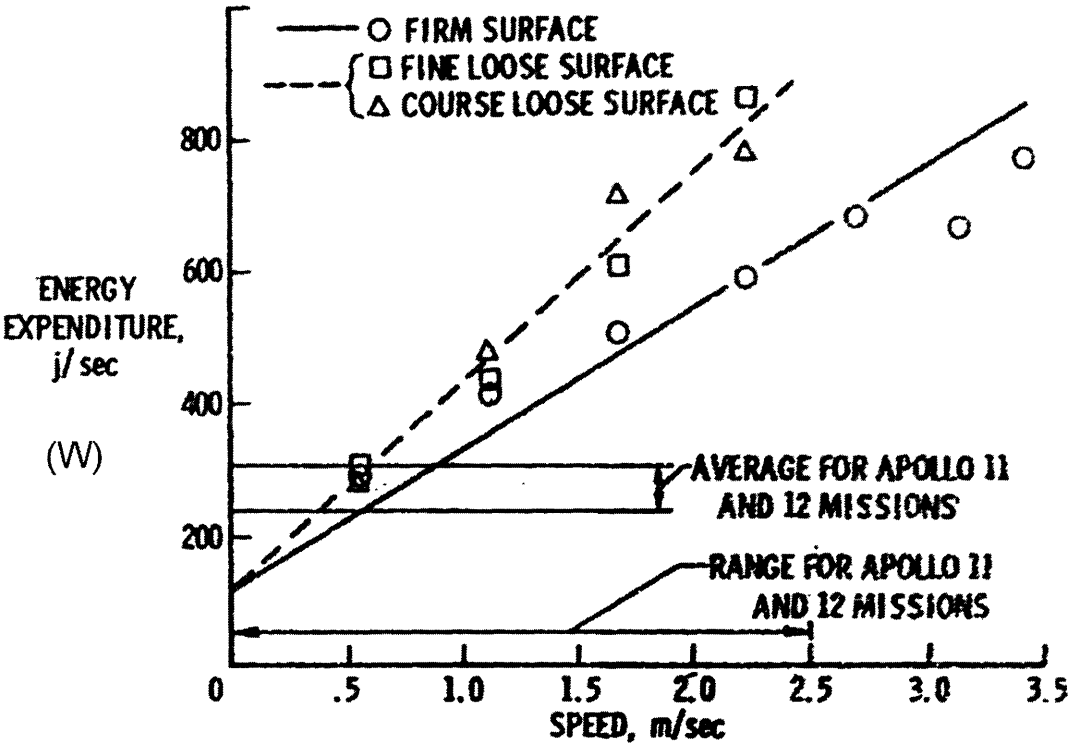

Figure 2-14: The effect of surface condition on energy expenditures in self-locomotion in simulated lunar gravity. Pressure suited subjects (25.5 kN/m^2). Caption and figure from Stone [1971].

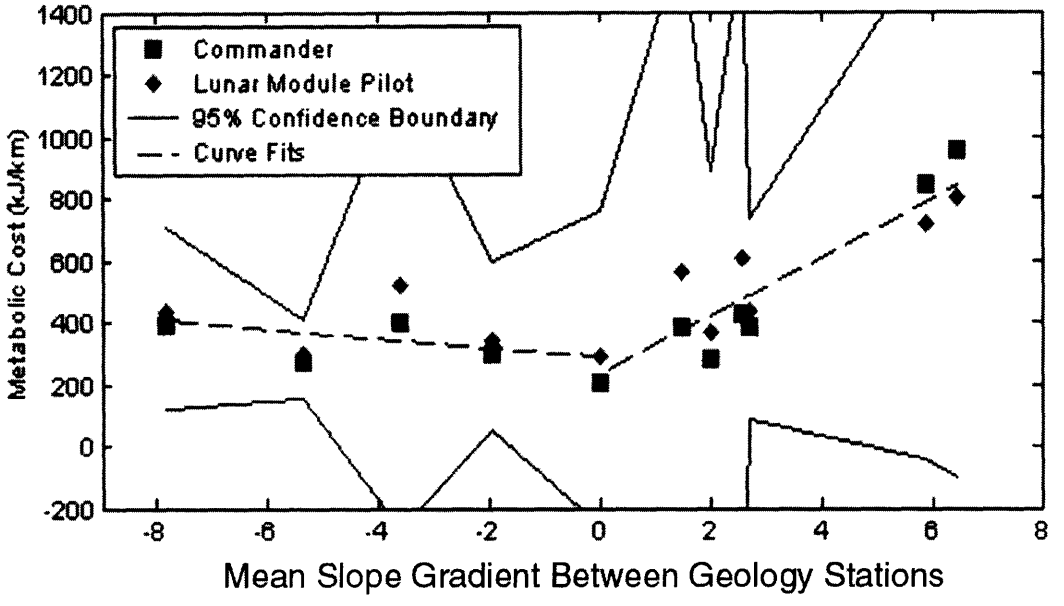

Figure 2-15: Carr [2001] synthesized data in Johnston et al. [1975] from the Apollo 14 walking traverses, showing a relationship between metabolic cost and surface slope.

15. These metabolic estimates were used in real-time mission planning decisions such as whether it would be feasible to extend an EVA.

One important feature lacking from previously published Apollo metabolic cost estimates is the impact of the lunar rover on metabolic rates. Figure 2-16 shows the original metabolic estimates for each Apollo lunar surface EVA "traverse segment"[6], grouped by whether the traverse was performed on the lunar rover or on foot (unpublished data, provided to the author by Jim Waligora). To interpret the results, it is important to know that the rover average speed was ≈ 2.7 m/s (6.0 mi/hr)[7], a reasonably fast running speed in lunar gravity. This allowed the astronauts of Apollo 15, 16, and 17 to cover more ground than had previous lunar explorers, but perhaps more importantly, the lower average metabolic rate achieved during rover traverses allowed the total EVA time to be extended.

Carr et al. [2003] reconstructed the Apollo 14 traverse and applied the load carrying model of Santee et al. [2001], which includes gravity as an explicit model component, to this reconstructed traverse. The Santee et al. [2001] model results agreed with the Apollo 14 metabolic cost estimates from Johnston et al. [1975] to within $\sim 11\%$ [Carr et al., 2003], despite the lack of model parameters to account for the space-suit (other than as an adjustment to the total mass).

The Santee et al. [2001] model, designed to model load-carrying by soldiers, can not be expected to accurately predict the impact of space suit joint-torques. Carr et al. [2003] concluded that some effect must be compensating for the unmodeled detrimental effect of mobility restriction and joint-torques imposed by the Apollo space suits. A detailed comparison of the Apollo 14 metabolic cost estimates (Unpublished data, C. Carr) indicates that the Santee et al. [2001] model over-predicts the metabolic cost at velocities with $Fr > 0.5$ and under-predicts the metabolic cost for velocities with $Fr < 0.5$, suggesting that some feature of space suits might reduce the metabolic cost of running or elevate the metabolic cost of walking.

Another important explanation for why the Apollo 14 estimates are not too differ-

[6]This dataset includes all traverse segments during the Apollo missions, except one of the Apollo 16 EVAs, for which the original Apollo data table was not available.

[7]http://ares.jsc.nasa.gov/HumanExplore/Exploration/EXLibrary/docs/ApolloCat/Part1/LRV.htm

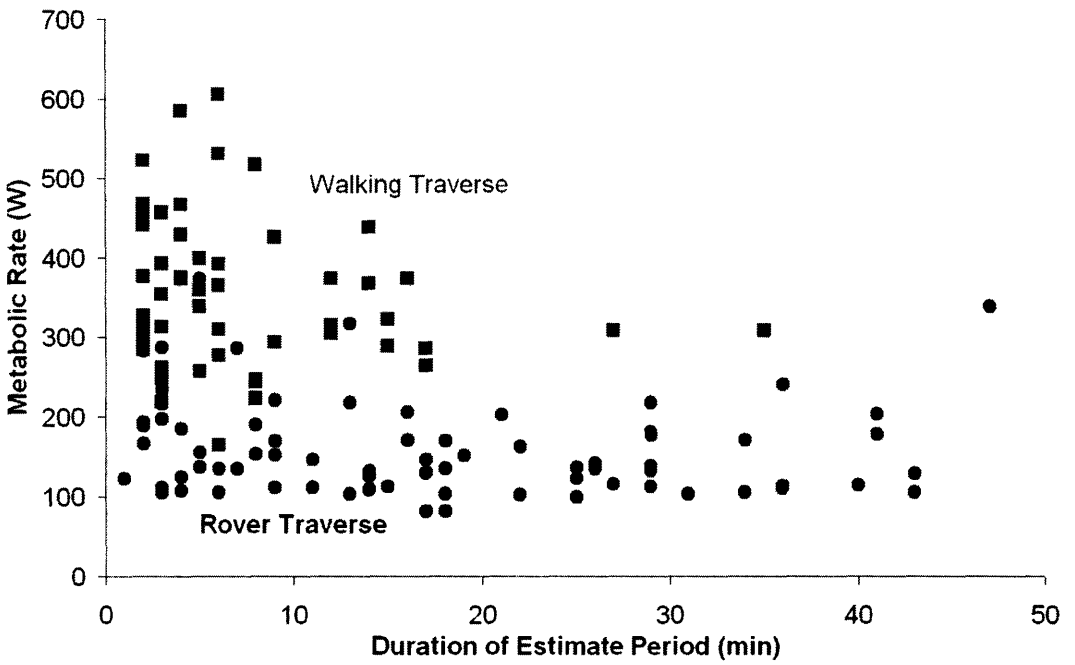

Figure 2-16: Original estimates for metabolic rate ($\dot{Q}_m$) from the Apollo missions: Each point represents a the metabolic cost estimate for a single "traverse segment." Data has been grouped by whether the traverse was performed on the lunar rover (filled circles) or on foot (filled squares). The data suggests that a major benefit of the lunar rover was to lower the average metabolic rate, thereby allowing extension of the EVA duration. (Unpublished data provided to the author by Jim Waligora).

ent from the estimates based on the Santee et al. [2001] model is the possibility that the detrimental effects of the space suit may be approximately balanced, in this case, by a reduction in weight supported by the suit occupant. Because of high longitudinal pressure forces, pressure suits become partly to fully self-supporting in reduced gravity environments. For example, a 100 cm^2 suit cross section (not unreasonable for a space suit ankle) at a suit pressure of 30 kPa would provide a longitudinal force of 300 N. On the Moon ($g = 1.62 m/s^2$ or $G = 0.165$) a 100 kg suit weights only 162 N; therefore, if a suit occupant stabilized the suit (maintained small knee flexion angles and provided the torques required to maintain upright suit and body posture), the suit weight would be entirely carried by the suit.

2.6 Summary and Conclusions

Muscle physiology limits the overall efficiency by which chemical energy is converted through metabolism to work. Walking and running utilize different methods of energy storage and release, and consequently differ in their relative recovery of energy. These differences contribute to the relative changes in the metabolic cost of walking and running as gravity is varied, with the metabolic cost of locomoting *at a given velocity* dropping in proportion to the reduction in gravity for running and less than in proportion for walking.

The framework described in this chapter, derived from basic thermodynamics, can be used to compare different studies in a clear, consistent manner. This framework was applied to locomotion, for which it clearly defines and differentiates between muscle efficiency and energy recovery, two concepts often confused in the existing running energetics literature. Furthermore, calculations based on data reported in the literature reveal that the human run-walk transition in Earth gravity occurs at the point for which energy recovery is approximately the same for walking and running.

Application of the framework to space suits demonstrated that suit pressurization has a significant impact on mechanical efficiency, mobility, and the metabolic cost of locomotion relative to unsuited conditions. Space suit torques in pressure suit

soft joints result largely from gas compression, and are approximately proportional to the internal gas pressure. Thermodynamic irreversibility increases due to energy dissipation in the restraint layer as the joint angle becomes large relative to its zero torque value.

Metabolic data from the Apollo lunar surface missions, not previously published, was presented and demonstrates that low metabolic rates were an important and beneficial consequence of performing traverses on the Moon using the Lunar Rover. Available data from the literature indicates that many factors substantially alter the cost of space-suited locomotion, including gravity, surface slope and surface condition. The results of modeling work by Carr et al. [2003] hint that space suits may affect walking and running differently, and that the impact during running may be less severe.

In the next chapter, these findings are synthesized and generalized via regression modeling of prior energetics data from studies of unsuited and suited locomotion.

Chapter 3

Regression Analysis: Cost of Transport During Locomotion In Space Suits

Abstract

I performed a cross-study analysis of past suited and unsuited locomotion energetics studies to try to understand how space suits affect cost of transport. I hypothesized that space suit legs act as springs during running, thereby maintaining or lowering cost of transport relative to space-suited walking.

I transformed data from past studies into a common format, and developed a regression equation for the specific resistance, a non-dimensional form of metabolic cost, based on the Froude number (a non-dimensional velocity), surface slope, earth-relative gravitational acceleration, and space-suit pressure. Acceptance criteria for regression factors included significance and a reduction in the residual variance. I divided suited data into fast running and walking or slow running groups and performed a group means hypothesis test and categorical regression of metabolic cost per unit weight (efficiency per unit time) and specific resistance (efficiency per unit distance).

The specific resistance regression achieved a DOF-corrected multiple R^2 of 0.83; all factors were significant ($p < 0.0005$). No additional evaluated factors met the acceptance criteria. The categorical regression, but not the hypothesis test, suggested that the fast running group had reduced efficiency per unit time; both tests suggested that the fast running group had increased efficiency per unit distance. Variations in specific resistance across studies were largely explained by a simple regression model. Several findings suggest that gas-pressure suit legs function as springs during running, including the finding of higher efficiency per unit distance during fast running, despite the increased work rate against space suit joint torques at higher velocities.

3.1 Introduction

Before humans first walked on the moon, Roth [1966], in his groundbreaking synthesis, summarized the state of knowledge of the bioenergetics of space suits for planetary exploration: walking in a pressurized space suit might require more than twice [Roth, 1966] to four times [Streimer et al., 1964] the energy expenditure as unsuited walking. In primary studies of locomotion energetics, researchers have evaluated the effects of velocity [Haaland, 1968, Annis and Webb, 1971, Kubis et al., 1972, Johnston et al., 1975, Wortz and Prescott, 1966, Sanborn and Wortz, 1967, Fox et al., 1975, Stauffer et al., 1987, Newman et al., 1994], surface slope [Haaland, 1968, Johnston et al., 1975, Margaria, 1976, Fox et al., 1975, Patton et al., 1995, Santee et al., 2001], reduced gravity [Robertson and Wortz, 1968, Wortz and Prescott, 1966, Fox et al., 1975, Newman et al., 1994, Farley and McMahon, 1992], increased mass carried [Wortz, 1968, Stauffer et al., 1987, Patton et al., 1995, Wickman and Luna, 1996, Santee et al., 2001], and space suits [Streimer et al., 1964, Robertson and Wortz, 1968, Annis and Webb, 1971, Lee et al., 2001]. Recent studies, geared toward space-suited work in microgravity, have focused on the static and dynamic torques required to move space suit joints [Dionne., 1991, Barer et al., 1994, Menendez et al., 1994, Morgan et al., 1996, Newman et al., 2000, Schmidt et al., 2001, Gonzalez et al., 2002, Yang and Yuan, 2002, Du et al., 2003].

With renewed interest in planetary exploration [Bush, 2004], I sought to understand how space suits modify the metabolic cost of locomotion by transforming data from past studies into a common format amenable to multiple regression analysis. To examine the effect of space suits and the relative importance of different factors, I analyzed locomotion studies in which subjects were suited or unsuited, carried no load or additional loads, walked or ran, and traveled on negative, level, or positive-sloped surfaces.

During locomotion in gas pressure space suits one must counteract suit joint-torques; at higher speeds one might expect this would require the occupant to do more work on the space suit per unit time. However, some joint torques may be beneficial: the knee joint torques of space suits may act as springs during running, reducing the required work rate. I hypothesized that fast running may be less efficient per unit time, but more efficient per unit distance, than walking or slow running in gas-pressure space suits.

3.2 Background

An extremely abridged review of locomotion is presented here; for a compact review of locomotion energetics see Margaria [1976] or the recent review by Saibene and Minetti [2003]. Davis and Cavanagh [1993] reviewed human locomotion in reduced gravity. Suited and unsuited locomotion in 1G and in reduced gravity is reviewed in Chapter 2. While Roth [1966] is somewhat out of date, it provides a useful and rather comprehensive review of pre-1966 studies in locomotion and space suit energetics.

Humans on land in earth gravity show three characteristic forms of locomotion [Minetti, 1998]: In walking, at least one foot maintains ground contact at all times, whereas in running there is no double support phase. Skipping is characterized by a stance phase involving an exchange of the support foot, and an extended aerial phase between two stance periods with the same supporting foot. Loping, a type of two-footed hopping performed by suited subjects in reduced gravity environments, is biomechanically similar to skipping without the support foot exchange.

While walking, kinetic and potential energies are out of phase, and there is a high percent recovery of potential energy; while running, kinetic and potential energies are in phase and the recovery depends upon storage of elastic energy in muscles and tendons, instead of the pendulum-like exchange of potential and kinetic energy in walking. Percent energy recovery stays high in reduced gravity (0.5-0.75g) but is decreased at 0.25g [Griffin et al., 1999]. Alexander [1989] has shown that humans (unsuited, at $1g$) choose walking or running at their current speed to minimize oxygen consumption.

Load-carrying studies have found a linear relationship between load carried and metabolic cost [Santee et al., 2001]. Hill-climbing studies have found a similar relationship between slope gradient and metabolic cost for positive slopes [Margaria, 1976, Santee et al., 2001]. Minimum metabolic cost is achieved for slightly negative slopes (8-10 degrees) [Margaria, 1976, Santee et al., 2001].

Non-dimensionalization of locomotion parameters has permitted testing of theories of invariant parameters of locomotion [McMahon, 1984, Minetti, 2001]. The Froude number, the ratio of inertial to gravitational acceleration, is computed as:

$$Fr = \frac{v^2}{gL} \tag{3.1}$$

where v is the velocity, g is the gravitational acceleration, and L is a characteristic length, usually taken, in studies of locomotion, as the leg length or height of the hip joint (approximately equal to the height of the center of mass in humans). The Froude number can be used to estimate accurately the run-walk transition speed and optimal speed of walking across a range of gravitational environments [Minetti, 2001].

The metabolic cost $\dot{Q}_m$ [W] is often normalized to create a figure of merit and to permit comparison across studies: The metabolic cost $\dot{Q}_m$ [W] normalized by the locomotion velocity v [m/s] gives the cost of transport, C [J/m],

$$C = \frac{\dot{Q}_m}{v}, \tag{3.2}$$

the energy required to transport a mass a unit distance. Further normalizing

by the total mass transported m [kg] gives a mass-specific cost of transport, C_m [J/(m·kg)],

$$C_m = \frac{C}{m}, \tag{3.3}$$

the energy required to transport a unit mass a unit distance. Normalizing by the gravitational acceleration gives the weight-specific cost of transport, a non-dimensional parameter called the specific resistance [Gabrielli and Karman, 1950], S:

$$S = \frac{C_m}{g} = \frac{\dot{Q}_m}{mgv}. \tag{3.4}$$

3.3 Methods

I reviewed past energetics studies of suited and unsuited locomotion, using as a primary reference the journal Aviation, Space, and Environmental Medicine and its precursor Aerospace Medicine. For each study I extracted data from tables or via digitization of figures in order to obtain metabolic cost data and to compute cost of transport, mass-specific cost of transport, and specific resistance. I performed multiple regression analysis to determine what factors best explain the computed specific resistance. I then performed a statistical test to evaluate my hypothesis.

3.3.1 Data Acquisition

When data were available in both tabular form and in figures, the tabular data were used. Figure data was scanned and digitized using a custom digitizing application that used a least-squares method, able to correct for any linear distortions of the source image, to determine the logical coordinates of digitized points. To test the accuracy of the digitizing process, 25 randomly generated coordinate pairs were plotted, printed on letter paper, scanned at 300 dpi, and digitized. Using the generated and digitized estimated coordinates, the average absolute percent position error was determined.

3.3.2 Energetics Data

The data required to normalize metabolic cost data in a consistent fashion were not always available in the published literature; I made the following assumptions in order to transform data in a consistent manner: Leg length was estimated as subject height/1.85, if subject height but not leg length data were available. If metabolic cost data were given in watts, these values were used; metabolic cost data given in terms of oxygen consumption were multiplied by the conversion factor, k $[W]/[mlO_2/s]$,

$$k = 4.33 \cdot RQ + 16.6, \tag{3.5}$$

where RQ is the respiration quotient, the ratio of moles of oxygen consumed to carbon dioxide expelled. All unknown respiration quotients were taken to be 0.87. In several cases, suit mass was not provided, but could be estimated or bounded from other sources in the literature.

To create a common format dataset, each study was assigned a unique identifier, as was each experimental condition for each study. Each experimental condition represented a single row in the dataset, and every column represented a published or computed datum from a given study and condition. Data were segmented in as fine-grained a fashion as possible; that is, published data were never averaged to produce a single row.

Experimental conditions (rows) were excluded from the dataset for several reasons: First, because computing cost of transport requires normalization of metabolic cost by the velocity, rows with zero velocity were excluded from the dataset. Low-speed measurements of metabolic cost taken immediately after high-speed locomotion would reflect the gradual recovery from high-speed conditions, and would exaggerate the metabolic cost at low speed; these rows were removed. Rows with unknown slope angle data were also excluded, as were rows representing redundant data reported in a previously analyzed study.

3.3.3 Regression Analysis

The Froude number Fr was selected as a regression factor on the basis of its success in predicting the run-walk transition, which is related to the mass-specific cost of transport [Alexander, 1989]. A binary variable suit was defined, indicating whether a given trial was suited ($suit = 1$) or unsuited ($suit = 0$). Suit might seem an appropriate choice for a regression factor. However, it was anticipated that some conditions in the dataset would involve unpressurized suits or partially pressurized suits; to account for these conditions, another variable called the pressure product p was defined that was equal to zero for suit=0 and equal to the differential suit pressure in $pounds/in^2$ for $suit = 1$. The pressure product was included in the regression, as space suit joint torques, and thus the work done on the space suit during a given movement, are proportional to the differential suit pressure. Reduced gravity is known to affect the metabolic cost and cost of transport, and so I included the Earth-relative gravitational acceleration, $G = g_{local}/g_{earth}$ as a factor. The strong effect of surface slope on the metabolic cost was demonstrated by data from the second lunar surface Apollo 14 extravehicular activity [Johnston et al., 1975, Carr, 2001]; the percent grade of the surface α (equal to the ratio of vertical altitude gain to horizontal distance multiplied by 100) was also included as a factor. Additional factors were also evaluated.

A mixed hierarchical regression was performed using each study as a cluster and solving with a random intercept and no interaction terms. The acceptance criteria for each factor in the regression model included a reduction in the remaining variance relative to the regression model without the factor, and an estimate for the factor coefficient that differed significantly from zero at the 0.95 level of significance. Where possible, factors were used in non-dimensional form in order to permit future interpretation across different conditions. The degrees-of-freedom corrected multiple R^2 was computed, using as the degrees of freedom (DOF),

$$DOF = N - F - I - 1, \tag{3.6}$$

where N was the number of conditions, F is the number of fixed terms in the regression, and I is the total number of clusters.

A sensitivity analysis was performed to quantify differences between the specific resistance calculated directly from the source data, S_i, and the specific resistance estimated using the regression model, $\hat{S}_i$. For each condition j within a study i , I computed:

$$dS_{ij} = S_{ij} - \bar{S}_i \tag{3.7}$$

and

$$d\hat{S}_{ij} = \hat{S}_{ij} - \bar{\hat{S}}_i \tag{3.8}$$

where $\bar{S}_i$ is the mean S_{ij} and $\bar{\hat{S}}_i$ is the mean $\hat{S}_{ij}$ within study i. To compare the deviation of condition j from the ideal sensitivity line ($\hat{S} = S$) I computed the deviation from the ideal sensitivity line as

$$e_{ij} = d\hat{S}_{ij} - dS_{ij}, \tag{3.9}$$

and computed the distance of condition j from the mean study condition as

$$d_{ij} = \sqrt{dS_{ij}^2 + d\hat{S}_{ij}^2}.$$

I will denote the estimate of the overall deviation from the ideal sensitivity line as the "fit parameter," and calculate it as

$$P_i^2 = 1 - \frac{\sum_{j=1}^{N_i} e_{ij}^2}{\sum_{j=1}^{N_i} d_{ij}^2}, \tag{3.10}$$

where P_i^2 is the fit parameter, and N_i is the number of conditions in study i. The fit parameter is similar to the Pearson Coefficient (r) but is geometrically different in

that it represents how well the conditions within a study are fit by the $\hat{S} = S$ line, not how well the conditions are mutually correlated. To permit comparisons, I also computed the Pearson Coefficient for each study (r_i), and calculated the slope of the linear least-squares fit to the $(S_{ij}, \hat{S}_{ij})$ data as:

$$\beta_{S,i} = \frac{\sum_{j=1}^{N_i} dS_{ij} \cdot d\hat{S}_{ij}}{\sum_{j=1}^{N_i} dS_{ij}^2}. \tag{3.11}$$

A within study fit in close agreement with the global fit would have $\beta_{S,i} \approx 1$.

3.3.4 Hypothesis Evaluation

To compare the efficiency of fast running versus walking and slow running in space suits, I segmented the suited subset of the data and performed a two-sample t-test. Although the run-walk transition in unsuited humans occurs near $Fr = 0.5$ even across different gravitational environments [Minetti, 2001], the effect of the space suit on the run-walk transition is not well understood. Because the Froude number is defined as a ratio of centripetal to gravitational acceleration, the condition $Fr \leq 1$ must be met during walking. Thus, running is guaranteed for $Fr > 1$.

Because it is theoretically possible to walk with $0.5 \leq Fr \leq 1$, I split the suited dataset into two groups using a categorical variable *suited-run*: fast running for $Fr > 1$ (*suited-run*$= 1$), and walking and slow running for $Fr \leq 1$ (*suited-run*$= 0$; in this analysis, I make no differentiation between loping and running, and refer to both under the category of running). Metabolic cost normalized by mass and gravity $M_{mg} = \dot{Q}_m/mg$ was used as a metric of efficiency per unit time (to avoid biases due to differing gravitational environments and masses), and specific resistance was used as a metric of efficiency per unit distance. Two-sample t-tests were then performed at the 0.95 level of significance to evaluate whether the means of M_{mg} and S differed between the two groups. A regression against the categorical variable *suited-run* was performed to evaluate further the significance and trend of any observed difference in

the means.

3.4 Results

Eighteen primary sources of locomotion energetics data were obtained from the literature: Table 3.1 lists these sources, segmented into suited studies (top 11 sources) and unsuited studies (bottom 8 sources), in chronological order of publication.

The source experiments included a variety of independent variables including velocity (11 studies), surface slope (5), type of space suit (5), gravity (4), type of reduced gravity simulator (4), load mass (3), suit pressure (3), test chamber altitude (1), and gender (1). These 18 sources represent 298 experimental conditions, of which 115 conditions involved space suits, and 183 conditions involved unsuited subjects and subjects carrying loads (weights, military gear, and/or chemical protective garments).

The mean number of subjects per study was 4.6 for suited studies, and approximately 10 for unsuited studies (in some studies not all conditions contained the same number of subjects, making the number of subjects per study approximate). The mean number of subjects per condition was 3.9 for suited studies and 9.6 for unsuited studies.

3.4.1 Validation of Digitizing Process

Average absolute percent position error for the set of 25 test coordinates was 0.2% and 0.1% for the abscissa and ordinate, respectively. The trend of position errors for each point in the set indicated a negative correlation with the order of digitization.

3.4.2 Energetics Data

Approximations used and exclusions made during data normalization are detailed in Table 3.2. After exclusion of 52 conditions, the dataset contained 100 suited and 146 unsuited conditions, or 246 total conditions. Of the 77 lunar gravity conditions, 62 were suited and 15 unsuited; there were 130 earth gravity conditions, 38 suited, and 92

Table 3.1: Primary Sources

Reference	Description*	Suit or Load†	Independent Variables‡	N§
[Streimer et al., 1964]	Treadmill locomotion	Three unk. suits	s, p	4
[Harrington et al., 1965]	Treadmill locomotion	Unk. ILC Dover Suit	v, a	4
[Wortz et al., 1967]	Treadmill locomotion	Gemini G2C	v, altitude	8
[Haaland, 1968]	Treadmill locomotion during simulated lunar mission	A5L, A6L, or A7L	v, a	2
[Robertson et al., 1968]	Partial gravity locomotion (4 dof inclined plane, 6 dof simulator)	A5L and RX-2 Suits	s, g, dof, p	6
[Annis & Webb, 1971]	Treadmill locomotion	Space Activity Suit	v, s	2
[Kubis et al., 1972]	Apollo 16 Time and motion study	A7LB Suit	v	2
[Johnston et al., 1975]¶	Apollo 14, 2nd Lunar EVA	A7L Suit	v, a	2
[Bishop et al., 1999]	Emergency Shuttle egress simulation	LES Suit	p	12
[Lee et al., 2001]	Emergency Shuttle egress simulation	LES & ACES Suits	s	4
[Wortz et al., 1966]	Partial gravity locomotion (4 dof & 5+ dof gimbaled system)	Unsuited	v, g, dof	8
[Sanborn, 1967]	Partial gravity locomotion (4 dof inclined plane, 4 dof & 6 dof gimbaled system)	Unsuited	v, dof	9-10
[Fox et al., 1975]	Partial gravity locomotion (2 dof slow rotation room & 4 dof inclined plane)	Unsuited	v, g, dof	2-4
[Webbon et al., 1981]	Treadmill liquid cooling garment tests	CPG	s	5
[Stauffer et al., 1987]	Load carrying at different velocities	Unsuited	v, m, gender	24
[Newman et al., 1994]	Partial gravity locomotion (water tank)	Unsuited	v, g	3-6
[Patton et al., 1995]	Load carrying during grade walking	Unsuited; CPG	a, m	14
[Santee et al., 2001]	Load carrying during grade walking	Unsuited	a, m	16

* Type of simulator for reduced gravity, if used, is indicated in parentheses (dof=degrees of freedom).

† Acronyms are standard space suit designators except CPG denotes Chemical Protective Gear.

‡ Independent variables in the original study: v=velocity, a=slope angle, s=suit, g=gravity, dof=simulator degrees of freedom, m=mass, p=suit pressure, others as noted.

§ Total number of subjects in each study; a range is given for studies in which different numbers of subjects participated in different experimental conditions.

¶ Data from each lunar surface astronaut were treated as a separate study because the Commander and Lunar Module Pilot experienced different conditions (paths, loads, and timing).

unsuited. The remaining 39 conditions represent unsuited locomotion at intermediate gravities (except four conditions in simulated 1/8g).

Figure 3-1 (upper left) shows that metabolic rates above 1000 W were seldom achieved; most metabolic rates above 500 W were achieved only in $1g$ conditions. Of the four variables examined ($\dot{Q}_m$, C, C_m, and S), mass-specific cost of transport C_m appeared to vary the least, for a given Froude number, across all conditions in the dataset; specific resistance data appeared to be segmented by gravity.

3.4.3 Regression Results

An initial regression of the type:

$$\hat{S}_i = \beta_{0,i} + \beta_{Fr} \cdot Fr + \beta_G \cdot G + \beta_p \cdot p + \beta_\alpha \cdot \alpha \tag{3.12}$$

yielded estimates

$$\{\bar{\beta}_0, \beta_{Fr}, \beta_G, \beta_p, \beta_\alpha\} = \{1.95, -0.518, -1.47, 0.193, 0.036\} \tag{3.13}$$

with

$$\bar{\beta}_0 = \sum_{i=1}^{N} \frac{\beta_{0,i}}{N}, \qquad N = 19. \tag{3.14}$$

All coefficients were significantly different from zero ($p < 0.0005$). The residual variance was 0.334 with standardized error 0.031. Insignificant factors, when added to the aforementioned regression) included the number of subjects ($p = 0.171$), the reduced gravity simulator degrees of freedom ($p = 0.267$), the suit mass ($p = 0.514$), the total mass transported ($p = 0.719$), the variable suit ($p = 0.743$), the load mass ($p = 0.904$), and the leg length (0.945). The only additional factor found to be significant was the velocity, ($p = 0.009$); addition of this term lowered the residual variance to 0.324 with standardized error 0.030, and increased the Fr p-value to 0.03. Replacing Fr with v alone ($p < 0.0005$ for all factors) yielded residual variance 0.328 with standardized error 0.031. Further results pertain to the initial regression

Table 3.2: Dataset Development

Reference	Study ID	Approximations*	Number of Conditions and Reason for Exclusion			
			Original	Excluded	Remaining	Reason
[Streimer et al., 1964]	1	Lh, body and suit mass	7	0	7	
[Harrington et al., 1965]	2	Lh	6	2	4	Zero velocity
[Wortz et al., 1967]	3	Lh, suit mass	4	0	4	
[Haaland, 1968]	4	Lh	6	0	6	
[Robertson et al., 1968]	5	Lh	42	10	32	Zero velocity
[Annis & Webb, 1971]	6	Lh	8	0	8	
[Kubis et al., 1972]	7	L	10	2	8	Unknown slope
[Johnston et al., 1975]	8	L	15	0	15	
	9	L	15	0	15	
[Bishop et al., 1999]	10	Lh, RQ	4	0	4	
[Lee et al., 2001]	11	Lh	2	1	1	Redundant data†
[Wortz et al., 1966]	12	Lh	28	14	14	Zero velocity
[Sanborn, 1967]	13	Lh	8	0	8	
[Fox et al., 1975]	14	Lh, RQ, subject and helmet mass	27	0	0	
[Webbon et al., 1981]	15	L, suit mass	2	0	2	
[Stauffer et al., 1987]	16	Lh, RQ	55	18	37	Redundant data‡
[Newman et al., 1994]	17	Lh, RQ	20	5	15	Zero velocity
[Patton et al., 1995]	18	Lh, RQ	9	0	9	
[Santee et al., 2001]	19	Lh, RQ	30	0	30	

* Approximations made in order to compute normalized quantities: Lh indicates leg length estimated as height / 1.85; L indicates assumed leg length; RQ indicates respiratory quotient.

† One of two conditions in this study was previously reported in [Bishop et al., 1999].

‡ Second measurements at low-velocity conditions were made immediately after high-velocity measurements and were dramatically different than low-velocity measurements made earlier in the trial.

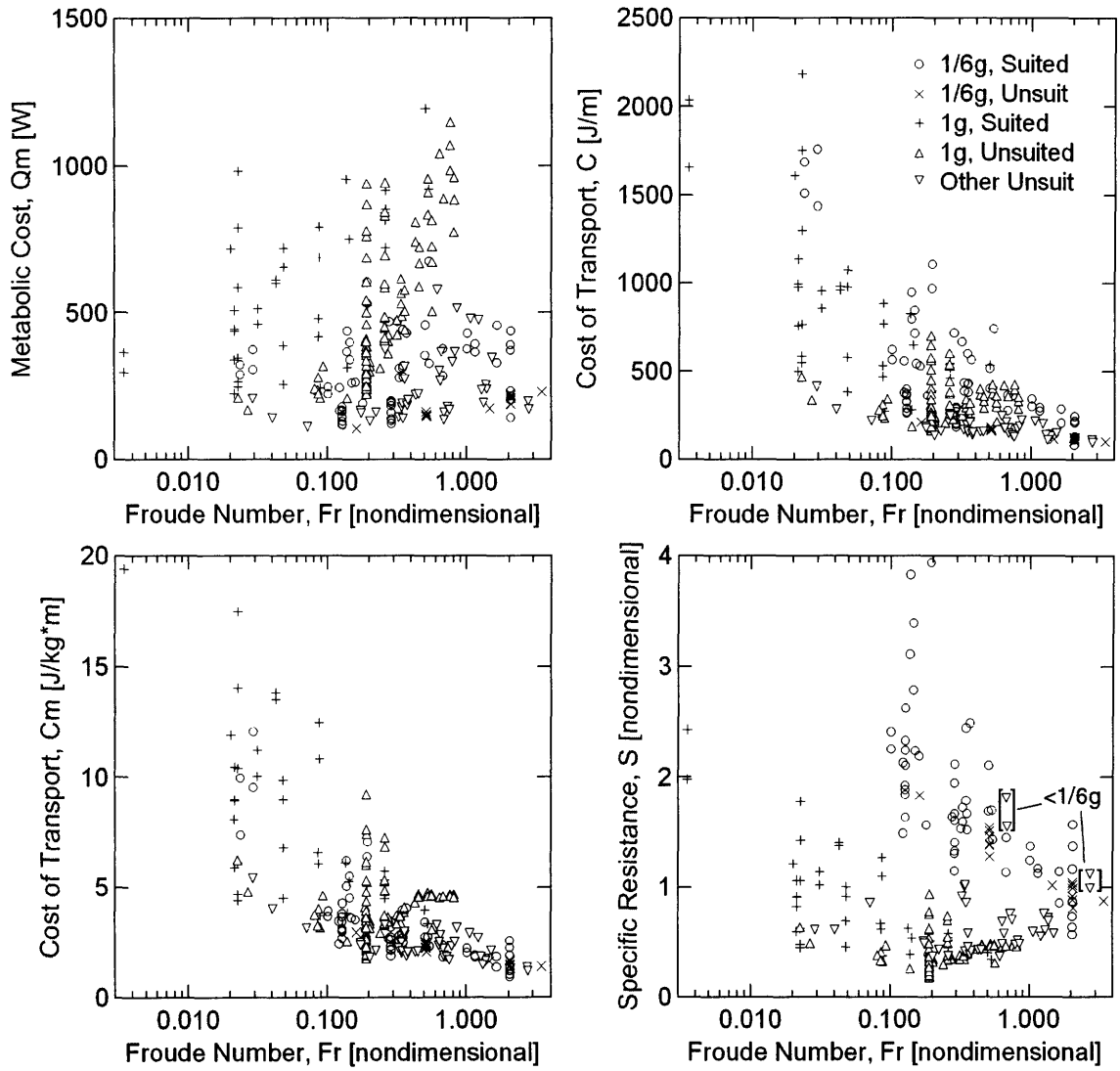

Figure 3-1: Metrics as a function of Froude Number: Metabolic cost (upper left), Cost of Transport (upper right), Mass-Specific Cost of Transport (lower left), and Specific Resistance (lower right). Other indicates a gravitational environment between earth equivalent ($1g$) and lunar equivalent ($1/6g$), except for four points in a $< 1/6g$ environment (indicated, lower right).

(without v as a factor).

The distribution of the random intercept $\beta_{0,i}$ is plotted in Figure 3-2 (upper left), and a one-sample t-test of the residuals was performed to identify outliers (Figure 3-2, upper right). Many of the large residuals were associated with small Froude numbers (Figure 3-2, lower left); when residuals were plotted versus study identifier (Figure 3-2, lower right) it was noted that most of the largest residuals (including all five positive outliers) were attributable to data from Apollo 14 [Johnston et al., 1975]. Examination of these residuals revealed that several of the Apollo 14 conditions included un-modeled masses or activity, as described in Table 3.3. After removal of these conditions, as indicated in Table 3.3, the linear regression procedure was repeated, giving:

$$\{\bar{\beta}_0, \beta_{Fr}, \beta_G, \beta_p, \beta_\alpha\} = \{1.64, -0.339, -1.16, 0.160, 0.024\}. \tag{3.15}$$

Once again, all coefficients were significant ($p < 0.0005$). The residual variance decreased 82% to 0.059 with a standardized error of 0.006. The distribution of the random intercept $\beta_{0,i}$ is plotted in Figure 3-3 (upper left), and appears less like a normal distribution than in the initial regression. The specific resistance values calculated from the source data is plotted, in Figure 3-3 (upper right), against S estimated from the regression model. A reference line of unity slope is shown for comparison; the DOF-corrected multiple R^2 was 0.83. Figure 3-3 (bottom) shows the residuals as a function of Froude number (left) and study identifier (right). The variance of $suit = 1$ residuals was approximately 3.8 times the variance of $suit = 0$ residuals ($p < 0.0005$).

A similar regression model with v instead of Fr produced residual variance 0.064; v was found to be significant ($p < 0.015$) when added to the original model, but the residual variance was unchanged.

An analysis of the within-study sensitivity (Figure 3-4) indicates a high level of variability in the level of fit of the regression equation for the data within each study; the poorest fit occurred for data from study 16 [Stauffer et al., 1987], which had

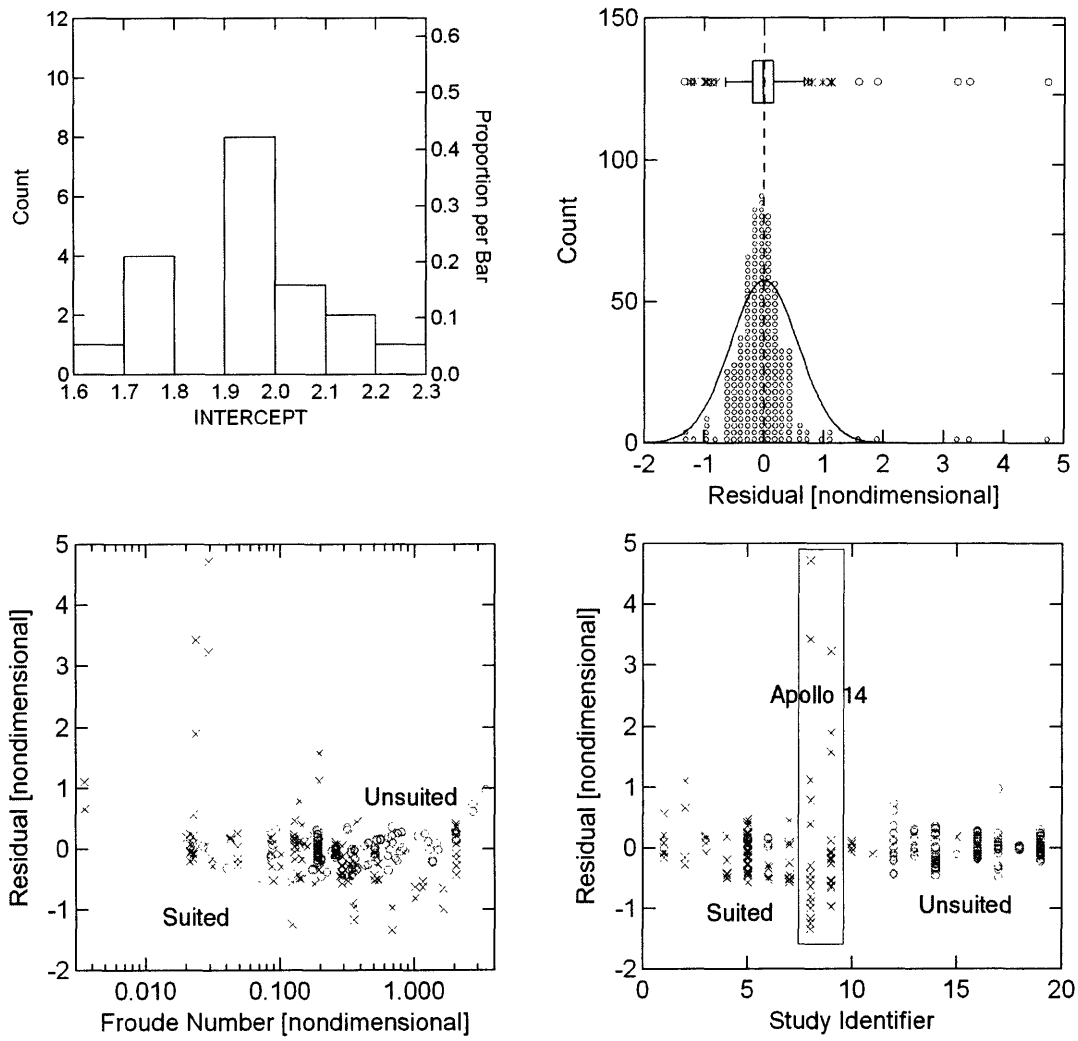

Figure 3-2: Results from the initial regression: Distribution of intercepts (upper left); Outlier identification (upper right); Many high residuals are associated with low Froude numbers (lower left); Many of the high residuals are associated with a particular study: the Apollo 14 extravehicular activity data (lower right, in box). Symbols × and ○ represent suited and unsuited conditions, respectively, in the lower left and lower right plots.

Table 3.3: Residual Analysis of Initial Regression

Reference	Study ID	Residual*	Explanation or Notes†	Excluded?
[Johnston et al., 1975]	8	4.73	Traverse from ALSEP site included geology activities.	Yes
	8	3.43	Traverse to ALSEP site: First time hauling heavily loaded (unmodeled) MET.	Yes
	9	3.23	Traverse from ALSEP site included geology activities.	Yes
	9	1.90	Traverse to ALSEP site: ALSEP modules attached to carry-bar vibrated, disrupting movement.	Yes
	9	1.58	Control problems with MET, including overturning; uphill grade.	Yes
	8	1.12	Control problems with MET, including overturning; uphill grade.	Yes
	8	0.78	CDR hauling MET up steepest part of traverse (α=11.3).	Yes
	8	0.39	CDR lifts back of MET to assist LMP in pulling of MET up slope and over obstacles.	Yes
[Harrington et al., 1965]	2	1.11	Lowest velocity (v=0.4 m/s) condition in 1g space suit trial.	No
[Newman et al., 1994]	17	0.96	Highest velocity (v=2.3 m/s) condition in underwater 1/6g unsuited trial.	No

* Included are the greatest magnitude positive residuals, indicated by ○ or * in Figure II (upper left), and other conditions from [Johnston et al., 1975] that included un-modeled masses or activity.

† ALSEP = Apollo Lunar Surface Experiments Package; CDR=Commander; LMP=Lunar Module Pilot; MET = Mobile Equipment Transporter, a (completely un-modeled) hand-pulled cart used to transport tools and rock samples. For in-depth details of the Apollo 14 mission, see [Jones, 2000].

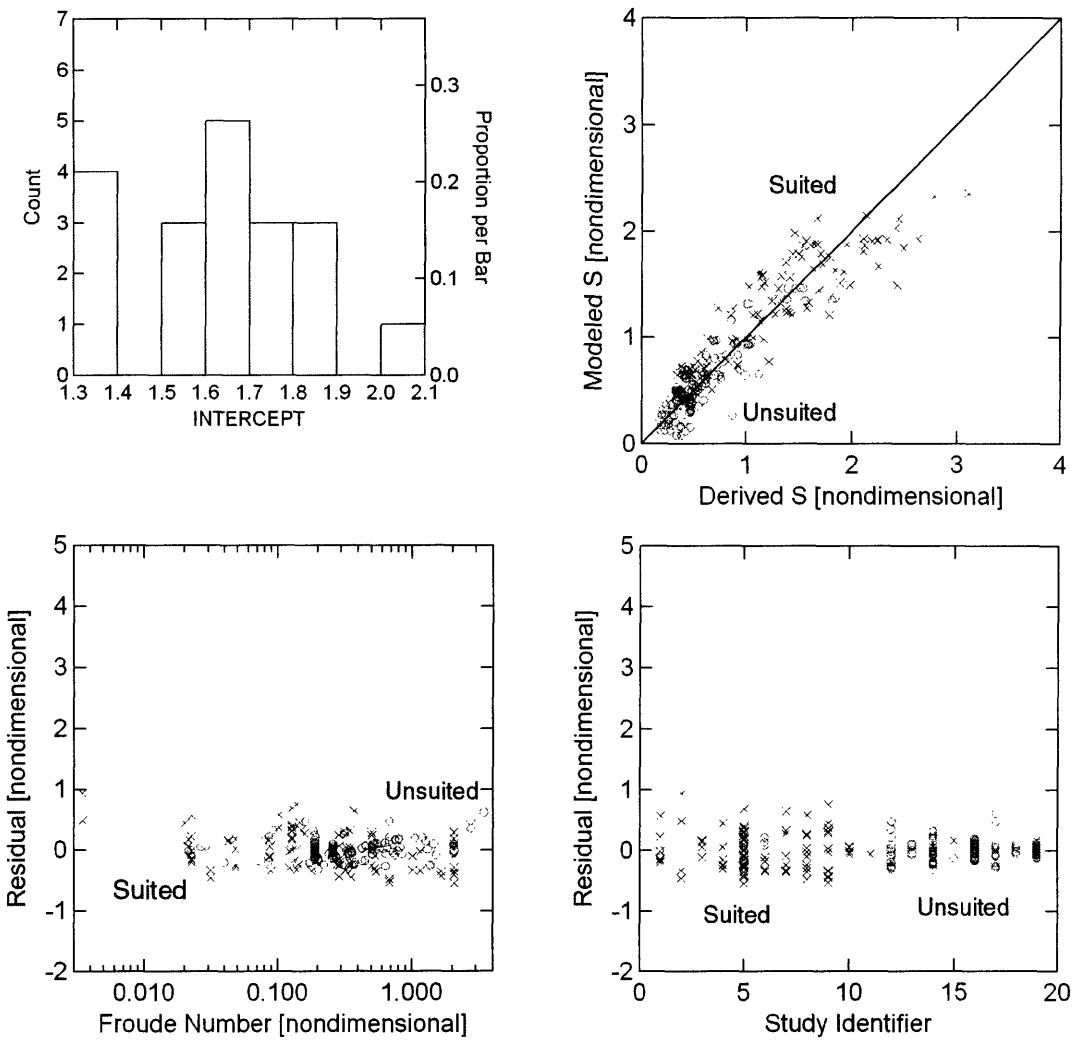

Figure 3-3: Results from the final regression: Distribution of intercepts (upper left); Specific resistance (S) from regression model versus derived from historical data, compared to a reference line of unitary slope (upper right); Residuals vs. Froude number (lower left); Residuals vs. Study ID (lower right). Symbols × and ○ represent suited and unsuited conditions, respectively.

sensitivity $\beta_{S,16} = -1.04$: this study focused on $1g$ load-carrying near and across the run-walk transition. Two studies of space suit locomotion in $1g$ (study IDs 6 and 10) had the highest sensitivities ($\beta_{S,6} = 1.62$,$\beta_{S,10} = 1.95$), and one of these (study 6) represented the only study of energetics in a mechanical counter-pressure space suit [Annis and Webb, 1971]; in these cases only, an increase in the specific resistance computed using the regression equation would tend to overestimate the actual increase in the specific resistance. Several studies (study IDs 2, 3, 4, 7, 15) had near-zero sensitivities; all of these studies except 15 included velocity as an independent variable during space suit locomotion, and all were in $1g$ except study 7. The two conditions of study 15 represented walking unsuited and walking with a slight-positive-pressure chemical protective garment in $1g$. Two studies of unsuited partial-gravity locomotion had sensitivities near unity ($\beta_{S,13} = 1.01$, $\beta_{S,14} = 0.97$). The remainder of the studies (1, 5, 8, 9, 12, 17, 18, 19) had sensitivities ranging between 0.38 and 0.79.

3.4.4 Hypothesis Testing

With removal of the eight conditions in Table 3.3, the suited datasets for M_{mg} and S (plotted in Figure 3-5, top) included 92 records, 14 with $Fr > 1$ and 78 with $Fr \leq 1$.

For M_{mg}, the two groups were not found to have difference variances ($p = 0.977$) and the means of the two groups were not significantly different in a pooled-variance t-test ($p = 0.134$, Figure 3-5, lower left). However, a regression on M_{mg}, performed with *suited-run* and a random intercept as the only factors, found both factors to be significant ($p < 0.0005$), with $\bar{\beta}_0 = 0.941$, $\beta_{suited-run} = 0.724$, and a residual variance and error of 0.112 and 0.021, respectively.

For S, the two groups were found to have difference variances ($p = 0.004$), and the means of the two groups were significantly different in a separate-variance t-test ($p < 0.0005$, Figure 3-5, lower right). A regression found both factors to be significant ($p < 0.0005$), with $\bar{\beta}_0 = 1.53$, $\beta_{suited-run} = -0.752$, and a residual variance and error of 0.233 and 0.043, respectively.

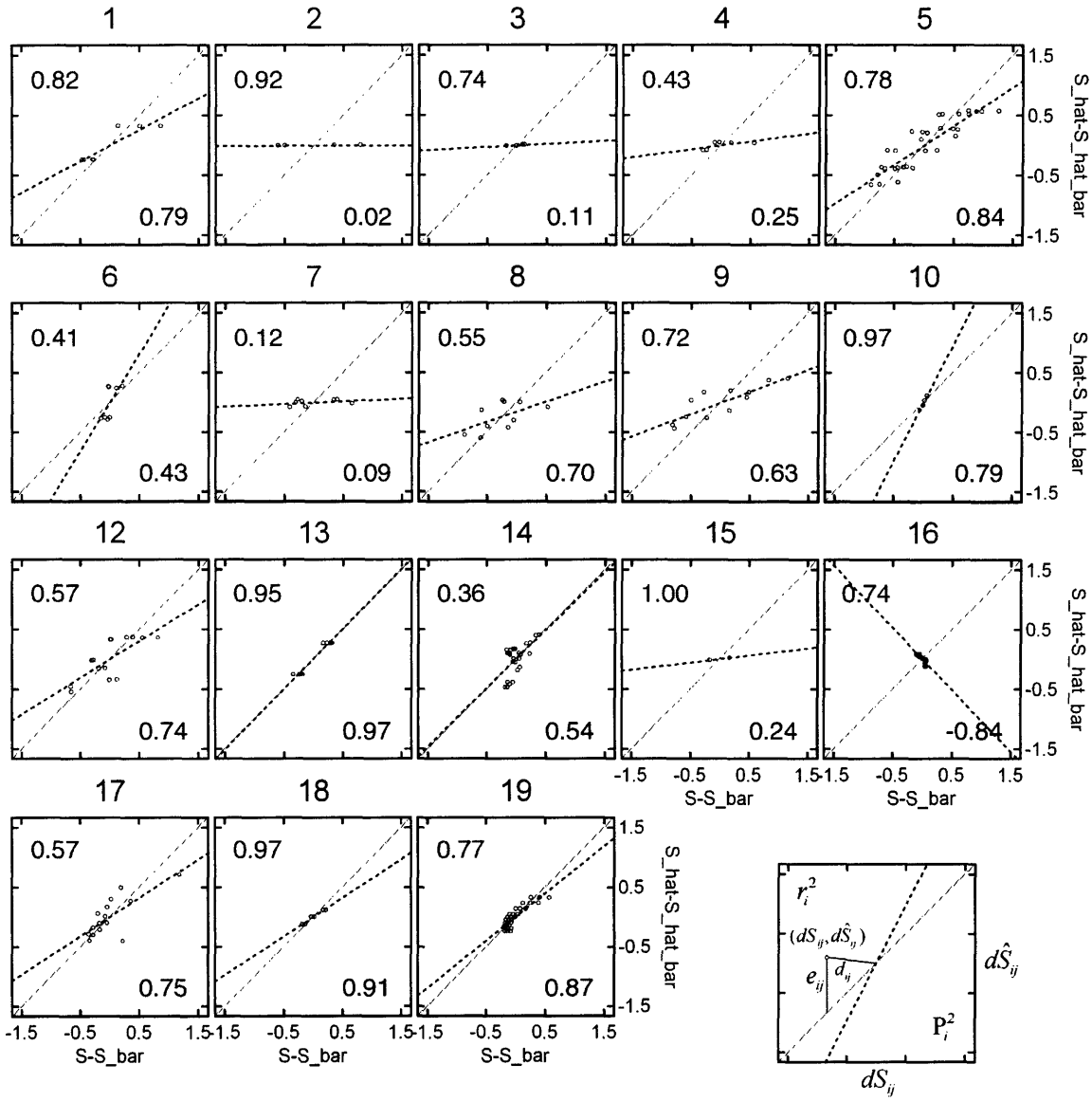

Figure 3-4: Within study sensitivity analysis: The number above each $d\hat{S}_i$ vs. dS_i plot is the study identifier. A reference line with unity slope indicates the ideal relationship between dS_i and $d\hat{S}_i$. The inset illustrates the geometry associated with the fit parameter P_i, shown in the lower-right corner of each plot. The square of the Pearson Coefficient r_i is shown in the upper left corner of each plot. The dotted line indicates the slope of the linear least-squares fit to the $(dS_{ij}, d\hat{S}_{ij})$ data within each study. Study 11 is excluded from the plot as this study included only one condition and, as a consequence, has undefined slope; because each study was permitted a random intercept, study 11 has $P_{11}^2 = 1$.

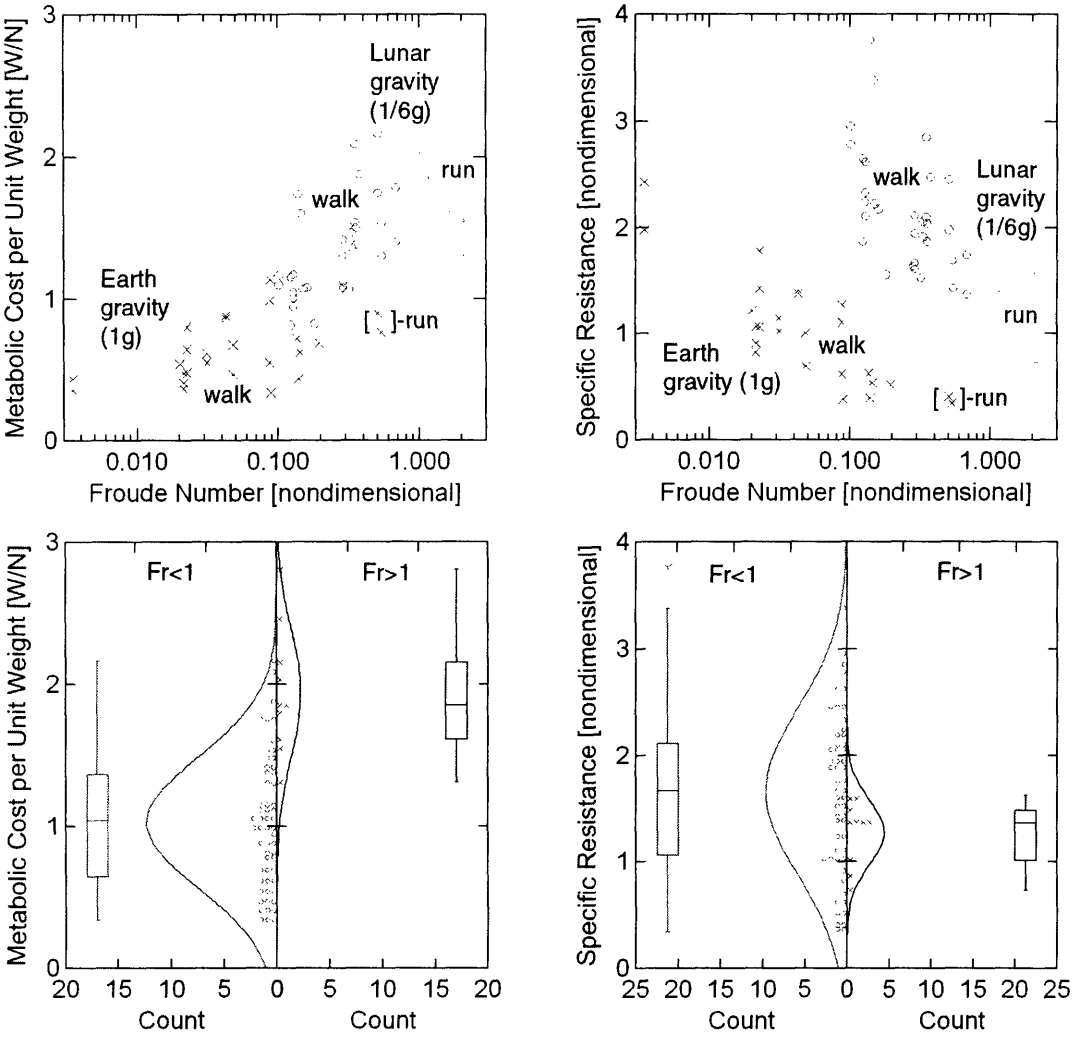

Figure 3-5: Hypothesis evaluation: Metabolic efficiency per unit time was based on the metabolic cost normalized by gravity and mass: dataset (upper left), two-sample t-test (lower left); Metabolic efficiency per unit distance was based on specific resistance: dataset (upper right), two-sample t-test (lower right). In the upper plots, symbol $\times$ identifies Earth-gravity conditions, $\circ$ identifies lunar gravity conditions with $Fr < 1$, and $+$ identifies lunar gravity conditions with $Fr > 1$. In the lower plots, symbols $\times$ and $\circ$ represent conditions with $Fr < 1$ and $Fr > 1$, respectively.

3.5 Discussion

I have intentionally based this analysis on an extremely diverse but comprehensive group of sources, and the results should be interpreted in that context. The sources selected were limited to those studies for which the data required for non-dimensionalization were available; many of the unsuited studies were selected out of convenience, and many other unsuited studies are available in the published literature. The study by Wickman and Luna [1996] on load carrying in reduced gravity is noticeably absent from the list of sources; this study was excluded partly because data on subject height and mass were not available. Wickman and Luna [1996] reported that heart rate, a relatively accurate predictor of metabolic rate over long but not short time frames, was occasionally used in place of suspect oxygen consumption data; I did not identify which energetics data was derived from which source, and consequently chose to exclude this source. Additional studies from the pre-Apollo era, often published in the form of NASA contractor reports or company-internal technical documents, remain to be analyzed. Additional metabolic data from Apollo is available, but has limited accuracy, and cannot readily be transformed because many of the relevant independent variables would need to be derived from multiple sources; doing so might compound errors inherent in the source data by introducing additional errors during the process of data normalization.

3.5.1 Sources of Error

Contributions to error in the analysis may originate from several sources: errors in digitizing of source data, errors in the source data itself, and assumptions made during data normalization. Digitizing errors were low, and the trend of errors associated with the order of points digitized was attributed to learning; digitizing can safely be excluded as a significant source of error and will not be discussed further.

One of the largest errors in the source data is likely to arise from the variety of approaches used to simulate reduced gravity. Fluctuations in the constant force required to simulate reduced gravity in a cable suspension system have been limited to

under 18% (% error at 3/8g) in a passive steel-spring-based system [Wu, 1999], under 16% (% error at 3/8g, 0.06g in general) in a passive rubber-tube based system [Griffin et al., 1999], 5% in one 10 m latex-hose-spring-based system [Davis and Cavanagh, 1993], or 2.2% to 10% in a system based on closed-loop control using a pneumatic actuator [Ray, 1993]. While the vertical force error can be substantial, the mean vertical force is unlikely to differ from the desired constant force by more than a few percent.

Another source of error is the uniform treatment of metabolic cost data originally estimated using a variety of methods. For example, estimates of metabolic cost from Apollo were based upon a thermoregulation model that included as inputs the oxygen tank pressure drop, an estimate of suit atmospheric leakage, heat removed by the liquid cooling garment, and the heart rate [Waligora, 1976]. Apollo metabolic cost estimates are likely to be accurate to within 5% to 10% [Waligora, 1976]. Most of the source studies relied upon measurements of inspired and expired oxygen (or of oxygen and carbon dioxide) to compute metabolic cost, but differing methods within this group of studies may introduce errors. For example, the technique of measuring oxygen consumption used by Harrington et al. [1965] "was thought to give values 8% lower than those obtained by standard [1966] spirometry techniques."[Roth, 1966] One study [Haaland, 1968] utilized heart rates in conjunction with a oxygen consumption vs. heart rate calibration procedure, in order to estimate metabolic rates during an 18-day simulation of a lunar mission.

A third source of error is the set of assumptions made in data normalization: the two most widely used approximations in this analysis were estimation of leg length as height/1.85, and assumption of the respiration quotient, RQ.

To evaluate the validity of the leg length assumption, I compared values derived using this estimation procedure to values derived using anthropometric data from NASA's Man-Systems Integration Standard [NASA, 1995] for men and women, from 5th, 50th, and 95th height percentiles. Because leg height data was not available, leg height was estimated as the mean of crotch height and weight height. This leg height estimate was compared to the estimate obtained by dividing the 5th, 50th, and 95th

percentile heights by 1.85. The average percent error of the height/1.85 procedure was 1.62%; the optimal divisor given this limited set of anthropometric data would have been approximately 1.875, for which the average percent error was 1.60%. Mohanty et al. [2001] developed a regression equation ($r = 0.84$) relating leg length to height in 505 South Indian Women; the height/1.85 procedure estimate differed on average by only 2.9% from the Mohanty et al. [2001] regression line, illustrating the relative accuracy of a simple approach to leg length estimation even in a population quite different from the population of locomotion energetics subjects.

It is widely known that an RQ of 0.7 corresponds to fat metabolism, while an RQ of 1.0 corresponds to carbohydrate metabolism. The actual RQ is dependent upon diet, which determines what energy sources are available, and exertion level, which is a major determinant of what food sources are actively being used. Moderate exercise may typically correspond to an RQ of about 0.85, while RQ near 1.0 may be achieved during intense exercise near conditions of maximum oxygen uptake. The value I assigned to unknown respiration quotients, 0.87, is the value used by NASA to estimate metabolic rate from oxygen consumption during on-orbit extravehicular activities [Snow, 2000](p. 7.1-11). Under a situation of intense exercise ($RQ \sim 1.0$), assigning $RQ = 0.87$ would under-predict energy utilization by 2.7%, while under "average conditions" ($RQ = 0.81$, an unlikely lower bound of activity for conditions in locomotion energetics studies), assigning $RQ = 0.87$ would over-predict energy utilization by 1.3%.

It appears that these assumptions used in data normalization probably contributed no more to overall error than may have been contributed by the variations in equipment and methods used by the authors of the primary sources. With that assurance, one can now interpret the results.

3.5.2 Energetics Data

Figure 3-1 illustrates the general trend of decreasing C, C_m , and S as a function of increasing Froude number. While running in $1g$ has a higher mass-specific cost of transport than walking, Farley and McMahon [1992] found that below $\approx 0.5g$ run-

ning has a lower cost of transport than walking.[1] In $1g$ locomotion, C_m decreases to a minimum near $Fr \approx 0.25$ [Minetti, 2001], then rises again as the walking speed increases to near $Fr \approx 0.5$; above the run-walk transition, C_m is approximately constant, independent of Fr, at least for moderate velocities. Margaria [1976] illustrates this relationship in a plot of C_m vs. velocity (p. 98) with an approximately quadratic curve for velocities below the run-walk transition and a horizontal line for velocities above the run-walk transition. I have plotted S vs. $\sqrt{Fr}$ in Figure 3-6 to demonstrate that the dataset of unsuited locomotion shows a similar pattern in $1g$, but not in reduced gravity: in $\leq 3/8g$ it appears that S declines in a monotonic fashion with increasing Froude number. The minima in specific resistance for $1g$ to $0.5g$ is consistent with the high-percent recovery observed by Griffin et al. [1999] at $1g$, $0.75g$, and $0.5g$; the disappearance of this minimum is consistent with the reduction in percent recovery observed by Griffin et al. [1999] at $0.25g$.

Because the work done on the spacesuit by the occupant is likely to increase with velocity due to increases in joint movement, suited S values not too distant from the unsuited S values at higher Froude numbers imply that an energy saving mechanism may help reduce the cost of transport at these velocities.

Videos of Apollo astronauts attempting to recover tools from the lunar surface show them jumping and landing on one leg, in order to compress their space suit knee joint and permit them to reach the surface with their gloves [Jones, 2004]. The relative difficulty in performing this act visually illustrates the substantial spring-back forces resulting from pressure-volume work done during knee flexion. Schmidt et al. [2001] have quantified the knee torques as a function of joint angle for the training version of the current NASA space suit, the class III Extravehicular Mobility Unity (EMU); these angle-dependent torques may function like a spring in parallel with each leg, reducing the cost of transport by reducing the loads borne by the body and transforming energy from kinetic to potential and back to kinetic energy during the rebound phase of running.

[1] Farley and McMahon [1992] reported cost of transport based on net metabolic cost, excluding basal metabolism.

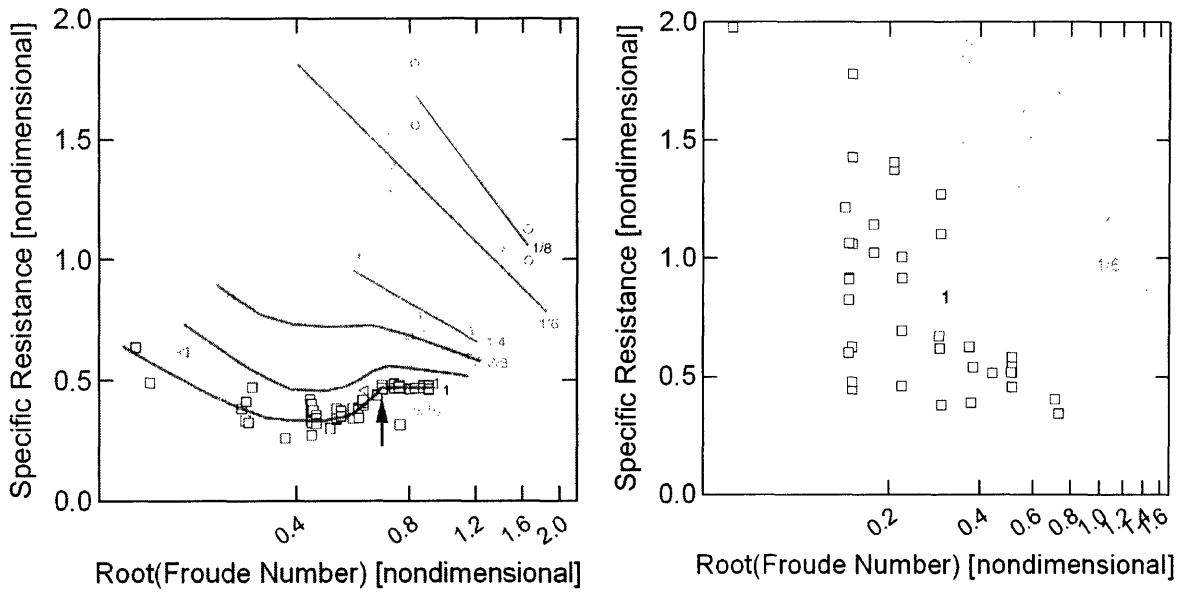

Figure 3-6: Interpretation of the effect of reduced gravity on the specific resistance during unsuited level locomotion (left). Numbers indicate the earth-relative gravitational acceleration (real or simulated) and each g-condition has a unique symbol. A logarithmic scale has been used for the abscissa to expand the low Fr range. In $1g$, specific resistance of level unsuited walking decreases as walking speed approaches $\sqrt{Fr} \approx \sqrt{0.25} \approx 0.5$, and increases as walking speed increases up to the run-walk transition (indicated by the arrow); above $\sqrt{Fr} \approx \sqrt{0.5} \approx 0.7$ the plateau associated with running is visible. There is no evidence, in this limited dataset, of a similar increase in specific resistance near $Fr = 0.5$ in moderately reduced gravity environments ($\leq 3/8g$). Unsuited conditions (left) appear to provide a lower bound to the specific resistance observed in suited conditions (right), with the suited specific resistance trending toward the unsuited specific resistance at higher Froude numbers.

3.5.3 Regression Analysis

The random intercept term of the initial regression appears to be approximately normally distributed (Figure 3-3, upper left), thereby supporting the implicit assumption that studies constitute random samples. The residuals also appear to be approximately normally distributed. As might be expected from the lower number of suited subjects per condition and the variations in space suit hardware, variance of the residuals for $suit = 1$ conditions was much higher than for $suit = 0$ conditions. For these two groups, the ratios of the standard deviation to the root of the mean number of subjects per condition differed by only 24%; this suggests that the difference in the variance of the residuals between the two groups was largely due to the reduced number of subjects in the $suit = 1$ conditions.

The high residual variance of the initial regression analysis is explained by the outlier residuals attributable almost entirely to un-modeled geologic activity and load-carriage during the Apollo 14 lunar extravehicular activities. Field geology activities were some of the most energy intensive activities performed on the lunar surface [Johnston et al., 1975], and field geology activities occurring during a time period book-kept as a traverse would tend to reduce the mean velocity (or Froude number) and increase the metabolic cost substantially. This is entirely consistent with the conditions that produced two of the three largest residuals (Table 3.3). Transportation of the Apollo Lunar Surface Experiments Package (ALSEP) or the Mobile Equipment Transporter (MET) created a weight distribution rather different than during other space-suited locomotion; in addition, much of the excess weight may have been borne by the astronaut and not supported in part by the space suit; inexperience with these loads or the space suit (ALSEP deployment occurred during the 1st EVA of the Apollo 14 mission) may also have contributed to the high residuals. Fatigue and control difficulties may also have played a role. For example, the lunar module pilot carried two ALSEP modules to the ALSEP deployment site (Table 3.3, 4th line) on a carry bar that he eventually cradled over his elbow joints during elbow flexion; he reported that the carry bar "was bouncing and flexing. It was throwing me totally

off stride. It had a natural frequency of vibration that was not a natural frequency of my movements. It was just kind of flopping around and throwing me totally off balance."[Jones, 2004] Control problems with the MET occurred frequently, with many near-tip-overs.

What is perhaps as interesting as the high residuals identified in the Apollo 14 data are the types of factors that were not found to be significant in the regression: Non-dimensionalization of the metabolic cost is likely to be responsible for the insignificance of factors such as the total mass, suit mass, and load mass. While velocity was found to be significant, it seemed more prudent to perform the second regression after elimination of the outliers than to change the baseline regression factors; in addition, I wanted the regression to include as few dimensional factors as possible.

The large drop in the residual variance in the second regression confirmed that the residual outliers were responsible for the large residual variance in the initial regression. The distribution of the random intercept appears less like a normal distribution than before. The plot of derived specific resistance (S) vs. modeled specific resistance ($\hat{S}$) (Figure 3-3, upper right) shows that across all studies, the regression model provides a good fit to the observed specific resistance data, with no large obvious discrepancies between suited and unsuited data. While velocity was found to be a significant factor in the second regression, the stated criteria for acceptance of additional factors included not only significance, but also a reduction in the residual variance; as the residual variance remained unchanged when v was added as a factor, the final regression equation includes as factors only Fr, G, p, and α.

In an analysis across such different studies, one would expect the within-study sensitivity to vary much more than the across study sensitivity; indeed this is what Figure 3-4 shows. The poorest within-study fit is for the only study (16) which unambiguously traces out the $1g$ run-walk transition, as discussed in the section entitled Cost of Transport and illustrated in Figure 3-6. The increase in S as the Froude number increases (whereas $\hat{S}$ decreases because $\beta_{Fr} = -0.34$) is responsible for the negative slope ($\beta_{S,16} = -1.04$) and very low fit parameter ($P_{16}^2 = -0.84$).

At a different extreme, the high sensitivity observed for study 6 [Annis and Webb, 1971] may result from the low-space suit torques of a mechanical counter pressure suit relative to a typical gas pressure space suit with the same effective internal pressure.

Wickman and Luna [1996] performed multiple regression modeling of energetics data and achieved an R^2 of 0.82; the current model achieves a similar level of fit across a much more diverse set of data, permits scale independent comparisons through the use of non-dimensional parameters, incorporates the impact of space suit pressure and surface slope, and does not require the use of two separate regression equations for walking and running (at least, not in gravitational environments of $\leq 3/8g$). Wickman and Luna [1996] reported non-zero coefficients for leg length and body mass in her regression equation for mass-specific metabolic cost ($M_m = \dot{Q}_m/m$); in the regression equation for specific resistance ($S = M_m/gv$) I found neither of these factors to be significant. However, the spread observed in the sensitivity analysis for some studies (for example, see Figure 3-4, study identifier 19, a study of unsuited locomotion with independent variables of grade and load [Santee et al., 2001]), suggests that load does affect the specific resistance.

The regression equation, while providing a good fit between studies, does not always provide a good fit within studies. Many improvements to the regression equation are possible, including the evaluation of interaction terms and transformation of factors into more appropriate forms. For example, addition of the interaction term $Fr \times p$ results in all $p < 0.0005$ with residual variance 0.052 and $\beta_{Fr \times p} = -0.108$, suggesting that at higher Froude numbers space suit pressurization may help to reduce the specific resistance; this may be indicative of the hypothesized space-suit leg-spring mechanism. One possibility to developing an improved regression equation would be to normalize and adapt the load-carrying model developed by Santee et al. [2001].

3.5.4 Hypothesis Evaluation

Metabolic rate normalized by weight (M_{mg}) seems an appropriate metric for efficiency per unit time of locomotion, if one seeks to compare locomotion across different gravity

levels. While the t-test suggested that the means of the $Fr > 1$ and $Fr < 1$ suited locomotion groups were not different, the regression is likely to be a more reliable indicator of the difference between these two groups: Therefore, fast running is more expensive per unit time than walking or slow running. However, the lack of data for $Fr > 1$ in $1g$ limits the generality of this comparison.

The suited specific resistance ($S = M_{mg}/v$) data showed a clear trend downward within a given gravitational environment; the hypothesis test and regression both support the conclusion that fast running in space suits is more efficient per unit distance than walking or slow running. A similar comparison cannot be performed between these two groups within $1g$ because no $1g$ data with $Fr > 1$ exists; however, comparisons between these groups within $1/6g$ would support the same conclusion but at a higher level of significance.

3.5.5 Summary and Conclusions

In this study, I investigated how space suits modify the metabolic cost of locomotion by transforming data from a wide variety of unsuited and suited energetics studies into a common format and performing multiple regression analysis. My conclusions fall into three categories: those concerned with the transformed metabolic cost data, the regression analysis, and the evidence that supports the hypothesis that space suits may act as springs during running.

A major finding of this study is the confirmation that fast running ($Fr > 1$) is less efficient per unit time but more efficient per unit distance than walking or slow running ($Fr < 1$) in space suits. This has broad implications for extravehicular activity including for the development of any distance-to-safe-haven rules and the planning of traverses. Another important finding was that the increase in specific resistance with Froude number, observed in $1g$ below the run-walk transition, is not observed in moderately reduced gravity ($\leq 3/8g$). In addition, the suited specific resistance approaches the unsuited specific resistance in many cases, and especially at higher Froude numbers.

An important result of the regression analysis is that variations in the specific

resistance across the analyzed studies can be explained largely by a simple linear regression model with only four parameters: Froude number, surface grade, earth-relative gravity level, and a derived factor called the pressure product, which is the only parameter of these four that captures any impact of the space suit on locomotion. The within-study analysis highlights the areas in which the regression model is weak: capturing the increase in specific resistance below the run-walk transition in gravities near $1g$, capturing the changes in S observed with different loads, and capturing only with poor sensitivity the within-study changes in specific resistance for several of the space suit studies.

A finding hinted at, but not demonstrated, by the data, is that the legs of the space suit may act as springs during running, reducing the specific resistance that would otherwise be required for locomotion. Several observations support this hypothesis: First, subjects moving in a space suit do work on the space suit while counteracting suit joint-torques, and at higher velocities, subjects increase their joint movement in proportion to the velocity. If the work done on the space suit increases as the Froude number increases, but the specific resistance decreases, some other energy saving mechanism must exist. Second, suited specific resistance can approach the unsuited specific resistance, particularly as the Froude number increases; this suggests than an energy saving mechanism exists that can make up for the energy cost of doing work on the space suit, which is not present in unsuited locomotion. Third, the negative coefficient of the interaction term $Fr \times p$ suggests that at higher Froude numbers space suit pressurization may help to reduce the specific resistance. Fourth, clear evidence exists of the large spring-back forces that can be exerted by space suit legs, both from videos of astronauts on the lunar surface, and from direct measurements of knee torques. The extent to which the legs of gas pressure suits act as springs during running has yet to be determined, but a better understanding of this phenomenon would have important implications for the cost of transport in both gas pressure and mechanical counter-pressure space suits.

Acknowledgments

This work was supported in part by USRA/NIAC contract 070605-003-006.

Chapter 4

Exoskeleton Characterization: A lower-body exoskeleton for simulation of space-suited locomotion

Abstract

In a previous historical analysis of suited and unsuited locomotion energetics (Chapter 3), I found evidence that space suits act as springs during running. Video images of Apollo astronauts on the lunar surface suggest that knee torques create, in large part, this spring effect. I hypothesized that a lower-body exoskeleton, properly constructed, could be used to simulate the knee torques of a range of space suits. Here I report characterization of a lower body exoskeleton. Equivalent spring stiffness of each exoskeleton leg varies as a function of exoskeleton knee angle and load, and the exoskeleton joint torque relationship closely matches the current NASA spacesuit, or Extravehicular Mobility Unit, knee torques in form and in magnitude. I have built a physical nonlinear spring, and demonstrated that this spring achieves space suit-like joint torques; therefore space suit legs act as springs, with this effect most pronounced

when locomotion requires large changes in knee flexion such as during running.

4.1 Introduction

Space suit development for future human planetary exploration requires an improved understanding of how space suits affect the kinematics, dynamics, and energetics of locomotion. In a previous analysis of historical data from suited and unsuited locomotion energetics studies (Chapter 3), I found evidence that space-suited running is more efficient per unit distance than space suited walking; this and other evidence suggests that space suits may act as springs during running, improving cost of transport relative to walking. Video images of astronauts locomoting on the lunar surface suggest that knee torques create, in large part, this spring effect(for example, see Apollo 16, 146:49:41 in Jones [2005]).

I hypothesized that if space suit knee joints act like springs in parallel with the legs, then springs in parallel with the legs could be used to simulate space suit knee joints. Here I report the characterization of a lower body exoskeleton with two spring-like legs.

4.2 Methods

I built a lower body exoskeleton consisting of a webbing-based harness (designed for acrobatics), three-degree-of-freedom hip joints, two spring-like exoskeleton legs, and two modified cycling shoes. I added a load-transfer cage to transfer exoskeleton hip torques from one side to the other, largely in order to ensure subject comfort. I then calibrated two representative exoskeleton legs in order to measure their stiffness and deformation as a function of leg geometry and applied load. From this calibration data I derived knee flexion and joint-torque estimates, and compared these estimates to knee joint-torque data from a space suit, the Extravehicular Mobility Unit (EMU) [Schmidt, 2001].

4.2.1 Exoskeleton Construction

Figure 4-1(A) shows a subject wearing the exoskeleton. A custom hip joint attached to the harness (Swivel Harness, Climbing Sutra, Las Vegas, NV) provides two rotational degrees of freedom: a bearing provides free rotation of the exoskeleton hip joint in (approximately) the sagittal plane; rotation can also occur around a pin joint attached to the bearing. The hip adapter at the top of each exoskeleton leg provides a third rotational degree of freedom. Together, these three degrees of freedom provide relatively complete hip mobility.

The cycling shoes (SH-M 038, Shimano, Osaka, Japan) contain a high-stiffness sole; to create a load path fully independent from the human leg, a spring steel plate with a pin joint adapter was attached to the bottom of each shoe taking advantage of the pedal-clip mounting hardware. Because this plate was attached after cutting away any interfering soft portion of the outer shoe sole, subjects can walk in the modified shoes without contacting the metal plate on the ground.

An exoskeleton leg, shown in two views in Figure 4-1(B), includes pin joint adapters at the hip and ankle joint, a friction-lock knee joint, and fiberglass bars that connect each knee joint to the pin joint adapters. For a given subject, the knee joint is set to a specific exoskeleton knee angle ϕ, chosen to ensure geometric compatibility with subject leg length and harness positioning, and locked in place. Compression of the exoskeleton leg deforms the fiberglass bars; the bending moments of the fiberglass bars (springs) result in spring-back forces.

The springs were machined from unidirectional fiberglass bar stock (GC-67-UB, Gordon Composites, Montrose, CO, USA) in thicknesses of 6.35 mm (0.250 in), 3.18 mm (0.125 in), and 1.57 mm (0.062 in). The thickest springs were intended to be the primary working springs of the exoskeleton, whereas the thinner springs were selected to provide control conditions: the thinnest spring was intended to be used to simulate the exoskeleton restrictions of motion but not to provide any appreciable spring forces. The intermediate thickness spring, I considered, might provide spring forces adequate to self-support the exoskeleton harness and load transfer cage.

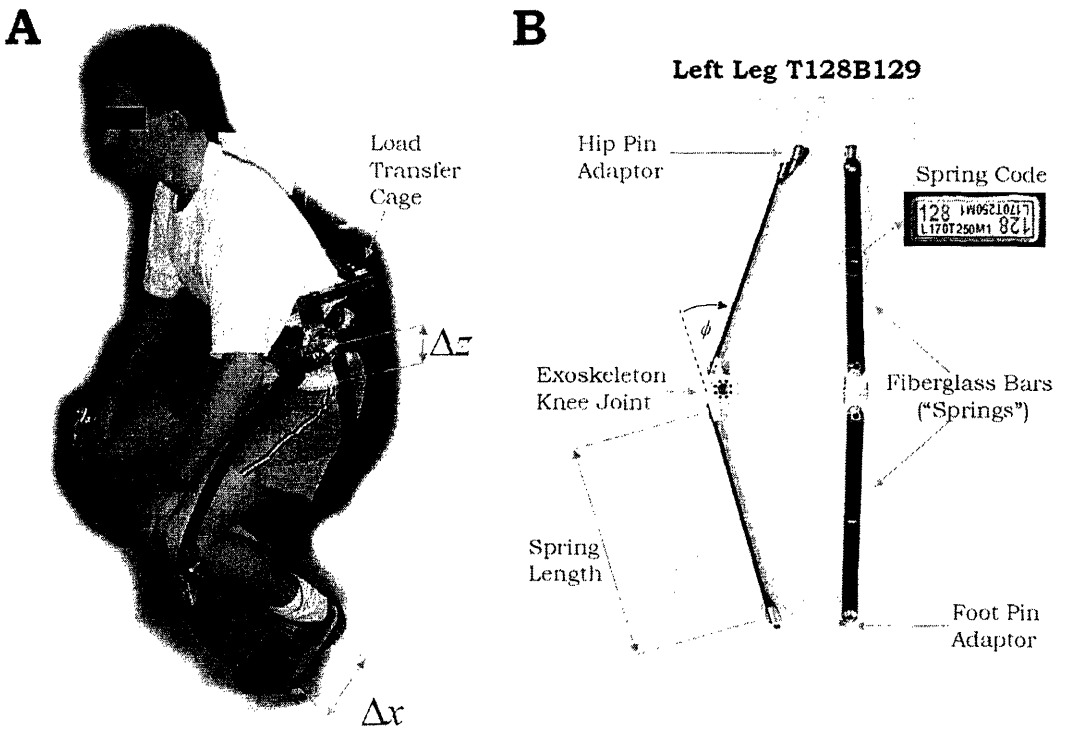

Figure 4-1: **A.** Subject crouching while wearing lower-body exoskeleton. The distance from the exoskeleton hip pin to the greater trochanter, the vertical offset Δz, represents the offset between the center of rotation of the exoskeleton hip and the center of rotation of the human leg. The distance from the exoskeleton foot pin to the axis of the lower leg, the forward offset Δx, represents the moment arm of the net ground reaction force at the center of pressure relative to the lower leg axis. These anthropometric measurements, along with others, are used to determine exoskeleton sizing and to perform joint-torque estimation. **B.** An exoskeleton leg is characterized as TxxxByyy where the xxx and yyy represent the three-digit spring codes, assigned during manufacturing, for the two fiberglass bars in a particular leg (the longer spring code LaaaTbbbMc specifies spring length aaa in tenths of inches, spring thickness bbb in thousandths of inches, and the order of manufacturing c). Given springs of a particular length, exoskeleton knee joint flexion angle ϕ can be adjusted to accommodate subjects with varying leg length; I set ϕ to achieve a zero-torque exoskeleton leg height compatible with normal standing posture for each subject, and then locked the exoskeleton leg knee joint in place.

Springs lengths of 49.5 cm (19.5 in.) and 43.2 cm (17.0 in.) were chosen to accommodate tall and short subjects, respectively. Because exoskeleton knee angle was expected to dramatically affect exoskeleton leg stiffness, these spring lengths were chosen to maintain exoskeleton knee angles within the range of 20-50°.

4.2.2 Exoskeleton Leg Calibration

The apparatus used to calibrate exoskeleton legs (Figure 4-2(A)) allows the stiffness of each exoskeleton leg to be systematically determined by varying the exoskeleton knee angle and the applied load. Exoskeleton leg stiffness can be computed from the change in height due to a change in the applied load. While I use height and load data to estimate the equivalent knee joint torques, I use a frequency-based method to estimate the stiffness.

By modeling the exoskeleton leg as a second-order system (Figure 4-2(B)) one can estimate stiffness by measuring the frequency of vertical oscillations resulting from an arbitrary vertical displacement d. The differential equation of the undriven system is given by

$$m\ddot{y} + b\dot{y} + ky = 0, \tag{4.1}$$

where each dot represents a time derivative, and $y(t)$ is the vertical oscillation of the hip pin as a function of time, t. Using the initial conditions $y(0) = d$ and $\dot{y}(0) = 0$, $Y(s)$, the Laplace transform of $y(t)$, is given by

$$Y(s) = \frac{mds + bd}{ms^2 + bs + k} = \frac{ds + bd/m}{s^2 + (b/m)s + (k/m)}. \tag{4.2}$$

Because the exoskeleton leg system oscillates, the characteristic equation $s^2 + (b/m)s + (k/m)$ has complex conjugate roots such that $(b/m)^2 < 4(k/m)$. Therefore the roots are given by

$$\lambda = \sigma \pm j\omega, \tag{4.3}$$

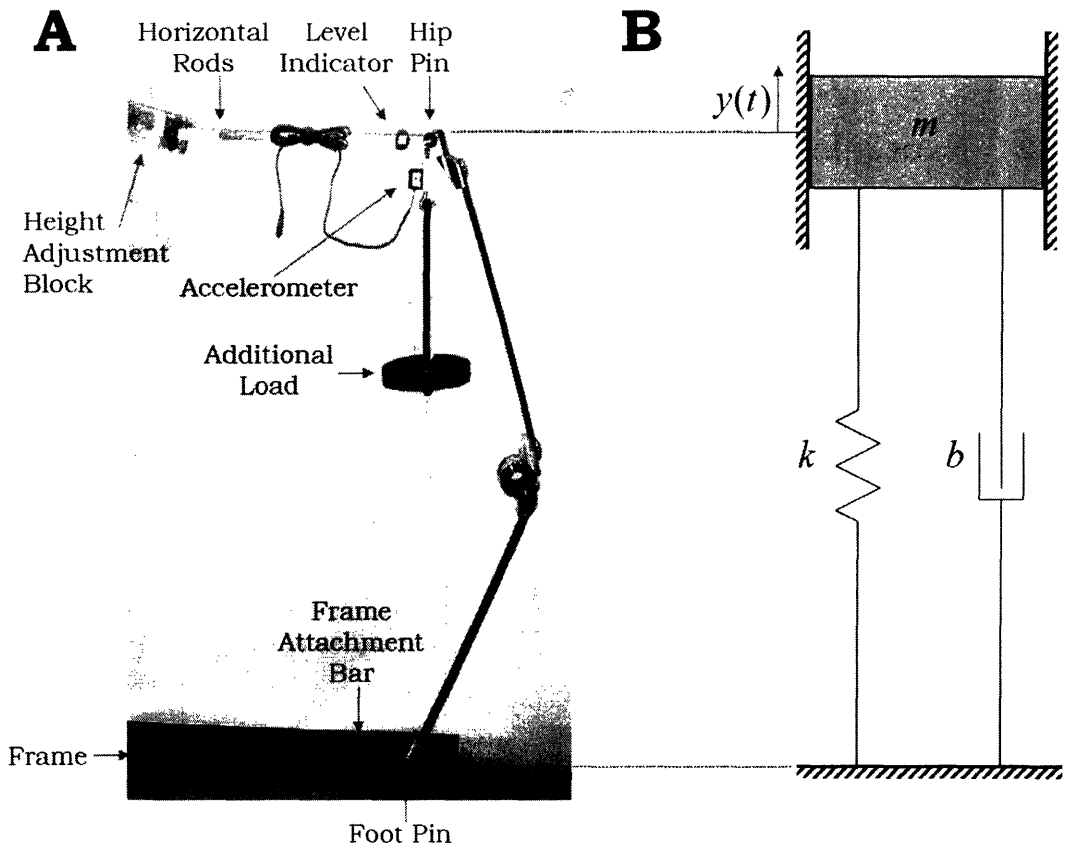

Figure 4-2: **A.** Experimental apparatus used to determine stiffness of exoskeleton legs. The height adjustment block and the frame attachment bars are both rigidly attached to a large immobile frame. The long horizontal rods constrain hip pin motion to approximately the vertical axis for small amplitude oscillations. For each load tested, height of the exoskeleton leg is read from the level indicator, and small oscillations around the equilibrium point are induced by adding a small amount of energy to the system by displacing the additional load downward. Oscillations are measured using the accelerometer. **B.** Model of exoskeleton leg used to estimate stiffness k and damping parameter b as a function of the total mass m, which is the sum of the spring self mass and the mass of the relevant experimental apparatus elements, including the additional load.

with

$$\sigma = -\frac{b}{2m} \tag{4.4}$$

and

$$\omega^2 = \frac{k}{m} - \sigma^2. \tag{4.5}$$

I computed the Fast Fourier Transform (FFT) of the vertical accelerations measured by the accelerometer, and estimated ω as $2\pi f$, where f was the frequency of the FFT power spectrum peak.

The envelope of the accelerometer data can be used to determine the damping of the system: The real component of the roots, σ, can be estimated as the negative reciprocal of the time constant of the envelope

$$E(t) = E_0 \cdot e^{-t/\tau} = E_0 \cdot e^{\sigma t}. \tag{4.6}$$

Here, $E(t)$ is the envelope of the acceleration data (determined from sampling the magnitude of low-pass filtered acceleration data at points where the derivative is near zero), E_0 is the best-fit magnitude, and $\tau = -1/\sigma$ is the best-fit time-constant.

I estimated cycle to cycle energy recovery of an exoskeleton leg as:

$$\eta = e^{-1/(\tau \cdot f)}, \tag{4.7}$$

where η is the ratio of energy stored in the exoskeleton leg to the energy stored in the exoskeleton leg in the previous cycle.

By defining ω_n as the natural frequency, Equation 4.5 can be rewritten as:

$$\omega_n{}^2 = \frac{k}{m} \tag{4.8}$$

with

$$\omega_n{}^2 = \omega^2 + \sigma^2. \tag{4.9}$$

To determine stiffness using Equation 4.8 one must determine the components of the total mass m, which are given by

$$m = m_{self} + m_{apparatus} + m_{load}, \tag{4.10}$$

where m_{self} is the spring self-mass, $m_{apparatus}$ is the mass of the experimental apparatus supported by the exoskeleton leg, and m_{load} is the additional load mass. I controlled m_{load} and estimated $m_{apparatus}$ as half the mass of the two simply-supported horizontal rods plus the mass of other apparatus components supported by the exoskeleton leg.

Define m_0 as the total mass with zero additional load, and consider measuring the frequency and damping under conditions of zero load and with a small load of Δm. If stiffness is assumed to be equal in both cases (true in the limit $\Delta m \rightarrow 0$, or if stiffness is independent of load), one can write two equations in the two unknowns m_0 and k, as given by

$$\omega_{n,0}^2 = \frac{k}{m_0}, \tag{4.11}$$

and

$$\omega_{n,\Delta}^2 = \frac{k}{m_0 + \Delta m}, \tag{4.12}$$

where $\omega_{n,0}$ and $\omega_{n,\Delta}$ are the natural frequencies in the two conditions as estimated using Equation 4.9. Solving equations 11 and 12 gives

$$m_0 = \frac{\omega_{n,0}^2}{\omega_{n,0}^2 - \omega_{n,\Delta}^2} \cdot \Delta m, \tag{4.13}$$

and

$$k = \omega_{n,0}^2 \cdot m_0 = \omega_{n,\Delta}^2 \cdot (m_0 + \Delta m). \tag{4.14}$$

For each exoskeleton knee angle tested, I made five measurements of the self mass $m_{self} = m_0 - m_{apparatus}$, using $\Delta m = 0.45$ kg (1.0 lb). I also compared the measured

self mass to that predicted for a cantilevered beam, which for a uniform beam with mass m_{actual} is given by

$$m_{self} = \frac{33}{140} m_{actual}. \tag{4.15}$$

At exoskeleton angles near 180°, the exoskeleton leg, if actually uniform in cross-section and stiffness, would approximate such a beam. At exoskeleton angles approaching zero, most of the self-mass load is carried in compression, and the pure bending force F_{bend} is given by

$$F_{bend} = m_{self} \cdot g_{effective}, \tag{4.16}$$

where

$$g_{effective} = g \cdot sin(\phi/2), \tag{4.17}$$

with gravitational acceleration g. Therefore $m_{self} \rightarrow \infty$ as $\phi \rightarrow 0$, and the uniform beam approximation for the exoskeleton self mass is given by

$$m_{self,beam} = \frac{33}{140} m_{actual} \cdot \frac{1}{sin(\phi/2)}. \tag{4.18}$$

For small ϕ, the exoskeleton leg will start behaving more and more like a rod, for which the resonant frequency-stiffness relationship is given by

$$\omega_n^2 = \frac{k}{m/\pi^2}. \tag{4.19}$$

The theoretical contribution to the estimated self-mass due to this rod-like behavior is therefore

$$m_{self,rod} = \frac{1}{\pi^2} m_{actual} \cdot \frac{1}{cos(\phi/2)}. \tag{4.20}$$

with the total theoretical self-mass given by

$$m_{self} = \frac{33}{140} m_{actual} \cdot \frac{1}{sin(\phi/2)} + \frac{1}{\pi^2} m_{actual} \cdot \frac{1}{cos(\phi/2)}. \tag{4.21}$$

I computed m_{actual} as the sum of all the components of a given exoskeleton leg.

For measurements under load conditions other than $\Delta m = 0.45kg$ I took the self mass as the mean m_{self} under the $\Delta m = 0.45kg$ condition at the same exoskeleton knee angle. Other load masses used, as allowed by the experimental apparatus for a given exoskeleton leg, were $0.91kg$ $(2.0lb)$, $1.81kg$ $(4.0lb)$, $2.72kg$ $(6.0lb)$, $3.63kg$ $(8.0lb)$, $5kg$, $7kg$, $10kg$, and $12kg$. For these load masses three measurements were made. For all measurements, I estimated the stiffness using the above procedure.

I also compared the stiffness at zero load to the theoretical stiffness at zero load computed from standard beam theory. The deflection in the pure bending direction produced by the bending force F_{bend} is given by

$$d_{bend} = \frac{L^3}{3EI} \cdot F_{bend}, \tag{4.22}$$

where L is the equivalent beam length of the exoskeleton leg, E is the flexural modulus ($35.2GPa$ to $37.9GPa$), and I is the moment of inertia of the beam cross section. For the thickest fiberglass bars, bar width $w = 3.175cm$ $(1.25in)$, thickness $t = 0.635cm$ $(0.250in)$, and the moment of inertia $I = wt^3/12$. I took L as the total length of the two fiberglass bar segments in a given exoskeleton leg that are not restrained from bending by the end adapters, and measured this distance to be equal to

$$L = 2(S - 4.48cm), \tag{4.23}$$

where S is the spring length as shown in Figure 1(B). The bending deflection results in a smaller downward deflection d_{down} as given by

$$d_{down} = d_{bend} \cdot \frac{1}{sin(\phi/2)}. \tag{4.24}$$

The theoretical stiffness at zero load ($m_{load} = 0$) is defined as the ratio of upward

force δF theoretically generated for an infinitesimal downward deflection δd_{down}. As related in the theoretical self mass computation, the bending force is related to the upward force by

$$F_{bend} = F \cdot sin(\phi/2). \tag{4.25}$$

Equations 4.22-4.25 can be solved to give the stiffness contribution $k_{exo-beam}$ due to the exoskeleton leg acting as a beam:

$$k_{exo-beam} = \frac{\delta F}{\delta d_{down}} = \frac{3EI}{L^3} \cdot \frac{1}{sin^2(\phi/2)}. \tag{4.26}$$

From the standard equation for rod stiffness one can similarly derive that the stiffness contribution $k_{exo-rod}$ due to the exoskeleton leg acting as a rod is given by

$$k_{exo-rod} = \frac{E_{rod}tw}{L} \cdot \frac{1}{cos^2(\phi/2)}, \tag{4.27}$$

with compressive modulus $37.2 \leq E_{rod} \leq 40.7GPa$. The spring-steel foot-plate also bends in response to the applied load, acting as a standard cantilevered beam. The effective stiffness of the foot-plate k_{fp} is given by

$$k_{fp} = \frac{3E_{fp}I_{fp}}{L_{fp}^3}, \tag{4.28}$$

where the spring-steel bending modulus $E_{fp} \approx 207GPa$, the moment arm of the load $L_{fp} \approx 5cm$, and $I_{fp} = w_{fp}t_{fp}^3/12$ with foot plate width $w_{fp} \approx 3.6cm$ and foot plate thickness $t_{fp} \approx 1.59mm$ $(0.0625in)$. The total theoretical stiffness at zero-load k_{theory} is given by

$$\frac{1}{k_{theory}} = \frac{1}{k_{exo-beam}} + \frac{1}{k_{exo-rod}} + \frac{1}{k_{fp}}. \tag{4.29}$$

4.2.3 Estimation of Knee Flexion and Joint Torques

Figure 4-3 shows the geometrical relationships between a compressed exoskeleton leg and the leg of the subject. From these relationships one can derive the knee torque T

that results from a exoskeleton spring-back force F. This spring-back force is given by $F = mg$, and because m is systematically varied and exoskeleton leg height h measured during exoskeleton leg calibration, the spring-back force $F(h)$ is known.

The leg length L can be expressed in terms of the exoskeleton leg height as

$$L^2 = (h - \Delta z)^2 + \Delta x^2. \tag{4.30}$$

The leg length expressed in terms of the knee flexion angle θ is given by

$$L^2 = L_1^2 + L_2^2 - 2L_1L_2cos(\pi - \theta). \tag{4.31}$$

Knee flexion angle θ can be computed as a function of h by computing L using Equation 4.30, and computing θ, from Equation 4.31, as

$$\theta = \pi - cos\left(\frac{L_1^2 + L_2^2 - L^2}{2L_1L_2}\right). \tag{4.32}$$

The knee torque moment arm r is given by

$$r = L_2cos\left(\frac{\pi}{2} - \alpha - \beta\right) - \Delta x \tag{4.33}$$

where

$$\alpha = sin^{-1}\left[\frac{L_1}{L}sin(\pi - \theta)\right], \tag{4.34}$$

and

$$\beta = sin^{-1}\left(\frac{\Delta x}{L}\right). \tag{4.35}$$

The knee torque vector $\mathbf{T}$ is therefore given by

$$\boldsymbol{T} = -\boldsymbol{r} \times \boldsymbol{F} \tag{4.36}$$

where the moment arm vector $\boldsymbol{r}$ and force vector $\boldsymbol{F}$ have the directions given in Figure 4-3. This sign convention ensures that the direction of positive equivalent

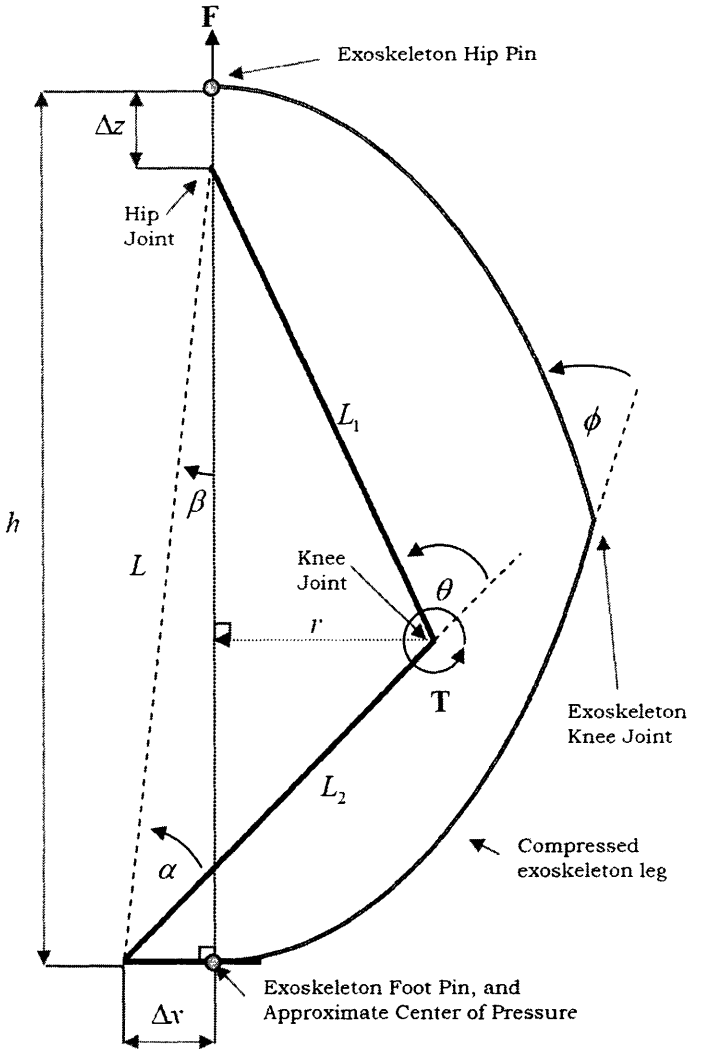

Figure 4-3: Geometry for computing knee joint-torque equivalent of exoskeleton spring force $\boldsymbol{F}$. All variables are described in the text.

torque T is consistent with the direction of positive knee flexion angles. Schmidt et al. [2001] used an opposite sign for her reported EMU knee torques; I modified the sign of her data to be consistent with this sign convention when comparing the two data sets.

While L_1+L_2, $L_2/(L_1+L_2)$, Δx, and Δz are subject specific quantities, I derived joint torques by assuming the value of $L_1 + L_2$ that leads to geometric compatibility for a given exoskeleton knee flexion angle, and using representative values for $L_2/(L_1+L_2)$, Δx, and Δz. I took $\Delta x = 12.7cm$, the average of the Δx values for the two pairs of exoskeleton shoes (European sizes 39 and 47) to be used by subjects. I took $\Delta z = 7.5cm$, a typical value based on exoskeleton fitting data from eight subjects. The ratio $L_2/(L_1 + L_2)$ represents knee height relative to leg length, which I took as 0.58, the ratio of the population mean knee height to population mean leg length for males [NASA, 1995].

I computed the stiffness of an exoskeleton leg as a function of the exoskeleton knee flexion angle relative to the EMU, and computed the goodness of fit after scaling the exoskeleton torque data by this relative stiffness. I performed the relative stiffness computation on 'fitted' knee flexion angles θ_{fit} given by

$$\theta_{fit} = \theta + \theta_Z, \tag{4.37}$$

where θ_Z is an angle offset that ensures that the exoskeleton-derived knee flexion angle of zero-torque coincides with the EMU-derived knee flexion angle of zero torque.

Using the joint-torque method to estimate θ as a function of h I also computed the cycle to cycle energy recovery η as a function of θ and normalized leg length $L/(L_1 + L_2)$.

4.3 Results

4.3.1 Exoskeleton Leg Calibration

Only exoskeleton legs with the $6.35mm$ $(0.250in)$ thick fiberglass bars were able to be calibrated; exoskeleton legs with lower-thickness bars had insufficient stiffness for the calibration apparatus and range of calibration masses available. Using the thick fiberglass bars, two exoskeleton legs with differing bar lengths were calibrated: Leg T130B131, with $43.2cm$ $(17in)$ bar lengths, and leg T110B111, with $49.5cm$ $(19.5in)$ bar lengths.

Each exoskeleton leg generally behaved as a second-order spring-damper system (Figure 4-4). At $\phi = 20°$, frequency measurements were infrequently impaired by contact between the calibration masses and the exoskeleton leg. At loads near $10kg$ to $12kg$, large oscillations were observed, in conjunction with side-to-side swaying of the calibration masses.

At zero additional load, stiffness estimates computed assuming no damping are lower than with-damping stiffness estimates by 12% to 29% ($380N/m$ to $590N/m$). At non-zero additional loads, no-damping stiffness estimates are consistently slightly lower than with-damping stiffness estimates, differing by only 0.01% to 3% ($0.5N/m$ to $25N/m$), with a mean difference of only 0.15% ($3N/m$); this difference grows consistently in magnitude as calibration mass increases (while holding the exoskeleton angle constant).

The actual self-mass measurements appear to agree with the theoretical predictions except for low exoskeleton knee flexion angles (Figure 4-5(A)). In contrast, stiffness results agree with theoretical predictions for low exoskeleton angles but not for high exoskeleton angles. The relative contributions from the beam and rod modes of the exoskeleton leg are quite different: the ratio of mean (for a given condition) stiffness values $\bar{k}_{exo-beam}/\bar{k}_{exo-rod}$ is typically less than 0.02%. In contrast, the ratio of mean stiffness values $\bar{k}_{fp}/\bar{k}_{exo-beam}$ is on the order of $2-4\%$.

Stiffness is a strong negative function of both exoskeleton knee angle ϕ and additional load m_{load} (Figure 4-6). The relationship between stiffness and load for a

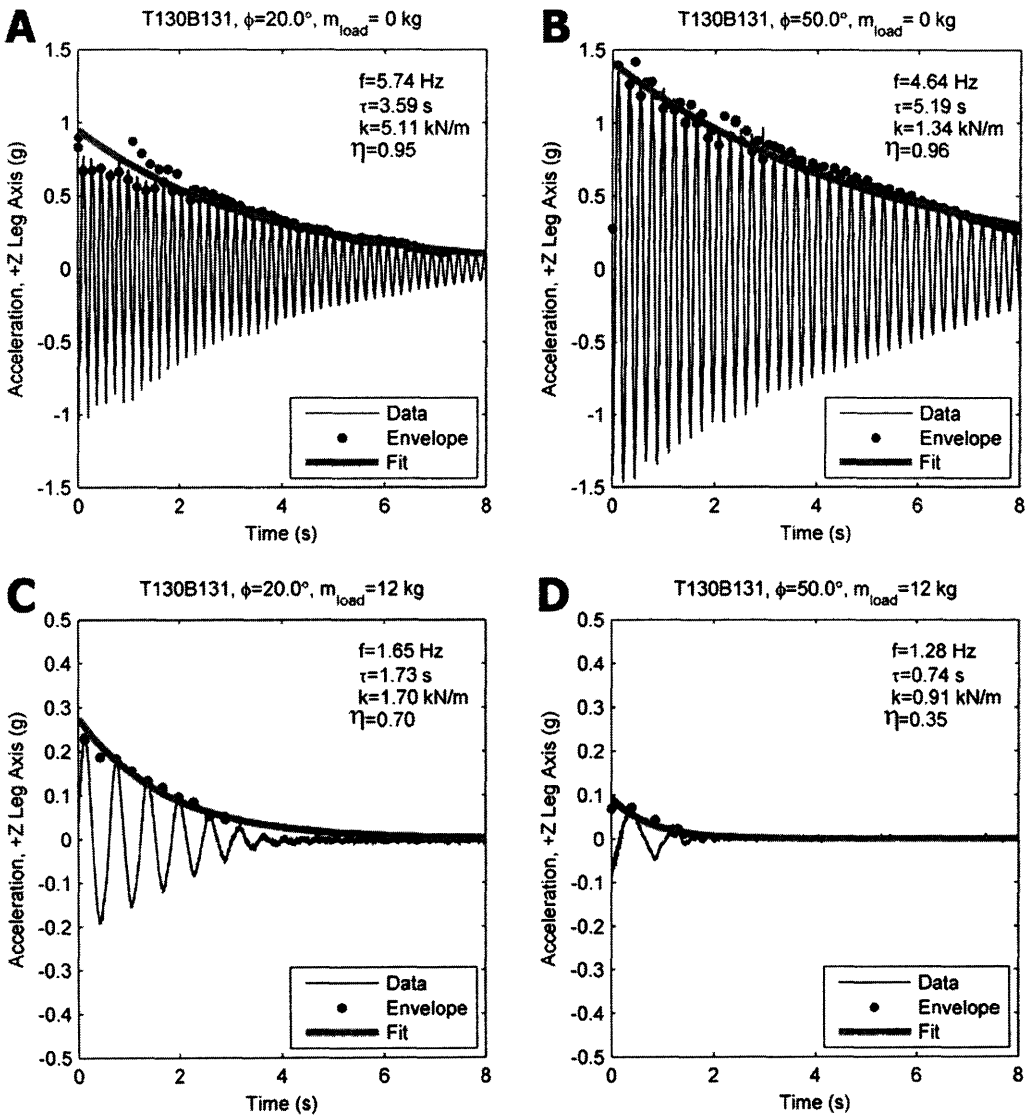

Figure 4-4: Calibration data from leg T130B131 (17.0" fiberglass bars) at the extrema calibration conditions for exoskeleton knee angle ($20° \leq \phi \leq 50°$) and load ($0kg \leq m_{load} \leq 12kg$). Inset within each plot are the oscillation frequency f, exponential time constant τ, and energy recovery η. **A.** Small angle, small load condition. **B.** Large angle, small load condition. **C.** Small angle, large load condition. **D.** Large angle, large load condition.

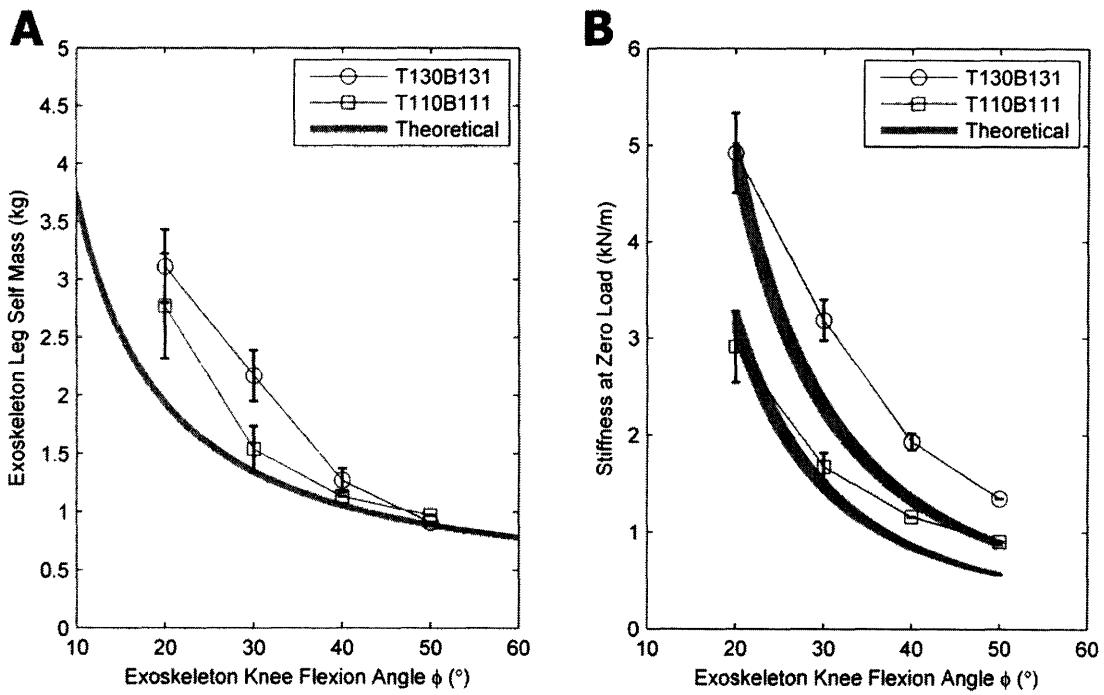

Figure 4-5: Exoskeleton leg calibration results compared to theoretical approximations. T130B131 is an exoskeleton leg with 43.2 cm (17 in) fiberglass bars, and T110B111 is an exoskeleton leg with 49.5 cm (19.5 in) fiberglass bars. **A.** Estimated self-mass at zero load ($m_{load} = 0$): Error bars for self-mass values represent $\pm 1\sigma$ (standard deviation) of the calculated self-mass, based on N = 4-7 valid measurements under each angle condition ($\bar{N} = 5.1$). **B.** Measured stiffness at zero load: Error bars for exoskeleton leg stiffness values represent $\pm 1\sigma$ of measured exoskeleton leg stiffness based on the identical set of measurements as in (A). The ordinate range of the theoretical curve at a given knee flexion angle represents the stiffness resulting from fiberglass bar flexural moduli ranging from 35.2 GPa to 37.9 GPa, the range specified by the manufacturer for the fiberglass bars.

particular exoskeleton angle becomes progressively less linear as exoskeleton knee angle increases; for example, for leg T110B111, such linear fits give an R^2 range of 0.99 ($\phi = 20°$) to 0.80 ($\phi = 50°$). A parabolic fit of the stiffness-load data for a given exoskeleton knee flexion angle gives a much better fit (Figure 4-6).

The stiffness surface represented by contours in Figure 4-6 (*Bottom*) can be approximated using

$$\hat{k} = \boldsymbol{X} \cdot \boldsymbol{\beta}^T \tag{4.38}$$

with

$$\boldsymbol{X} = \left[\begin{array}{cccccc} 1 & \phi & m_{load} & \phi \cdot m_{load} & \phi^2 & m_{load}^2 & (\phi \cdot m_{load})^2 \end{array} \right], \tag{4.39}$$

where $\boldsymbol{\beta}^T$ is a column vector of regression coefficients, and $\hat{k}$ is the estimated stiffness. For leg T130B131, the coefficients are given by

$$\boldsymbol{\beta}^T = \left[\begin{array}{ll} 1.0 \cdot 10^4 & N/m \\ -3.1 \cdot 10^2 & N/(m \cdot \circ) \\ -4.3 \cdot 10^2 & N/(m \cdot kg) \\ 7.2 \cdot 10^0 & N/(m \cdot kg \cdot \circ) \\ 2.7 \cdot 10^0 & N/(m \cdot \circ^2) \\ 6.8 \cdot 10^{-1} & N/(m \cdot kg^2) \\ 8.1 \cdot 10^{-4} & N/[m \cdot (kg \cdot \circ)^2] \end{array} \right] \tag{4.40}$$

with an adjusted R^2 of 0.99. For leg T110B111, the coefficients are given by

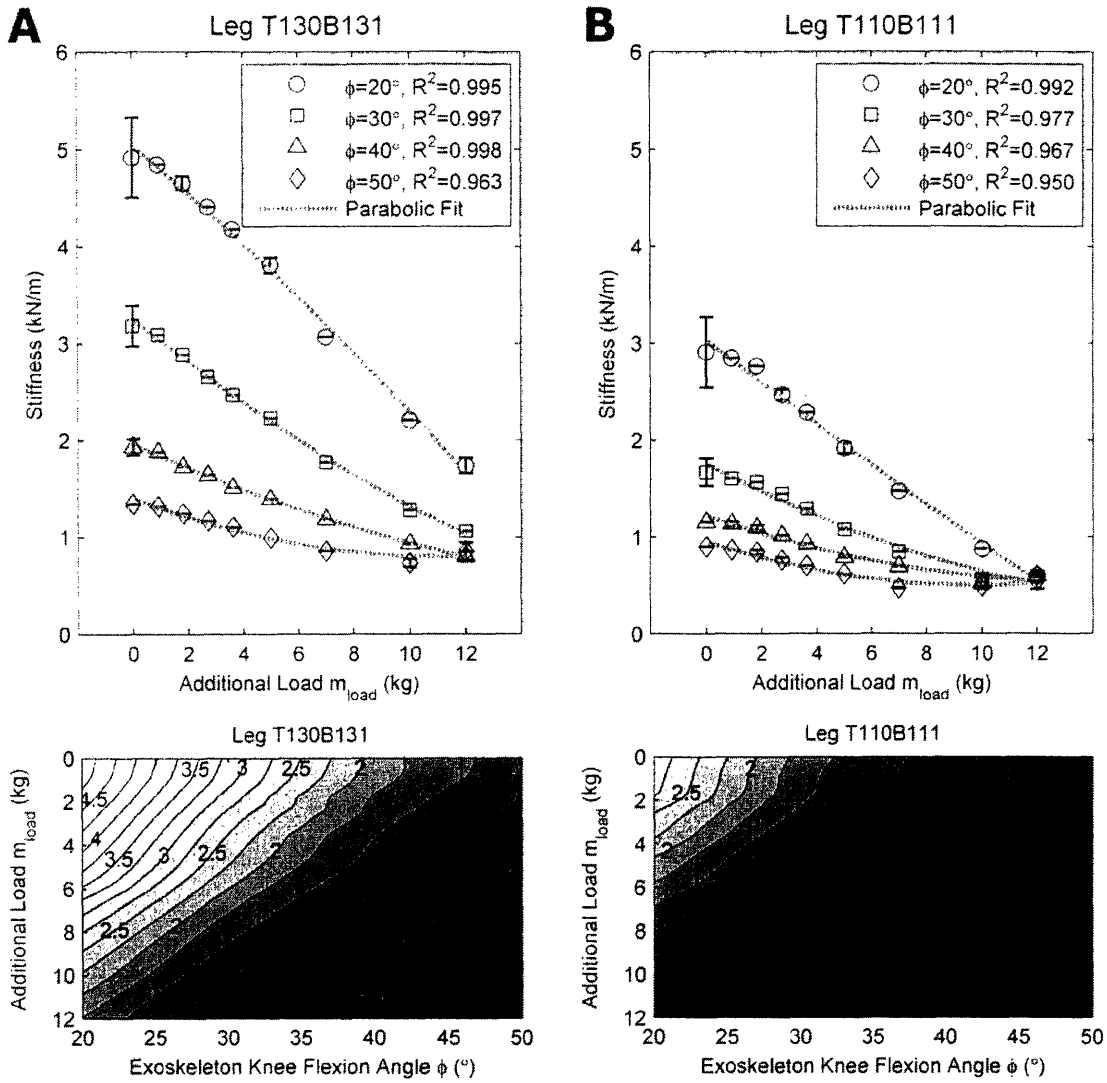

Figure 4-6: Frequency-based stiffness estimates as a function of additional load and exoskeleton knee flexion angle for **(A)** exoskeleton leg T130B131, with 43.2 cm (17 in) fiberglass bars, and **(B)** exoskeleton leg T110B111, with 49.5 cm (19.5 in) fiberglass bars. Stiffness estimates at zero additional load are based on N = 4-7 valid measurements ($\bar{N} = 5.1$). Other stiffness estimates are based on $N \geq 3$ valid measurements, except for two conditions for which $N = 2$, and one condition (Leg T130B131, $\phi = 50°$, $m_{load} \approx 4.5kg$) for which $N = 1$. Error bars for stiffness values (*Top*) represent $\pm 1\sigma$ (standard deviation) of the stiffness. Labels on contour plots (*Bottom*) represent mean stiffness values in kN/m.

Table 4.1: Torque comparison of Exoskeleton Legs and EMU Knee Joint

	Leg T130B131 (17.0" bars)			Leg T110B111 (19.5" bars)		
ϕ (°)	θ_z (°)	S [a]	R^2 [b]	θ_z (°)	S [a]	R^2 [b]
20	41.4	1.7	0.97	43.2	1.2	0.95
30	41.3	1.3	0.98	42.9	0.9	0.91
40	42.2	1.1	0.98	43.3	0.8	0.90
50	40.4	0.9	0.98	42.3	0.7	0.88

[a] The quantity S represents the stiffness of a given exoskeleton leg relative to the EMU knee joint.
[b] R^2 values were obtained after using a scale factor S to best scale the exoskeleton joint-torque curve to match the EMU knee torque data.

$$\beta^T = \begin{bmatrix} 6.1 \cdot 10^4 & N/m \\ -1.9 \cdot 10^2 & N/(m \cdot \circ) \\ -3.9 \cdot 10^2 & N/(m \cdot kg) \\ 7.2 \cdot 10^0 & N/(m \cdot kg \cdot \circ) \\ 1.7 \cdot 10^0 & N/(m \cdot \circ^2) \\ 5.9 \cdot 10^{-1} & N/(m \cdot kg^2) \\ -1.9 \cdot 10^{-4} & N/[m \cdot (kg \cdot \circ)^2] \end{bmatrix} \tag{4.41}$$

with an adjusted R^2 of 0.97.

4.3.2 Estimation of Knee Flexion and Joint Torques

Equivalent knee torques for the exoskeleton legs tested agree in form and magnitude with joint torques reported by Schmidt et al. [2001] for the EMU (Figure 4-7). Table 4.1 gives the EMU-relative stiffness for each tested exoskeleton leg configuration; the relative stiffness for each exoskeleton leg changed by a factor of 1.7-1.9 over the range $20° \leq \phi \leq 50°$, and this range is inclusive of an EMU-relative stiffness of one for both leg T130B131 and T110B111. On average, the shorter length fiberglass bars (used in T130B131) provide a better match in form to the EMU joint-torque data (Figure 4-7(A), *Right*).

For the exoskeleton leg with shorter fiberglass bars (T130B131), estimated energy recovery stayed above 60% for knee flexion angles $< 50°$ (Figure 4-8(A), *Middle*); the

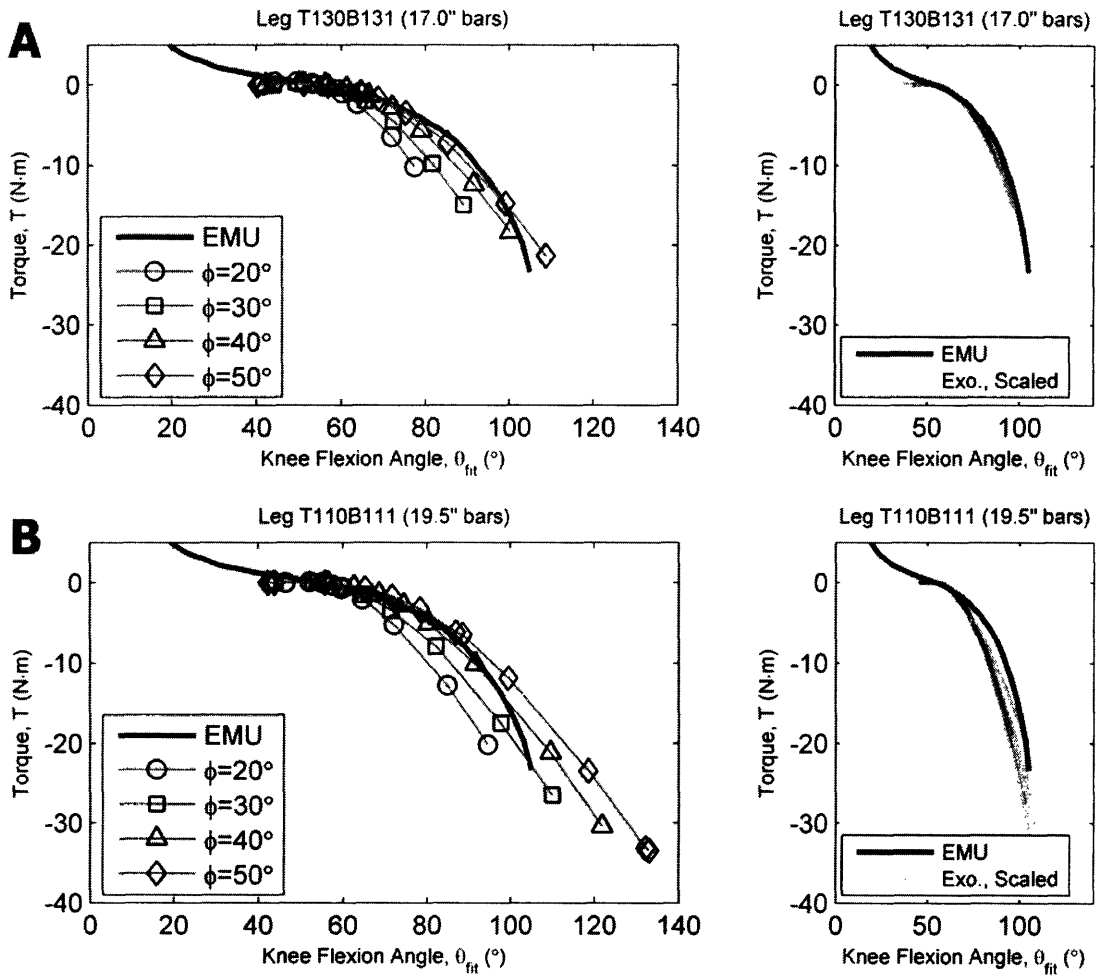

Figure 4-7: *Left*: Estimated Knee Joint-Torques for exoskeleton legs with 17.0" **(A)** and 19.5" **(B)** fiberglass bars as a function of exoskeleton knee angle ϕ. Space suit knee-torque data from the Extravehicular Mobility Unit (EMU) from Schmidt [2001] is shown as a reference. *Right*: Exoskeleton joint torques have been scaled by their EMU-relative stiffness S (see Table 4.1) and plotted to permit comparison of the form of the exoskeleton joint torque curves as compared to the EMU.

other exoskeleton leg has generally lower energy recovery, reaching a low of $\eta \approx 45\%$ for $\phi < 50°$. Energy recovery for a given knee flexion angle or normalized leg length does not appear to be a strong function of exoskeleton knee flexion angle for $\eta \approx 50\%$ or greater.

4.4 Discussion

4.4.1 Exoskeleton Leg Calibration

Damping is overestimated by the exoskeleton leg calibration system, primarily because the testing apparatus does not perfectly constraint motion to within the vertical direction. For small oscillations, the horizontal rods constrain exoskeleton hip joint motion, to first order, to the vertical direction; this approximation is not applicable for large magnitude oscillations.

During large magnitude oscillations, energy is transferred to other degrees of freedom of the calibration apparatus. This energy transfer is best illustrated by the swaying of the calibration masses at high additional loads. This swaying destructively interferes with the vertical oscillations, further removing energy from the vertical oscillation mode. This creates a higher damping condition, and causes an underestimate of the ratio of energy recovery η as compared to the actual ratio of energy recovery than would be present at this load condition when the exoskeleton is worn by a subject.

This overestimate of damping also elevates the estimated natural frequency and produces an overestimate of stiffness. At zero additional load, excess damping due to the non-ideal nature of the testing apparatus is minimized, and the with-damping estimates are likely to be much more accurate. At non-zero additional load, no-damping and with-damping stiffness estimates are very similar, suggesting that the effect of overestimated damping on stiffness estimates is minimal. The major impact of overestimating damping appears to be a reduction in the estimated ratio of cycle to cycle energy recovery η; the magnitude of this underestimate - or better, more

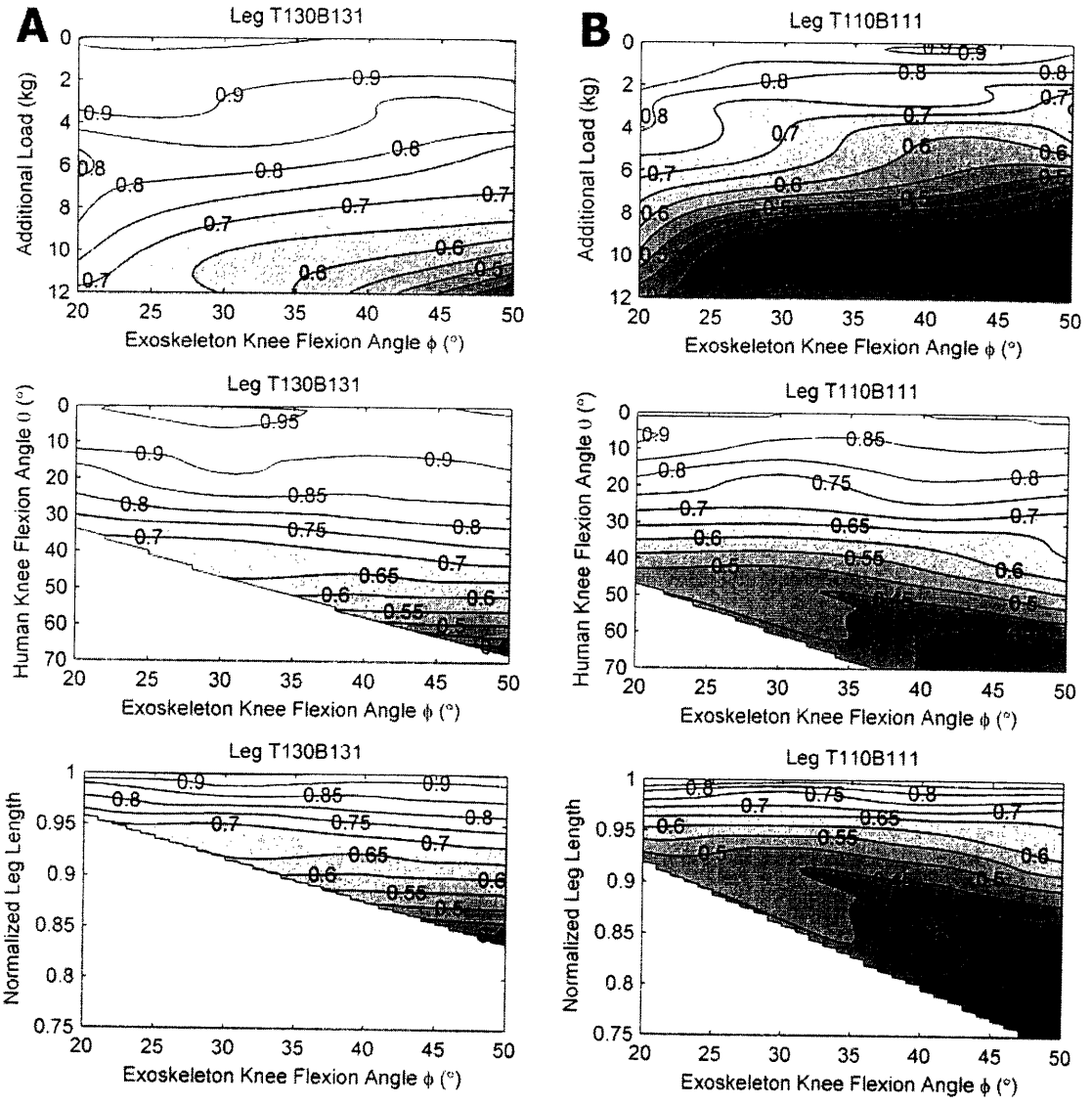

Figure 4-8: Contours of cycle to cycle energy recovery ratio η for exoskeleton legs with **(A)** $43.2cm$ $(17in)$ fiberglass bars, and **(B)** $49.5cm$ $(19.5in)$ fiberglass bars, as a function of exoskeleton knee flexion angle. Energy recovery ratio is plotted as a function of additional load m_{load} (Top), human knee flexion angle θ $(Middle)$, and normalized human leg length $L/(L_1 + L_2)$. White areas at the bottom left of the *Middle* and *Bottom* plots represent regions for which no data was collected; because exoskeleton leg stiffness decreases as a function of exoskeleton knee flexion angle, the same range of calibration masses yields a lower range of human knee flexion angles and normalized leg lengths at low ϕ as compared to high ϕ.

accurate values for η - could be better determined by constraining motion of the exoskeleton leg and calibration masses to the vertical.

Non-idealities of the calibration apparatus may also affect the variability of zero-load stiffness measurements. The higher variance in zero-load stiffness estimates associated with lower exoskeleton knee flexion angles (see Figure 4-6) is likely to be associated with imperfect alignment and mechanical play of the pin joints and rods, the effects of which are exacerbated by rapid oscillations caused by high-stiffness exoskeleton leg configurations.

While the calibration apparatus does have some limitations, the exoskeleton leg calibration procedure provides an effective method to determine exoskeleton leg stiffness. Furthermore, the approximations made in computing leg stiffness are generally valid over a broad range of conditions, as illustrated by the extent to which the stiffness measurements are self-consistent and agree with theoretical approximations.

Exoskeleton legs are physically unlike a uniform beam or a rod. Nevertheless, the uniform beam and rod approximations are useful in predicting exoskeleton self-mass and stiffness at near zero additional load, when bar deflections are small. At low exoskeleton knee angles, the effective gravitational loading in the direction of bending is very small, and the highly non-uniform exoskeleton leg behavior is most like a uniform beam. As ϕ increases, the impact of the non-uniform nature of the exoskeleton leg increases, causing the observed deviation between the theoretical estimates based on the uniform beam assumption and the actual stiffness measurements (Figure 4-5(B)).

The standard uniform beam solutions assume small deformations; the decreasing linearity of the stiffness-load relationship as a function of ϕ may be a consequence of the large deformations of the exoskeleton leg at high exoskeleton knee flexion angles.

Exoskeleton leg stiffness is dominated by the bending stiffness of the fiberglass bars, with the foot plate accounting for not more than a few percent of the measured stiffness. Because of the large magnitude of $k_{exo-rod}$ and the form of Equation 4.29, $k_{exo-rod}$ can be neglected, for all practical purposes, in the stiffness estimate.

The stiffness surfaces, for which contours are shown in Figure 4-6(*Bottom*), can be represented with high accuracy by a general quadratic equation in ϕ and m_{load},

permitting accurate estimates of stiffness for untested exoskeleton leg geometries.

4.4.2 Estimation of Knee Flexion and Joint Torques

The EMU knee joints are designed to have a zero-torque position of around 50°, close to neutral body posture in weightlessness, and thus convenient for working in microgravity. A gas pressure suit designed for planetary exploration could be designed with a different zero-torque knee flexion angle, but would likely have a joint-torque relationship similar in form to the EMU (relative to the zero-torque knee flexion angle). Therefore, adjusting the knee flexion angle by an offset (see Equation 4.37) prior to comparing exoskeleton equivalent joint-torques with the EMU data is warranted.

Because equivalent knee joint torques for the spring-like exoskeleton legs are similar in form and magnitude with knee joint torques reported for the EMU, the EMU knee joint is confirmed to behave like a non-linear spring. The EMU knee joint-torque relationship is like other soft-goods (fabric) space suit joints, although flight versions of the EMU include an additional multilayer insulation blanket that makes the joints somewhat more stiff.

Schmidt et al. [2001] argue based on physical modeling that EMU soft-goods joint-torques result predominantly from gas compression, and not from beam-like bending of the restraint layer (in the latter joint torques would depend substantially on material properties). This implies that similar soft-goods space-suit joints, including the knee joints of the space suits used on the Moon during the Apollo missions, also act like non-linear springs.

Because the relative stiffness varies with exoskeleton knee flexion angle, subjects with different leg lengths, using the same set of fiberglass bars, will experience knee joint-torques of similar form but of different magnitudes. By tailoring fiberglass bar to leg length, knee joint-torques could be matched across subjects.

Exoskeleton-induced knee joint-torques have been computed on the assumption that the axis of rotation of the knee joint and the axis of the exoskeleton knee joint are parallel. The exoskeleton provides only one degree of freedom at the ankle, but

because the exoskeleton has three degrees of freedom at the hip, subjects can cause the exoskeleton knee axis to become less well aligned with the human knee axis of rotation by medial or lateral rotation of the ankle.

While medial ankle rotation is limited by the end-stop of the hip assembly, lateral ankle rotation is permitted; subjects may use lateral ankle rotation as a strategy to reduce knee torques. In contrast, pressure suits force the axis of rotation of the knee joint to be approximately parallel to the bending axis of the suit knee joint through geometric compatibility of the body surface with the inner surface of the pressure suit.

4.4.3 Energetics: Exoskeleton *versus* Pressure Suit

While the exoskeleton and the EMU are likely to induce similar knee torques, there are important differences between the two that are likely to affect the energetics of locomotion in different ways. First, the longitudinal pressure forces in pressure suits, absent in the lower-body exoskeleton, allow pressure suits to be partially or entirely self-supporting in reduced gravity. Second, while the lower-body exoskeleton somewhat reduces hip mobility, the exoskeleton provides excellent hip mobility in comparison to a pressure suit; the limited hip mobility in pressure suits prevents normal pelvic tilt and pelvic rotation, two elements of gait that help to improve cost of transport by reducing the magnitude of center of mass motion. Third, the exoskeleton does not restrict upper body motion to the same extent as a pressure suit (near-body arm motion is only slightly limited by the extent of the load-transfer cage, shown in Figure 4-1). In normal unsuited locomotion, arm swings help balance trunk torques induced by the lower limbs [Li et al., 2001]; arm swinging in a pressure suit requires the wearer to exert additional forces to overcome intrinsic joint torques (predominantly due to joint volume changes), inertial joint torques, and gravity torques. Fourth, gas pressure suits generally limit ankle mobility to a greater extent than does the exoskeleton, due to the need to constrain pressure forces. Fifth, gas pressure suit helmets can obscure or distort the normal field of view.

Given these differences, how might the non-linear spring-like nature of the ex-

oskeleton and pressure suits affect the energetics of walking and running in similar or different ways?

While walking, kinetic and potential energies are out of phase and are inter-converted in an inverted compass-style gait. This pendular exchange of energy results in cycle to cycle recovery of energy of 60-65% while walking at $0.15 \leq Fr \leq 0.5$ in environments with Earth-relative gravity of $0.5 \leq G \leq 1$ [Griffin et al., 2004a]. Energy recovery while walking decreases in environments with $G < 0.5$ because the relative excess of kinetic (forward) energy as compared to potential (vertical) energy does not permit as much inter-conversion as in higher G environments.

The lower-body exoskeleton and pressure suits are likely to affect walking in different ways. Pressure suits impair the normal mechanisms that help to minimize center of mass motion and achieve high levels of energy recovery during walking. This is consistent with the earlier finding that fast running ($Fr > 1$) in a space suit has a lower cost of transport $[J/(kg \cdot m)]$ than walking or slow running ($Fr < 1$) 3. The lower-body exoskeleton, because of its comparatively good hip mobility, may not significantly impair energy recovery during walking.

It is possible that the exoskeleton might improve energy recovery during walking? Biewener et al. [2004] reported knee flexion angles during walking at $1.5m/s$ ($Fr \approx 0.2$ in Earth gravity) ranging from 4-26°. For the exoskeleton legs tested, energy recovery ranges from approximately 70-90% over this range of knee flexion angles (Figure 4-8, *Middle*), better than the expected pendular energy recovery of in normal walking. $\bar{\eta}$ values, averaged over $20° \leq \phi \leq 50°$, were 89% and 81% for the exoskeleton legs with shorter and longer fiberglass bars, respectively. This suggests that exoskeleton springs have the potential to improve energy recovery during walking, but whether they decrease or increase the cost of transport during walking $[J/(kg \cdot m)]$ depends upon whether walking kinematics and dynamics can adjust to take advantage of the high-return nature of the exoskeleton springs.

While running, kinetic and potential energies are in phase with one another; this limits energy inter-conversion, resulting in lower energy recovery during running than during walking. However, kinetic energy can be stored as elastic energy in muscles

and tendons; for example, the Achilles tendon alone can conserve 35% of the total mechanical energy required during each stride Farley et al. [1991].

The spring-like nature of an exoskeleton leg and pressure suit joint may improve energy recovery during running if the leg or joint has sufficiently high energy recovery and has a stiffness that is 'tuned' to complement that of the human leg. While a discussion of stiffness tuning is beyond the scope of this paper, interested readers can find the basic theory in the groundbreaking work on the impact of surface stiffness during running by McMahon and Cheng [1990].

Does the exoskeleton have adequate energy recovery to improve the cost of transport? Kerdok et al. [2002] reported maximum leg length changes during $3.7m/s$ running that correspond to $L/(L_1 + L_2) \approx 87\%$. At this normalized leg length, exoskeleton leg energy recovery was estimated to be about 38-40%. At least two factors make this number significant: First, this is the marginal energy recovery (energy recovery for an infinitesimal bit of energy stored in the exoskeleton leg spring at a normalized leg length of 87%), and the mean energy recovery would be somewhat higher. Second, the estimated energy recovery is an underestimate due to the exaggerating damping of the calibration apparatus under conditions of high calibration loads. It is likely that the exoskeleton leg can improve energy recovery of energy that is normally lost during running.

Consider another example: Biewener et al. [2004] reported knee flexion angles during running at $3.5m/s$ ($Fr \approx 1.3$ in Earth gravity) ranging from 16-46°. For the exoskeleton legs tested, energy recovery ranges from approximately 50-85% over this range of knee flexion angles (Figure 4-8, *Middle*). $\bar{\eta}$ values were 79% and 65%, respectively, for the exoskeleton legs with shorter and longer fiberglass bars, much higher than the nominal energy recovery in running.

Even given these numbers, the high energy recovery of the exoskeleton leg may not be enough to improve cost of transport. For example, the stiffness of the exoskeleton leg may impede ground clearance during the swing phase, or disrupt the running gait in other ways. Whether exoskeleton legs can reduce the cost of transport in running depends upon, as in walking, whether a locomoting human can adjust their

kinematics and dynamics to take advantage of high-recovery energy storage without incurring substantial costs that negate these potential benefits.

Do space suits have high energy recovery? To the extent that joint torques result from gas compression, energy recovery will depend upon the extent to which the work done on the gas is thermodynamically reversible. Joint-torque profiles of space-suit joints reveal varying levels of hysteresis, a direct indicator of irreversibility, as a function of the joint angle [Schmidt, 2001]. This hysteresis can result from irreversibility of the gas compression process, and is also related to losses associated with energy dissipation in the restraint layer. Energy recovery of space suit legs is demonstrably significant, as evidenced by many episodes on the Lunar surface in which astronauts used their knee joints to spring from a crouched to a standing position (examples include Apollo 16: 144:35:24, 166:57:55; Apollo 17: 144:50:52, 165:36:33, in Jones [2005]).

4.4.4 Conclusions

I have built and characterized a passive lower-body exoskeleton that simulates a pair of non-linear springs in parallel with the legs. Stiffness of the tested exoskeleton legs is, as expected, a function of the exoskeleton knee angle and decreases with the applied load, or equivalently, with increased knee flexion. The equivalent knee joint-torques of the tested exoskeleton legs closely match knee joint-torques of the EMU in both form and magnitude, suggesting that space suit legs act as springs. Because the forces generated by such springs are higher at greater knee flexion angles, the spring effect of space suit legs is likely to be most pronounced when locomotion requires large knee flexion angles, such as during running. Although not described in this paper, the joint-torque estimation approach developed herein can be reversed in order to compute stiffness from space suit joint-torque data.

While the current work does not predict when, specifically, exoskeleton legs will reduce or increases cost of transport during locomotion, the current work highlights some of the important differences between the lower-body exoskeleton and space suits, useful for interpreting the results of past and future energetics experiments. Exoskele-

ton legs used during locomotion are likely to share some of the energy recovery benefits of space suits, without the same level of mobility restriction.

To support future planetary exploration, future locomotion and energetics studies using fully integrated space suit systems are highly desirable. However, exoskeletons offer an alternative that is less expensive, doesn't require pressurization or use consumables, and permits better observation of limb motions. Although different than space suits in many ways, exoskeletons may help elucidate the mechanisms by which space suits impact human movement.

Acknowledgments

The author thanks Dr. Hugh Herr for providing, in large part, the design of the lower-body exoskeleton used in this work. I also thank MIT undergraduate researcher Conor Lenahan for his assistance in exoskeleton leg calibration. This work was supported in part by USRA/NIAC contract 070605-003-006.

Chapter 5

Exoskeleton Energetics: Implications for suited and unsuited energetics

Abstract

I hypothesized that locomotion with the exoskeleton would improve net energy recovery, reduce the cost of transport, and lower the Froude number of the run-walk transition relative to unsuited locomotion.

I measured the energetic cost and other variables during treadmill locomotion, with and without a lower body exoskeleton, in simulated reduced gravity ($G = 0.165, 0.379$) and in Earth gravity ($G = 1$). Subjects walked or ran at constant Froude numbers of 0.25 or 0.60, respectively, and walked and ran at a self-selected run-walk transition. Using the framework developed in Chapter 2, $1g$ measurements of specific resistance during unsuited locomotion were used to estimate the specific resistance of unsuited locomotion in the reduced gravity conditions. Net energy recovery was estimated for all exoskeleton conditions, based on metabolic cost measurements from the exoskeleton and unsuited conditions.

Six subjects completed the experiment after giving informed consent. Exoskele-

ton locomotion significantly lowered the cost of transport $[J/(kg \cdot m)]$ and specific resistance $[J/(N \cdot m)]$ relative to the unsuited condition, increased the estimated net energy recovery, and lowered the Froude number of the run-walk transition relative to the unsuited condition. Theoretical and actual values for the unsuited specific resistance in reduced gravity conditions showed no statistically significant differences. The exoskeleton control condition (an exoskeleton leg with 1/8th the stiffness of the primary exoskeleton leg with space-suit-knee-like stiffness) had the lowest cost of transport of the three conditions tested.

Although order effects cannot be ruled out, it appears that the high energy recovery of the exoskeleton legs led to the observed reduction in the cost of transport and specific resistance during exoskeleton locomotion. The lower costs of transport of the exoskeleton control condition suggests how one might design a tuned space suit: an exoskeleton or space suit leg stiffness that results in minimum metabolic cost during locomotion. The findings explain the previously observed effect of space suits on running: exoskeleton locomotion improved recovery during both walking and running, but because space suits impair walking recovery, the benefit of spring-like legs is most prominent during space-suited running. The results of the study and the success of the theoretical model also point to a potential role for energy recovery in the run-walk transition, although more data is needed to evaluate the linkage between recovery and gait transitions.

5.1 Introduction

Space suits adversely impact the achievable mechanical efficiency of work, limit mobility, and increase the metabolic costs of locomotion relative to unsuited conditions (Chapter 2). Results of the regression modeling of historical unsuited and suited energetics data suggested that space suits may act as springs during running (Chapter 3). Characterization of a lower-body exoskeleton with legs that are non-linear springs demonstrated that the Extravehicular Mobility Unit (EMU) knee joints act like springs, with this effect likely to be most pronounced during running (Chapter

4).

While the lower-body exoskeleton induces joint-torques similar in form and magnitude to the knee joint-torques of the EMU, locomotion performance in the exoskeleton is likely to differ from performance in otherwise similar conditions in a space suit because of the substantial differences between the two, discussed in Chapter 4. While space suits significantly impair hip mobility [Schmidt, 2001], the exoskeleton has generally good hip mobility. These differences are beneficial, because they permit the isolation and study of different contributions to the effect of space suits on locomotion energetics.

To understand how space suit knee joint torques affect the energetics of walking and running, I conducted a energetics study of exoskeleton locomotion, hereafter referred to in short form as *exolocomotion.* In addition to elucidating some of the mechanisms by which space suits affect locomotion energetics, studying exolocomotion may also help to improve understanding of the basic mechanisms underlying unsuited locomotion energetics, including evaluating whether recovery may play a role in gait switching (see Chapter 2).

I hypothesized that exolocomotion with high-energy-recovery exoskeleton legs would elevate the net energy recovery in both walking and running. I expected this to reduce the cost of transport $[J/(kg \cdot m)]$ and specific resistance $[J/(N \cdot m)]$ relative to the unsuited condition in reduced gravity conditions, whereas in Earth-gravity conditions I expected the increase in recovery might come at the expense of total metabolic rate, just as it does in space suits. Furthermore, if recovery is linked to gait switching, the increase in net recovery should lead to a reduction in the run-walk transition Froude number relative to the unsuited condition[1], consistent with video data of astronauts walking and running on the lunar surface (C. Carr, unpublished data).

[1]An easy way to think about this is that in the limit of 100% recovery during running (at any speed), one could transition to running easily at any speed – indeed it would be hard not to do so–. Walking cannot attain high recovery at any speed because at very low or very high walking speeds an effective exchange of kinetic and potential energy cannot occur.

5.2 Methods

5.2.1 Experimental Protocol

Six subjects, three men and three women, participated in the experiment after giving informed consent to participate in the experimental protocol as approved by the MIT Committee on the Use of Humans as Experimental Subjects. Each subject attended an introductory session involving anthropometric measurements, fitting of an exoskeleton, and an exoskeleton familiarization period. Subjects completed the primary session on a separate day.

For the primary session, all subjects completed the same sequence of three trials over a several hour period in a single day, as illustrated in Figure 5-1. Subjects ran and walked during the first trial in an *unsuited* condition, wearing normal athletic shoes. In the second trial, denoted as the *ExoControl* condition, subjects wore a lower-body exoskeleton (see Chapter 4) with fiberglass bars (springs) of intermediate thickness (0.3175 cm or 0.125 in). In the *ExoControl* condition, the intermediate thickness springs were used with the intention to simulate the restrictions of motion of the exoskeleton without the effect of stiff legs. In the third trial, denoted as the *Exoskeleton* condition, subjects wore the lower-body exoskeleton with springs of thickness 0.635 cm (0.250 in), intended to simulate the knee torques of the EMU.

Trials included ten three-minute stages: an initial basal metabolic measurement stage, and three gravity conditions (G_{Moon}, G_{Mars}, G_{Earth}) each with three stages. For the first and last stages during each gravity condition, subjects walked or ran for the entire three-minute stage at a specified Froude number, a non-dimensional velocity given by

$$Fr = \frac{v^2}{gL}, \tag{5.1}$$

where Fr is the Froude number, v is the treadmill velocity, L is the leg length, and g is the simulated gravity level given by $g = g_{earth} \cdot G$, with Earth relative gravity G and Earth gravity taken as $g_{earth} = 9.81 m/s^2$ ($G_{earth} = 1$). Froude numbers

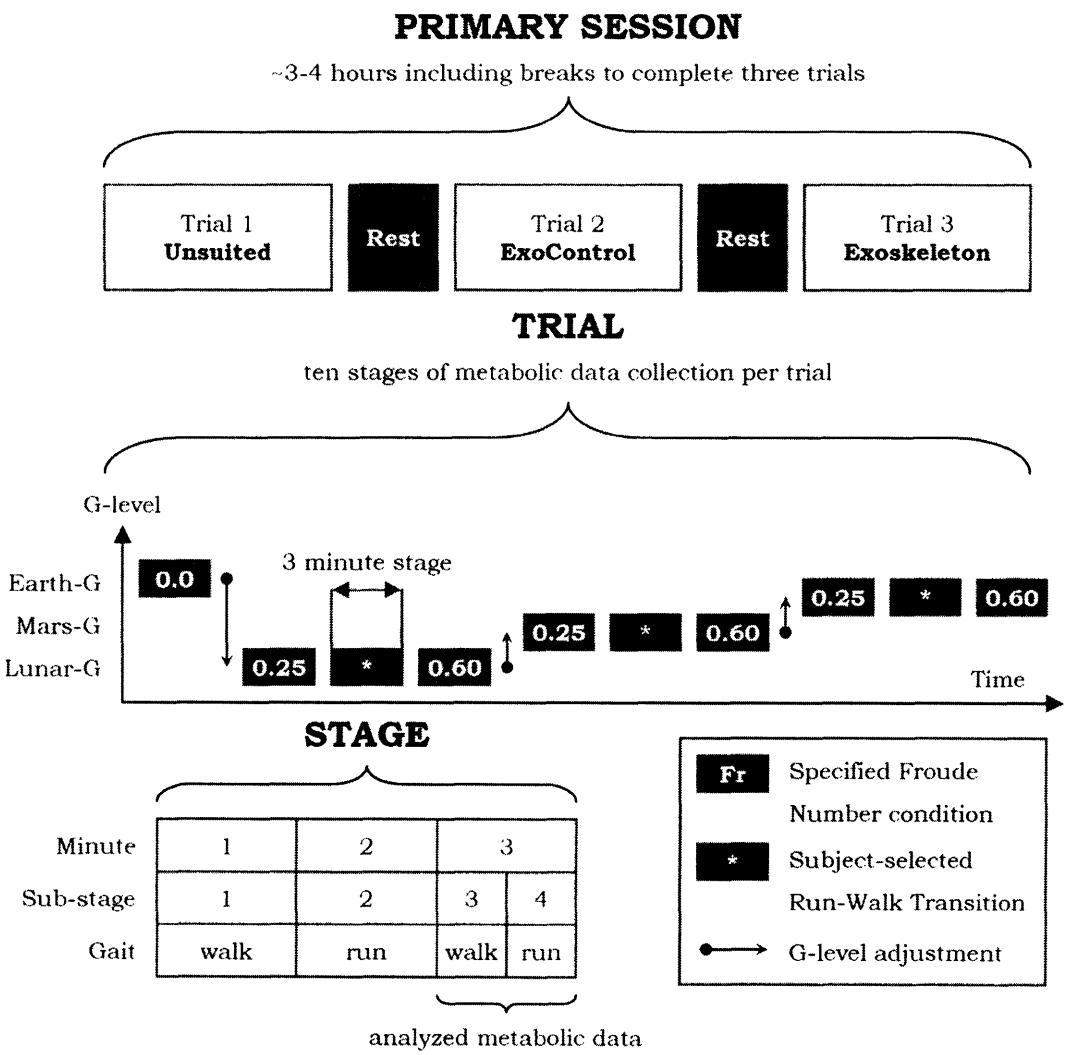

Figure 5-1: Exolocomotion Experiment Design

prescribed for walking and running conditions were 0.25 and 0.60, respectively.

In the middle stage during each gravity condition, subjects walked or ran at a self-selected velocity after being instructed to adjust the velocity up or down to find the speed at which they were indifferent to whether they were walking or running. During this middle stage, subjects switched gaits several times in a consistent controlled fashion using the sequence illustrated in Figure 5-1. In some cases, the experiment conductor adjusted the velocity up or down at the request of the subject.

Moon and Mars conditions were simulated using the Moonwalker, a spring-based partial body-weight suspension system (Figure 5-2).

The {Moon, Mars, Earth} order of simulated gravity levels provides the subject with a roughly increasing workload over time, desirable to limit fatigue. This order also allows the subject to become comfortable moving in the exoskeleton under slow conditions prior to fast conditions, in which the cost of a misstep could be greater. Furthermore, the subject experiences the most uncomfortable gravity condition first, and has the psychological benefit of knowing that the discomfort associated with partial body-weight suspension will only resolve –not worsen– as the trial continues.

While the G-level was adjusted, the subject stood flat-footed on the treadmill, occasionally making small hops at the indication of the experiment conductor who monitoring the real-time G-level. These hops helped to eliminate the effects of stiction on the observed G-level, which was estimated for display as,

$$G = 1 - \frac{F}{m_{total} \cdot g_{earth}}, \tag{5.2}$$

where F is the net upward force on the total transported mass m_{total}. The total transported mass m_{total} was determined by weighing the subject along with shoes, harness, and if applicable, the exoskeleton, using the Moonwalker load cell during the first gravity adjustment session in each trial. All masses except body mass were already known, and body mass was computed as the difference between total mass and known masses.

Treadmill velocities for each prescribed Froude number stage were calculated in

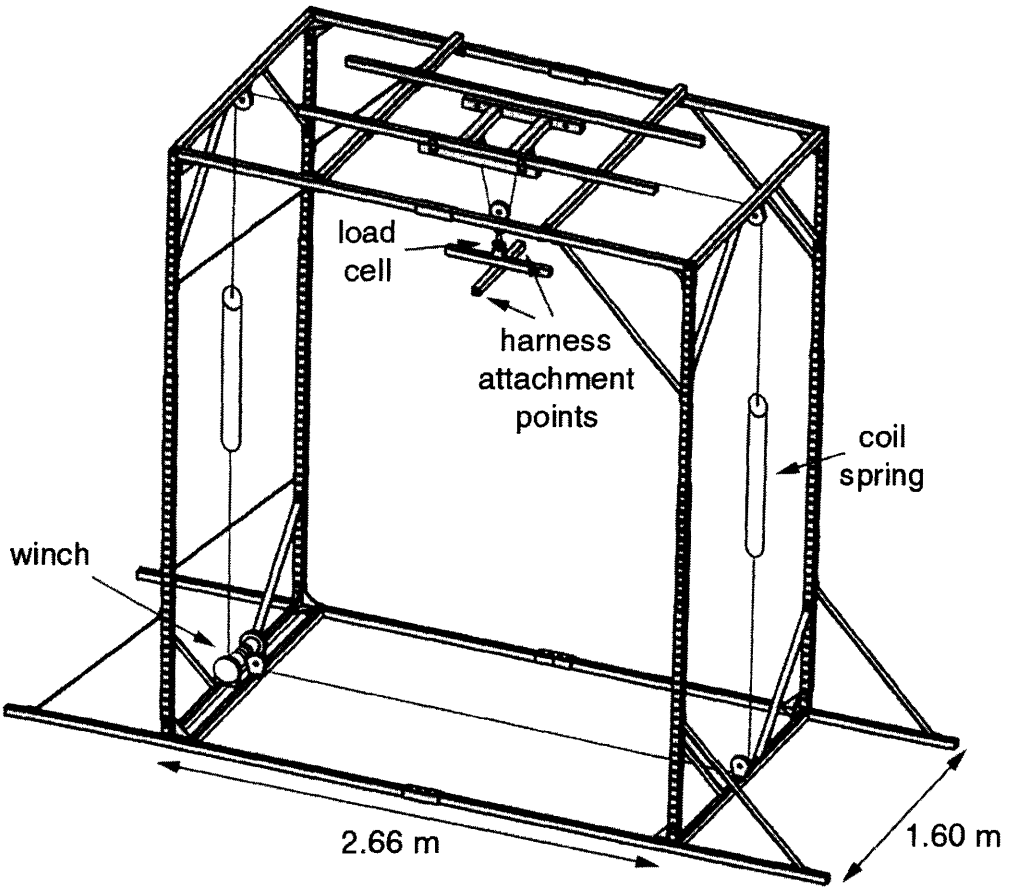

Figure 5-2: The Moonwalker is a partial body-weight suspension device with three degrees of freedom: front-rear translation, vertical translation, and yaw rotation. A treadmill was placed in the center of the Moonwalker structure, and a harness attaches to the Moonwalker via metal shoulder clips. Leg loops, shoulder straps, and an abdominal strap secure the subject in the harness and permit static control over the extent of body-weight suspension by adjustment of the line tension using the winch. A load cell (SM-500, Interface, Scottsdale, Arizona) in combination with an 2kHz-bandwidth signal conditioner (DMD-460WB, Omega Engineering, Stamford, Connecticut) measures the force applied to the subject. The coil springs elongate under increased tension, and produce a crude simulation of constant-force body-weight suspension. In practice, vertical oscillations produce substantial deviations in the simulated G-level (deviations for this experiment are reported in the results section). This drawing was adapted from Wu [1999].

real-time based on the actual G-level (obtained during G-level adjustment) and the subject leg length (measured during a prior introductory session). The test conductor adjusted the velocity of the treadmill, and the treadmill velocity display was completely obscured from the subject's view during all conditions.

5.2.2 Data Collection

A metabolic analyzer (VO2000, MedGraphics, St. Paul, Minnesota), auto-calibrated on room air before before each trial, recorded O_2 consumption and CO_2 production rates throughout each trial by sampling expired air from a special face-mask system with flow-sensing capability. Data from the last minute of each stage was analyzed[2]. A heart rate monitor worn by the subject allowed monitoring of heart rate.

A $\pm 10g$ accelerometer (CXL10LP3, Crossbow Technology, San Jose, California), mounted near the center of mass, was used to record approximate motion of the center of mass.

A custom treadmill velocity measurement system based on optical sensing of treadmill rear roller revolutions was used to record the treadmill velocity. This system was implemented because of the limited resolution (0.1 MPH) and unknown accuracy of the treadmill (Trotter CXT^{Plus}, Cybex Corporation, Medway, MA), and is described in detail in Appendix B.

Analog signals from the treadmill velocity measurement system, moonwalker load cell, and gait accelerometer were simultaneously sampled and digitized at 1 kHz using an analog and digital i/o module (PMD-1608FS, Measurement Computing, Middleboro, MA) connected to a laptop computer running custom software implemented in MATLAB (The Mathworks, Natick, Massachusetts).

[2]A prior validation experiment had shown that data from the third minute of treadmill walking or running approximated steady-state conditions, whereas the first two minutes represented a transient response (C. Carr, unpublished data).

5.2.3 Gait Analysis

Calculation of gait parameters was limited by the lack of kinematic or kinetic measurements; gait analysis consisted of computing the Froude number and cadence for each sub-stage condition.

The actual Froude number achieved in each condition was computed using the measured treadmill velocity, the subject leg length, and the actual mean G-level achieved over the sub-stage condition.

Cadence (step frequency), denoted by f, was calculated using a combination of accelerometer and moonwalker load-cell data because of 60Hz noise and a poor accelerometer electrical connection that caused loss of most body-Z-axis accelerometer data.

Non-dimensional cadence was computed as

$$\Lambda = \frac{fL}{v}, \tag{5.3}$$

where Λ is the non-dimensional cadence, L is subject leg length and v is the treadmill velocity. If ψ is the excursion angle swept out by the leg during a single stance period, then the non-dimensional cadence is related to the excursion angle during an idealized compass gait (with no double support and no aerial phase) by

$$\Lambda = \frac{1}{2sin\left(\frac{\psi}{2}\right)}. \tag{5.4}$$

Because actual gait normally involves either a double support phase (in walking) or an aerial phase (in running[3]), Equation 5.4 can be adjusted to read

$$\begin{aligned} \Lambda &\geq \tfrac{1}{2sin\left(\frac{\psi}{2}\right)} \quad \text{for walking, or} \\ \Lambda &\leq \tfrac{1}{2sin\left(\frac{\psi}{2}\right)} \quad \text{for running.} \end{aligned} \tag{5.5}$$

If one compared Λ values for walking and running, one would expect the observed differences to originate from differences in the excursion angle or the magnitudes of

[3]Groucho running [McMahon et al., 1987] excepted.

the double support phase (in walking) or aerial phase (in running). Non-divergence would imply either similar excursion angles, or a change in the excursion angle that counteracts the effects of the double support and/or aerial phase.

5.2.4 Energetics Analysis

Metabolic rate $\dot{Q}_m$ [W] was estimated by multiplying the O_2 consumption rate by the conversion factor, k $[W]/[mlO_2/s]$,

$$k = 4.33 \cdot RQ + 16.6, \tag{5.6}$$

where RQ is the respiration quotient, the ratio of moles of oxygen consumed to carbon dioxide expelled. The constants in Equation 5.6 are standard values for the free energy released from metabolism of oxygen and food at the specified respiration quotient. Mass-specific metabolic rate $\dot{Q}_{m,kg}$ $[W/kg]$, mass-specific cost of transport $C_m = \dot{Q}_{m,kg}/v$ $[J/(m \cdot kg)]$, and specific resistance $S = C_m/g$ $[J/(N \cdot m)]$[4] were estimated using the total mass transported, m_{total}.

To test the framework for metabolic cost developed in Chapter 2, specific resistance for {reduced gravity, unsuited} conditions was estimated based on the {Earth gravity, unsuited} condition.

First, I computed the net cost of locomotion, $\dot{Q}_{loco} = \dot{Q}_m - \dot{Q}_b$. Recovery, η, in the $G = 1$ unsuited condition was estimated as a function of v and G using data from Griffin et al. [1999], while muscle efficiency, E_{musc} was estimated as a function of G using the Hill model (see Appendix A for details on the gravitational dependence of E_{musc}).

The total positive work rate of the locomotion muscles was then estimated, following the derivation in Chapter 2, as

$$\dot{W}_{in} = \dot{Q}_{loco} \cdot \frac{E_{musc}}{1 - \eta}. \tag{5.7}$$

[4]Specific resistance, a non-dimensional parameter with descriptive units of $J/(N \cdot m)$, is the amount of energy required to transport a load of unit weight a unit distance

where $\dot{W}_{in}$ is the total positive work rate of the locomotion muscles. The total rate of positive work done on the center of mass in a different condition (indicated with a prime, $'$), assuming similar kinematics and kinetics that scale directly with mass and gravity, can be estimated as

$$\dot{W}'_{in} = \dot{W}_{in} \cdot \frac{G'}{G} \cdot \frac{m'}{m}. \tag{5.8}$$

From this result, Equation 5.7 can be used to solve for the new net cost of locomotion,

$$\dot{Q}'_{loco} = \dot{W}'_{in} \cdot \frac{1 - \eta'}{E'_{musc}}, \tag{5.9}$$

which gives

$$\dot{Q}'_{m} = \dot{Q}'_{loco} + \dot{Q}_{b}, \tag{5.10}$$

and finally

$$\dot{S}' = \frac{\dot{Q}'_{m}}{m' \cdot g' \cdot v'}. \tag{5.11}$$

In order to estimate the impact of the ExoControl and Exoskeleton conditions on recovery, I performed a related procedure. First, $\dot{W}_{in}$ was estimated from the measured metabolic data at each G-level in the unsuited condition. $\dot{W}'_{in}$ was then calculated for each corresponding ExoControl or Exoskeleton condition. This $\dot{W}'_{in}$ value, taken together with the measured S in each condition, was used to estimate the net energy recovery of the hybrid human-exoskeleton system according to

$$\eta' = 1 - \frac{\dot{Q}'_{loco} \cdot E'_{musc}}{\dot{W}'_{in}}. \tag{5.12}$$

Table 5.1: Subject Characteristics

Subject	Height [cm]	Leg Length [cm]	Ratio[a]	Gender	Symbol
1	172	86.0	2.00	Male	○
2	175	84.5	2.07	Male	□
3	179	94.0	1.90	Male	△
4	170	87.5	1.94	Female	▽
5	168	89.5	1.88	Female	◇
6	163	90.0	1.81	Female	☆
$m \pm s$	171 ± 5.6	88.6 ± 3.4	1.93 ± 0.09	–	–

[a] Ratio of height to leg length.

5.3 Results

Table 5.1 lists selected subject characteristics, including symbols used to plot subject-specific data. Subject age was 23.1 ± 2.5[5] excluding one 40-year-old subject. Body mass with light athletic clothing (excluding shoes) was 64.6 ± 5.6 kg.

Table 5.2 lists selected exoskeleton characteristics for each subject. Mean exoskeleton masses were 6.78 ± 0.14 and 7.13 ± 0.14 under the ExoControl and Exoskeleton conditions respectively, with the variation arising from differences between subjects in exoskeleton spring length (43.2 cm or 49.5 cm) and shoe size (European size 47 or 39). Mean total masses were 66.2 ± 5.7 kg (unsuited), 72.3 ± 5.7 kg (ExoControl), and 72.7 ± 5.8 kg (Exoskeleton). Body mass variance accounts for 96% of the variance in total mass. The mean EMU-relative stiffness for the range of exoskeletons used by the subjects was essentially unity (Table 5.2).

Basal metabolism $\dot{Q}_{b,kg}$ was 1.51 ± 0.15 [W/kg] across all conditions and subjects. While basal metabolism measurements were highly variable, the mean basal metabolic rates observed under the ExoControl and Exoskeleton conditions were not significantly different than the unsuited condition (Table 5.3). In several cases, no metabolic data was recorded during a particular 3-minute basal metabolic measurement stage.

[5] Quantities are $m \pm s$ (estimated mean$\pm$estimated standard deviation) unless otherwise denoted; $m \pm$SE or simply SE indicates standard error.

Table 5.2: Exoskeleton Characteristics

Subject	Spring Length [cm]	Δx^a [cm]	Δz^b [cm]	ϕ^c [°]	S^d
1	43.2	14.0	7.0	43	1.00
2	43.2	14.0	5.5	36	1.13
3	49.5	14.0	9.0	36	0.83
4	43.2	11.4	8.0	40	1.05
5	43.2	11.4	6.0	40	1.05
6	43.2	11.4	10.0	45	0.97
$m \pm s$	44.3 ± 2.6	12.7 ± 1.4	7.58 ± 1.39	40 ± 1.7	$\mathbf{1.00 \pm 0.10}$

[a] S Forward offset; see Figure 4-1.
[b] S Vertical offset; see Figure 4-1.
[c] S Exoskeleton knee angle; see Figure 4-1.
[d] S is EMU relative stiffness; see Chapter 4 for details on how this is computed.

Table 5.3: Basal Metabolic Rate $\dot{Q}_{b,kg}$ [W/kg]

Subject	Condition			Overall
	Unsuited	ExoControl	Exoskeleton	
1	1.65	-	0.83	1.24
2	1.65	0.72	1.95	1.44
3	2.51	1.08	1.58	1.72
4	1.54	0.68	1.72	1.31
5	1.35	1.26	0.86	1.16
6	5.64	0.38	0.45	2.16
$m \pm$SE	2.39 ± 0.67	0.82 ± 0.14	1.23 ± 0.24	$\mathbf{1.51 \pm 0.15}$
p-value[a]	–	0.067	0.152	–

[a] Two-sample equality of means t-test; a p-value < 0.05 would imply a significant difference of the mean relative to the Unsuited condition.

Table 5.4: Simulating Partial Gravity

Variable	G-Level	G ($m \pm s$)	G (Conf. Int.)[a]	p-value[b]	df[c]	%Error
G^{d}_{target}	Lunar	0.165	–	–	–	–
	Mars	0.376	–	–	–	–
G^{e}_{adjust}	Lunar	0.179 ± 0.013	$0.173 - 0.186$	< 0.0005	17	+8.6
	Mars	0.373 ± 0.012	$0.367 - 0.379$	< 0.0005	17	−0.7
G^{f}_{actual}	Lunar	0.156 ± 0.030	$0.150 - 0.162$	< 0.0005	107	−5.5
	Mars	0.361 ± 0.026	$0.356 - 0.366$	< 0.0005	107	−3.9

[a] Confidence interval for the previously quoted mean.
[b] One sample t-test relative to G_{target}
[c] Degrees of freedom for the t-test.
[d] G_{target} is desired G-level (G_{Moon} or G_{Mars})
[e] G_{adjust} is the G-level achieved when moonwalker G-level adjustment is performed.
[f] G_{actual} is the mean G-level achieved during each sub-stage.

How well was the G-level set during adjustment, and how did this relate to the actual G-level experienced by the subjects? Table 5.4 compares the target G-levels with the G-levels measured during G-level adjustment, G_{adjust}, and the actual mean G-level experienced for a given stage G_{actual}. In the Lunar-gravity condition, the mean G_{actual} was 14.1% lower than the mean G_{adjust}; in the Martian-gravity condition, a decline of 3.9% occurred. The mean standard deviation of the G-level within each stage, $\bar{s}_G$, was 0.071 ± 0.011 or 0.061 ± 0.003 during the Lunar or Mars condition, respectively.

How well were the desired Froude numbers achieved? Table 5.5 compares the target Froude numbers with the Froude numbers actually achieved, based on the mean G_{actual} and measured treadmill velocity in each condition. The largest Froude number errors occurred in the Lunar gravity condition, in which the largest G_{actual} errors also occurred. Errors decreased with increasing G-level after removal of the five $G = 1$ conditions for which subjects did not reach or maintain the assigned treadmill speed (these conditions occurred in either the ExoControl or Exoskeleton condition). Froude number errors tended to be larger during walking than during running. In Earth-gravity conditions, the mean error magnitude was 1.5%, which corresponds to a velocity error of 1.2%, close to the 0.8% RMS quantization error of the indicated treadmill velocity (see Appendix B).

Table 5.5: Actual Froude Numbers Achieved

G-Level(s)	Gait	Fr $(m \pm s)$	Fr (Conf. Int.)[a]	p-value[b]	df[c]	%Error
All	Walk	0.281 ± 0.050	$0.267 - 0.295$	< 0.0005	53	12.4
	Run	0.595 ± 0.101	$0.567 - 0.623$	0.719	53	-0.8
Moon	Walk	0.330 ± 0.060	$0.300 - 0.360$	< 0.0005	17	32.0
	Run	0.647 ± 0.125	$0.585 - 0.710$	0.127	17	7.8
Mars	Walk	0.267 ± 0.010	$0.262 - 0.272$	< 0.0005	17	6.8
	Run	0.599 ± 0.038	$0.580 - 0.617$	0.884	17	-0.2
Earth	Walk	0.246 ± 0.004	$0.244 - 0.248$	0.002	17	-1.6
	Run	0.539 ± 0.092	$0.493 - 0.585$	0.012	17	-10.2
	Run[d]	0.592 ± 0.011	$0.585 - 0.599$	0.022	12	-1.3

[a] Confidence interval for the mean G-level G_{actual}.
[b] One sample equality of means t-test relative to target Froude numbers of 0.25 and 0.60 for Walk and Run conditions, respectively. A p-value < 0.05 indicates the mean Fr number was significantly different than the target.
[c] Degrees of freedom for the t-test.
[d] After removal of five conditions in which subjects did not reach or maintain the assigned speed.

5.3.1 Exolocomotion Gait

Cadence values, shown in Figure 5-3, decline with reductions in gravity ($p < 0.0005$), and have a significant spread between the walking and running cadence values ($p < 0.0005$). Non-dimensional cadence values, shown in Figure 5-4, still have a significant spread between the walking and running cadence values ($p < 0.0005$), but the spread is opposite in sign and half the magnitude of the dimensional cadence spread, with Λ values for running lower than Λ values for walking. Unlike f, the Λ values increase with reductions in gravity ($p < 0.0005$).

Self-selected run-walk Froude numbers increased as $G-$level decreased ($p < 0.0005$), reaching a median value of 0.81 in the Lunar condition (Figure 5-5). Median and mean self-selected run-walk Froude numbers were lower for the ExoControl and Exoskeleton conditions ($p < 0.0005$) as compared to the Unsuited condition.

5.3.2 Exolocomotion Energetics

Mass-specific metabolic cost $[W/kg]$, shown in Figure 5-6, increased with G-level and Froude number, and was significantly lower for ExoControl and Exoskeleton conditions in comparison to the Unsuited condition (all $p < 0.0005$). However, the

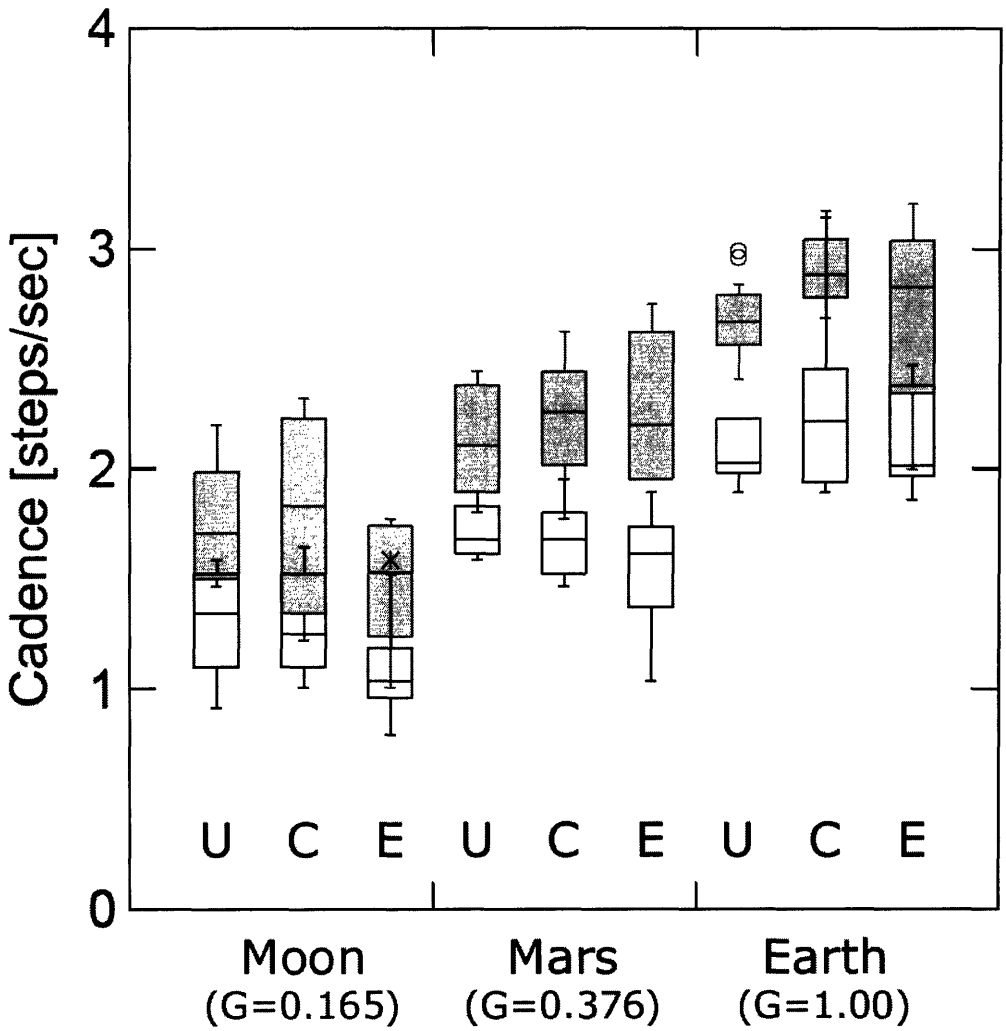

Figure 5-3: Quartiles for the cadence (total number of steps/sec) for walking ($Fr = 0.25$, unfilled boxes) and running ($Fr = 0.60$, filled boxes) conditions, as a function of the target $G-$level and exoskeleton condition (U=*Unsuited*, C=*ExoControl*, E=*Exoskeleton*). Symbols $*$ and $\circ$ indicate outliers.

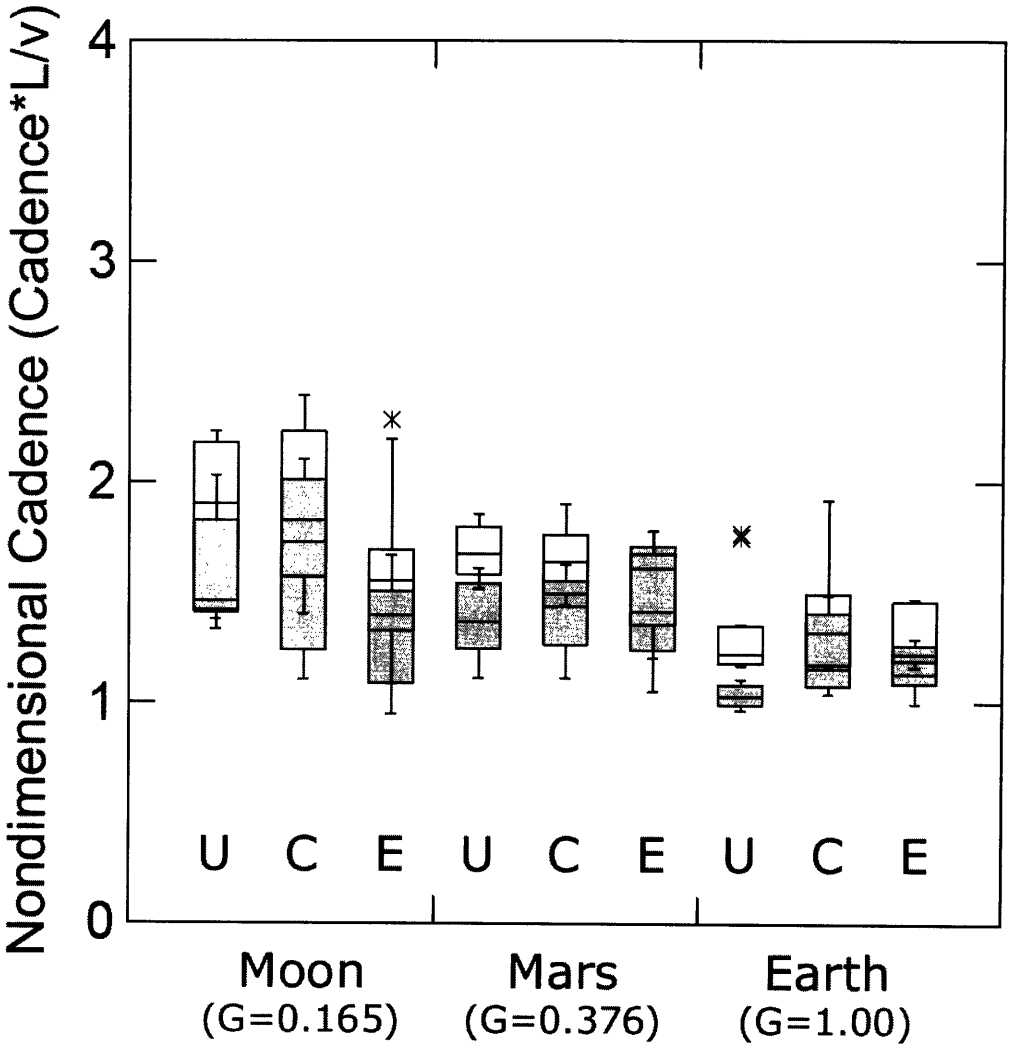

Figure 5-4: Quartiles for non-dimensional cadence ($f \cdot L/v$) for walking (Fr = 0.25, unfilled boxes) and running (Fr = 0.60, filled boxes) conditions, as a function of the target $G-$level and exoskeleton condition (U=*Unsuited*, C=*ExoControl*, E=*Exoskeleton*). Symbols $*$ and $\circ$ indicate outliers.

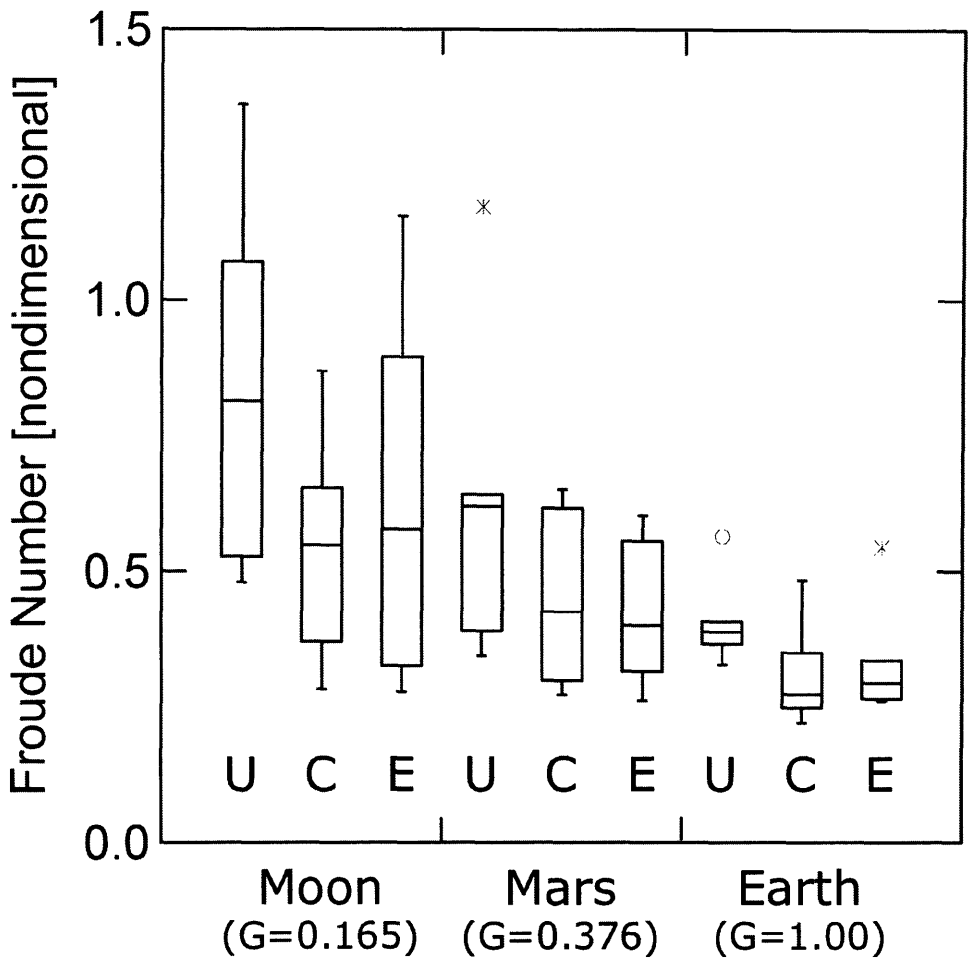

Figure 5-5: Quartiles for the self-selected run-walk transition Froude numbers for each combination of the target $G-$level and exoskeleton condition (U=*Unsuited*, C=*ExoControl*, E=*Exoskeleton*). Symbols $*$ and $\circ$ indicate outliers.

highest absolute mass-specific metabolic cost occurred in the {Exoskeleton, running, Earth gravity} condition, which also had the highest mean metabolic cost.

During unsuited walking, cost of transport $[J/(kg \cdot m)]$ was found to increase with reductions in gravity (Figure 5-7, $p = 0.001$). In the running and run/walk unsuited conditions, changes in gravity did not lead to a significant change in the cost of transport. In the ExoControl and Exoskeleton walking conditions, changes in gravity also did not lead to significant changes in cost of transport. However, during the run/walk and running conditions, cost of transport declined as gravity was reduced for both ExoControl and Exoskeleton conditions ($p \leq 0.014$).

Specific resistance $[J/(N \cdot m)]$, shown in Figure 5-8, significantly increased with G-level reduction across all three exoskeleton conditions ($p < 0.0005$). There was a significant effect of the exoskeleton condition, ($p \leq 0.001$), and specific resistance was, on average, higher in the unsuited condition and lower in the ExoControl and Exoskeleton conditions. There was also a negative association with increases in the Froude number ($p = 0.023$), and a significant cross effect with the exoskeleton configuration and the G-level (Figure 5-8, *bottom right*).

The measured and theoretical S values for the Unsuited condition, shown in Figure 5-9, are in excellent agreement. In the walking ($Fr = 0.25$) condition, the theoretical estimates differ from the measured estimates by -17% and 4.5% for Lunar and Mars conditions, respectively. In the running ($Fr = 0.60$) condition, the estimates differ by only 8.7% and 3.4%. These error are comparable in size to the errors in controlling the Froude number or the errors in setting the G-level. None of these differences were significant (Table 5.6).

Unsuited values for energy recovery, shown in Figure 5-10, represent input values based on the literature [Griffin et al., 1999, Kaneko, 1990], used to estimate the positive work done on the center of mass in each G-level condition. Presence of the exoskeleton, either in the ExoControl or Exoskeleton conditions, elevated the computed net energy recovery substantially, and more than counteracted the decline in energy recovery associated with unsuited walking as gravity is reduced. Walking recovery was elevated more than running recovery in Earth- and Mars-gravity conditions.

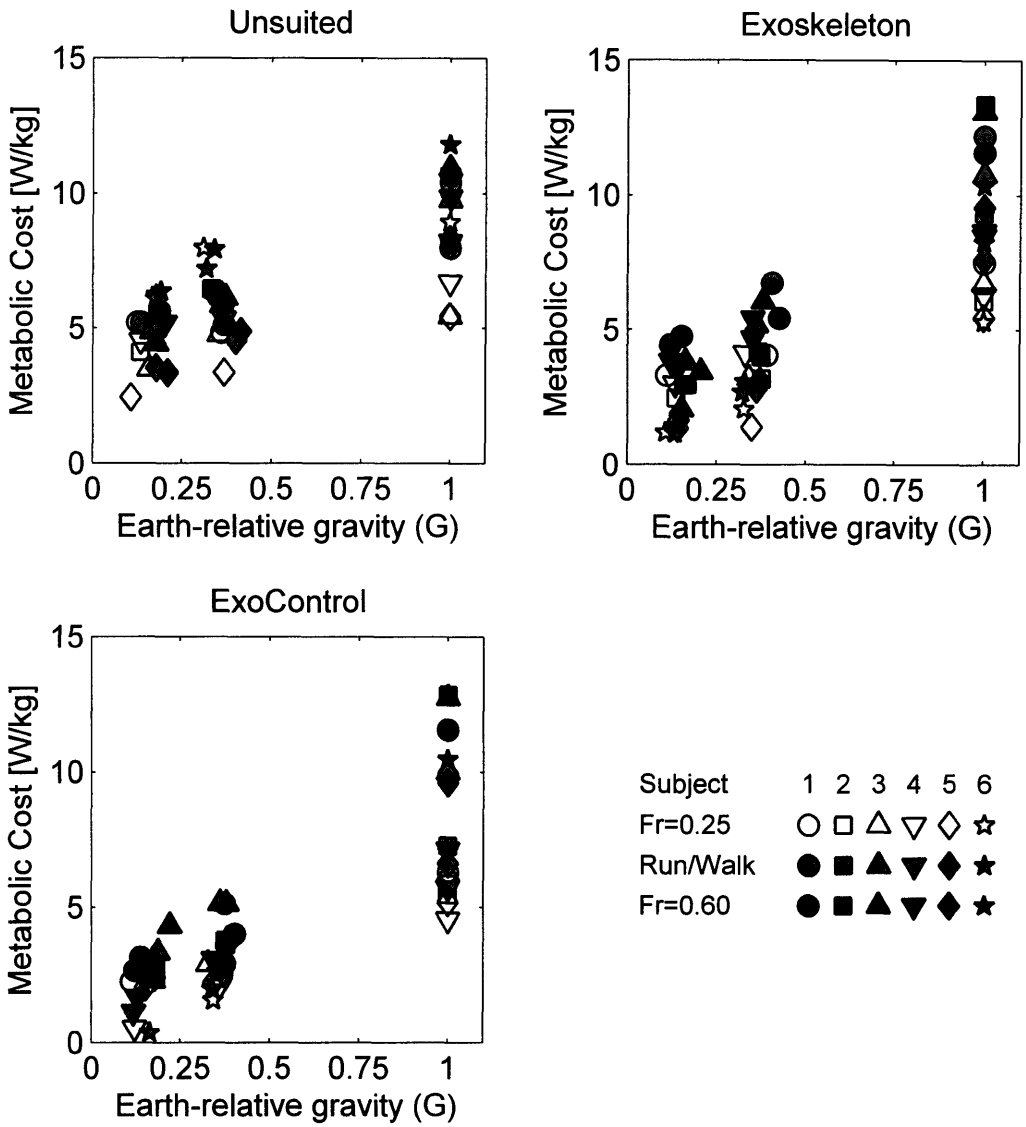

Figure 5-6: Metabolic cost $[J/kg]$ for all six subjects as a function of G-level. Unfilled symbols represent the walking ($Fr = 0.25$) condition, gray-filled symbols represent the run-walk condition ($Fr = 0.50$), and black-filled symbols represent the running ($Fr = 0.60$) condition.

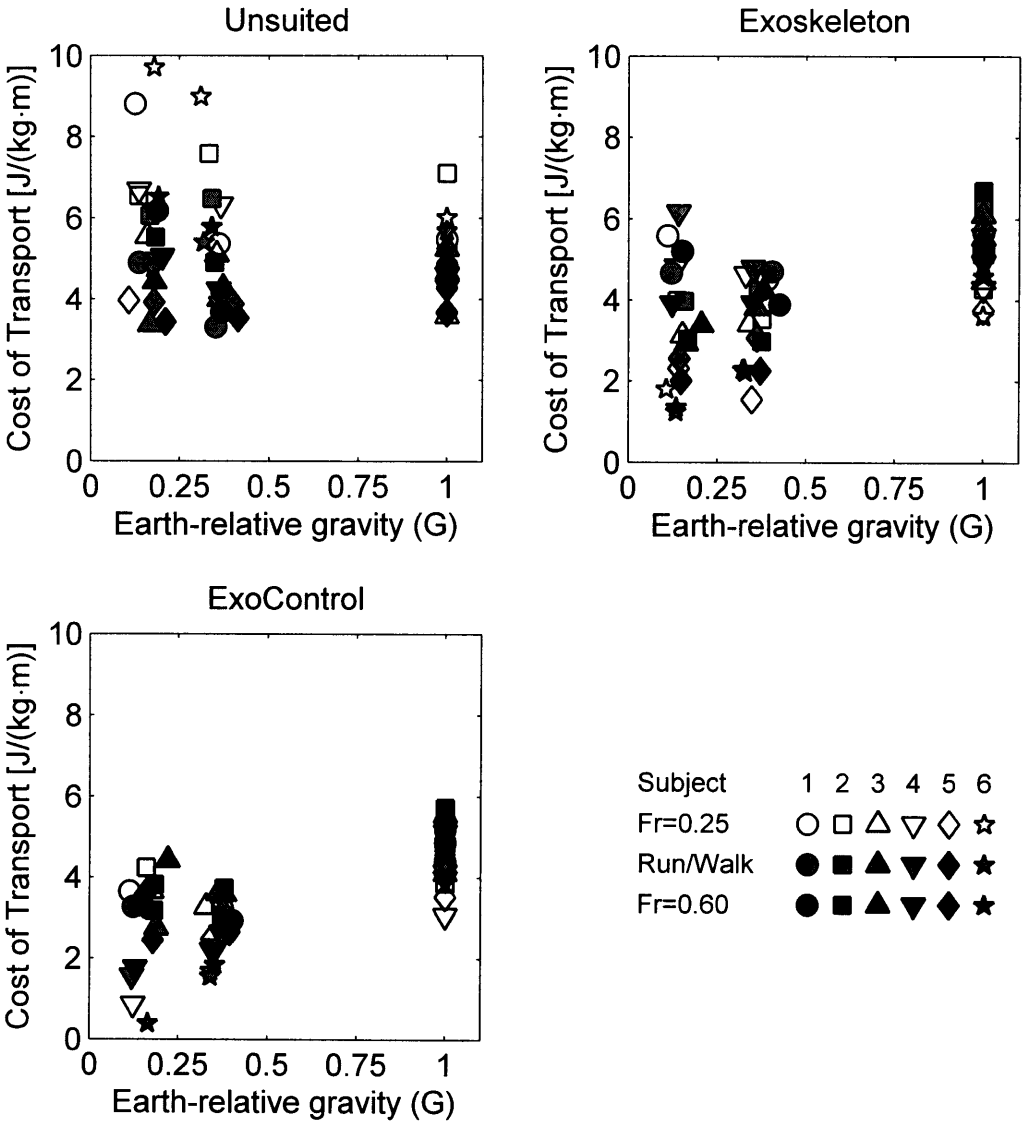

Figure 5-7: Cost of transport $[J/(kg \cdot m)]$ for all six subjects as a function of G-level. Unfilled symbols represent the walking ($Fr = 0.25$) condition, gray-filled symbols represent the run-walk condition ($Fr = 0.50$), and black-filled symbols represent the running ($Fr = 0.60$) condition.

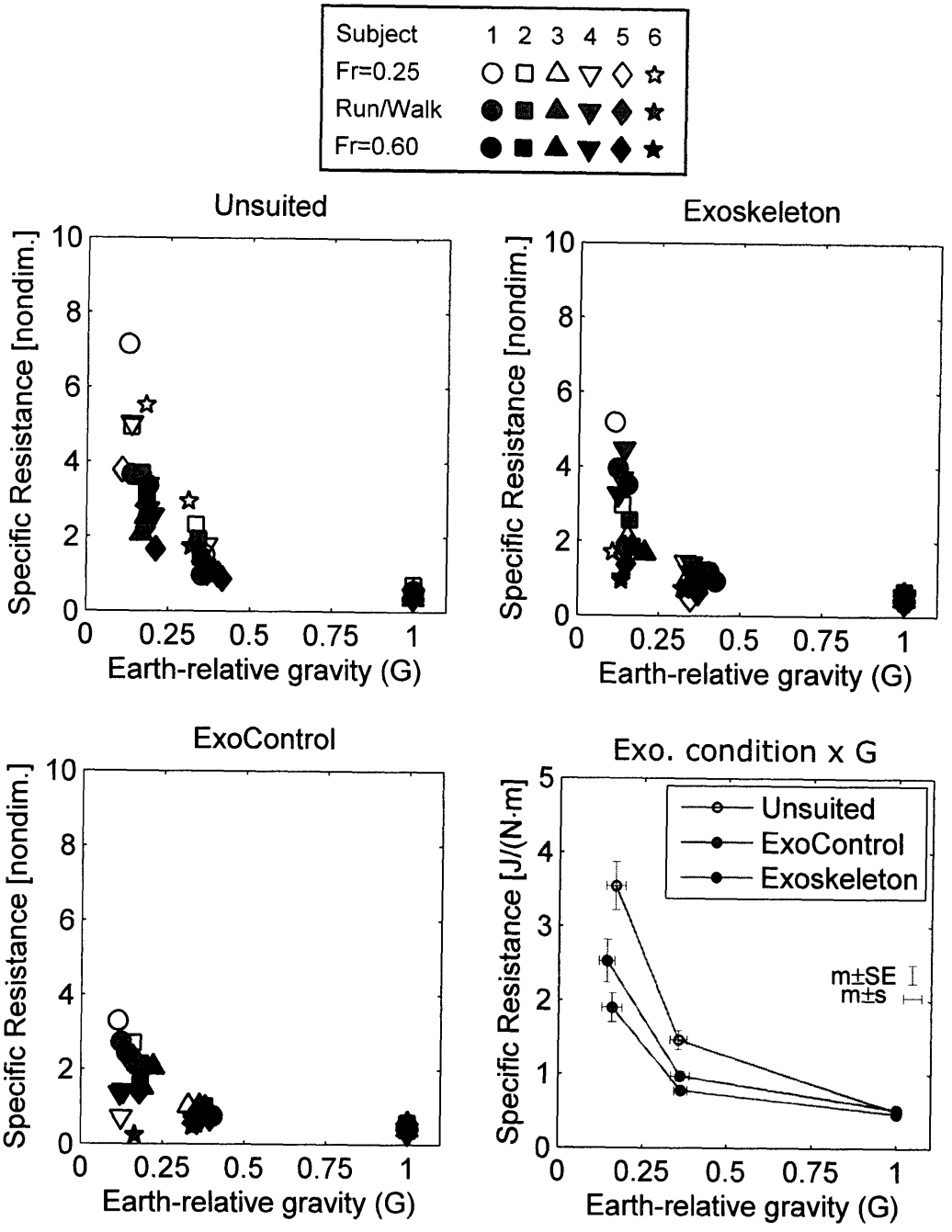

Figure 5-8: Specific Resistance $[J/(N \cdot m)]$ for all six subjects as a function of G-level. Unfilled symbols represent the walking ($Fr = 0.25$) condition, gray-filled symbols represent the run-walk condition ($Fr = 0.50$), and black-filled symbols represent the running ($Fr = 0.60$) condition. *Lower right*: Specific resistance values, averaged across all subjects and all Froude number conditions within each combination of exoskeleton configuration and G-level, reveal the significant cross-effect between the exoskeleton conditions and the G level.

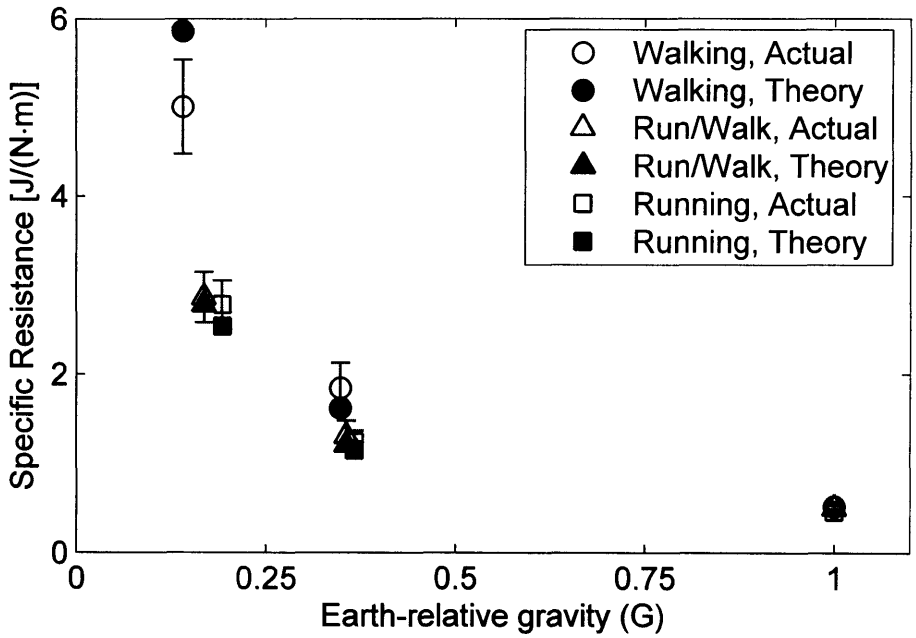

Figure 5-9: Unsuited specific resistance as a function of G-level: Unfilled symbols represent values computed directly from metabolic data. Filled symbols, the theoretical values, were estimated based on the $G = 1$ data using the approach described in the methods. Thus, theoretical results are shown only for the reduced gravity conditions. Symbols ○, △, and □ indicate walking ($Fr = 0.25$), run/walk, and running ($Fr = 0.60$) conditions, respectively. Error bars, one per actual measurement, are $m \pm SE$.

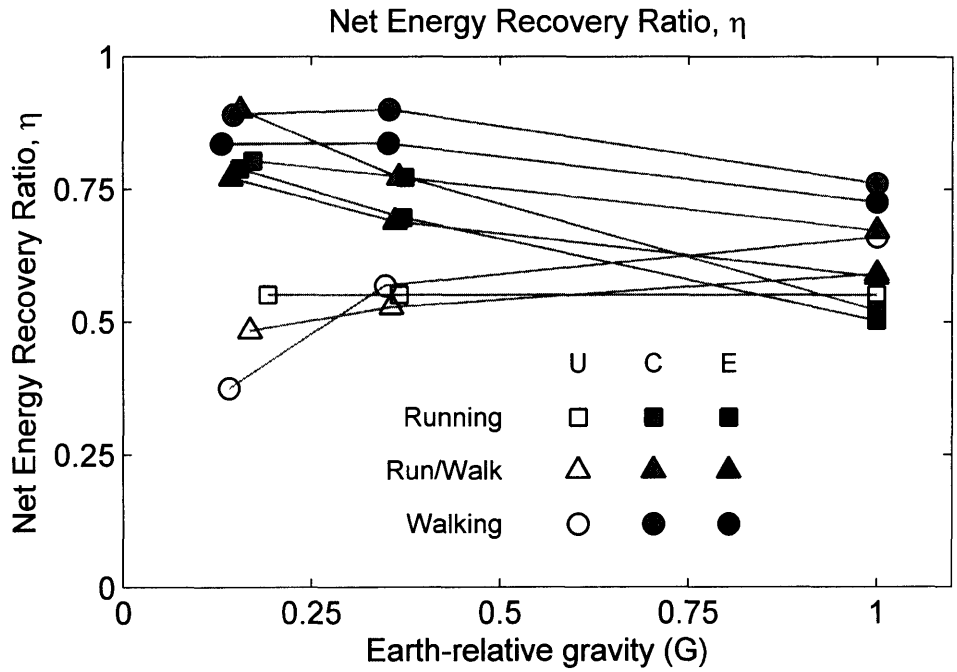

Figure 5-10: Computed net energy recovery ratio as a function of G-level and exoskeleton condition: Unfilled symbols represent the Unsuited condition, gray-filled symbols represent the ExoControl condition, and black-filled symbols represent the Exoskeleton condition. Symbols ○, △, and □ indicate walking ($Fr = 0.25$), run/walk, and running ($Fr = 0.60$) conditions, respectively. Exoskeleton conditions are denoted by U (Unsuited), C (ExoControl), and E (Exoskeleton).

Table 5.6: Specific Resistance Comparison

Condition	G	S_{actual}	S_{actual} (Conf. Int.)[a]	S_{theory}	% Difference	p-value[b]
Walking						
Moon	0.140	5.00	3.64 – 6.37	5.86	17.2	0.167
Mars	0.348	1.84	1.12 – 2.57	1.61	-12.2	0.458
Earth	1.00	0.518	0.370 – 0.665	–	–	–
Run/Walk						
Moon	0.168	2.86	2.13 – 3.59	2.77	-3.0	0.777
Mars	0.356	1.30	0.862 – 1.75	1.21	7.4	0.596
Earth	1.00	0.50	0.432 – 0.571	–	–	–
Running						
Moon	0.192	2.78	2.07 – 3.48	2.53	-8.7	0.418
Mars	0.367	1.24	0.917 – 1.56	1.14	-7.6	0.488
Earth	1	0.46	0.388 – 0.535	–	–	–

[a] Confidence interval for the observed values S_{actual}.

[b] One sample equality of means t-test relative to theoretical value ($df = 5$). A p-value < 0.05 would indicate that the mean S value is significantly different than the theoretical value.

5.4 Discussion

A major limitation of this experiment included a lack of kinematic and kinetic measurements; the availability of center of mass motion data from the accelerometer would have helped to overcome some of these limitations. While the repeated measures experiment design prevented order effects from being analyzed, this design was a reasonable compromise that was made to limit subject fatigue and maintain a low subject drop-out rate (no subjects dropped out). The limitations of the Moonwalker, discussed below, contributed substantially to experimental errors.

The basal metabolic rate measurements were highly variable due to problems in obtaining reliable metabolic measurements at low flow rates using the high-flow pneumotach required for subsequent measurements; subjects may also have disrupted basal metabolic measurements by talking or nose-breathing. However, the basal metabolic rate averaged across all trials and subjects (1.51 ± 0.15 (SE)) compares favorably with Farley and McMahon [1992], who found basal metabolic rate to be independent of gravity and equal to 1.47 ± 0.112 (SE) W/kg ($N = 4$).

The difference between the Lunar-condition G-level at adjustment and as experienced by the subjects demonstrates that subject stance and posture affected the G-level more than the errors in setting the G-level; subjects were frequently observed to walk on tip-toes during the Lunar gravity condition, which would tend to increase the effective G-level, not decrease it. The observed reduction is likely to be due to limitations of the moonwalker: in simulated lunar gravity, additional spring stretch produces large forces, enabling subjects to suspend themselves easily in the air (for example, during the body mass measurement).

Specified Froude numbers were generally slightly but significantly different from their target values, largely due to the limitations of the moonwalker: the non-constant force nature of the moonwalker springs made the moonwalker applied load vary significantly with body position, directly contributing to the larger Froude numbers errors at greater reductions in gravity. In $G = 1$ conditions, the Froude number errors are largely explained by the quantization error of the indicated treadmill velocity.

5.4.1 Exolocomotion Gait

Measured cadence values in the $G = 1$ running condition are near optimal for running in Earth gravity [Kaneko, 1990] (see Figure 2-9). Walking cadence values are not greatly lower than running cadence values because the $Fr = 0.25$ and $Fr = 0.60$ conditions have a relative velocity ratio of 0.65. The decline in cadence with reduced G-level is consistent with data reported by Davis and Cavanagh [1993].

As expected, non-dimensional cadence values for running are slightly less than those for walking. The similarity of non-dimensional cadence values across walking and running, and as a function of the G-level, is an indirect indicator that kinematics may not have changed substantially over the range of conditions studied. The more modest rise in Λ values as gravity is reduced suggests a slight change in the excursion angle, calculated using the Equation 5.4 approximation as 45-50° for $G = 1$ to 33-40° for $G = 0.165$.

The observed increase in the median self-selected Froude number with reduced G-level is consistent with the findings of Kram et al. [1997], who measured the run-walk

Table 5.7: Unsuited Self-Selected Run-walk Froude Number Comparison

G-Level	Mean Fr^a	Kram et al. [1997] Mean Fr^b	%Difference[b]
Moon	0.84	0.91	-7.4
Mars	0.62	0.57	8.4
Earth	0.41	0.45	-9.9

[a] Froude number at self-selected run-walk transition in unsuited condition.
[b] Linear interpolation of Froude number at run-walk transition using data from Kram et al. [1997].

transition at a range of simulated gravity levels using a detailed 'titration' procedure to determine the velocity of transition. For this study I used a much more simple procedure because of subject time considerations, and therefore expect less consistent results; the magnitude of the difference between the values observed and the findings of Kram et al. [1997] was less than 10% in all gravity conditions (Table 5.7), and the average difference was only -3%.

5.4.2 Exolocomotion Energetics

One surprising feature of the energetics results was that cost of transport at constant Froude numbers was relatively independent of G-level in the unsuited condition. This is different, but does not contradict, the relatively linear declines observed in the *constant velocity* reduced gravity walking and running measurements by Farley and McMahon [1992].

The success of the theoretical predictions of specific resistance values across all Froude number conditions, without any statistical differences between the observed and predicted values, suggests that the mathematical form of the model is reasonable, and that reasonable parameter values have been chosen. The goodness of fit (Adjusted R^2 of 0.98 for measured versus theoretical S) is somewhat surprising, because of the nature and extent of the assumptions that went into the estimates: First, they assume a very crude derivation of the gravitational dependence of muscle efficiency (see Appendix A). Second, the model as implemented to date is based on an assumption of 55% energy recovery during running, with no compensation for G or velocity; the data on walking energy recovery from Griffin et al. [1999] is much more

extensive. Third, when the total positive work rate by locomotion muscles ($\dot{W}_{in}$) was transformed from one state to another, $\dot{W}_{in}$ was assumed to scale directly with the gravity and mass ratios of the two conditions, making an implicit assumption of contant kinematics and kinetics. Nevertheless, a single equation,

$$\dot{Q}_m - \dot{Q}_b = \dot{W}_{in} \cdot \frac{1-\eta}{E_{musc}}$$

successfully predicted the observed metabolic cost across G and v, and across both walking and running gaits.

Perhaps the most surprising feature of the energetics results was the large effect caused by the low-stiffness springs used in the ExoControl condition. It was not anticipated that they would affect cost of transport and other variables to the extent that they did. The ExoControl springs were not calibrated (see Chapter 4), but by basic beam theory should be approximately 1/8th as stiff as the Exoskeleton springs (the latter are roughly equivalent to the EMU knee joints, with peak stiffness values in the 1-5 kN/m range, depending on the leg geometry). The ExoControl exoskeleton legs appear to have very high energy recovery, and several subjects commented on their relative easy of movement in reduced gravity; one subject described wearing these legs while walking in reduced gravity as 'effortless...I forgot they were there.'

It is possible that net energy recovery ratios are overestimated due to increases in $\dot{W}_{in}$ relative to the similar unsuited condition. However, Griffin et al. [1999] found that vertical displacements of the center of mass changed by less than 10% during simulated reduced gravity walking in the range $0.25 \leq G \leq 1.0$. While the observed net energy recovery ratios are high, they are consistent with the measured recovery values for the exoskeleton legs. An open question is whether each exoskeleton leg can store enough enery to account for a significant fraction of $\dot{W}_{in}$ during reduced gravity locomotion; this value has not been computed, but could be estimated if reliable kinematics data were available. It is possible that the ExoControl exoskelton legs have appropriate stiffness to significantly improve recovery and not significantly impair normal kinematics.

A remaining question involving both exolocomotion gait and energetics is why the unsuited run-walk transition occurs at higher Froude numbers at low gravity - if recovery signals gait switching, why doesn't the relative decline in walking recovery lead to a switch to running at lower Froude numbers rather than at higher Froude numbers? At least two factors may be involved.

First, the swinging of arms and legs creates a downward force that helps keep the body on the ground during reduced gravity walking, and this effect is magnified in a center-of-mass partial-body-weight suspension system in which the arms and legs are acted upon by normal levels of gravity. Kram et al. [1997] estimated the size of this effect for humans locomoting in reduced gravity, and used it to compute corrected run-walk transition Froude numbers, which were nearly constant (≈ 0.5) over a ten-fold range of gravity.

Second, I have made a broad assumption that energy recovery in running is not affected by gravity. While the directly reduced-gravity-proportional reduction in mass-specific metabolic cost found by Farley and McMahon [1992] argues against a significant change in energy recovery during running, at least for *constant velocity* running in $0.25 \leq G \leq 1.0$, it is possible that energy recovery in running declines substantially below $G = 0.25$ and at low velocities.

How do these exolocomotion findings relate to space suit energetics? All the same mechanisms at work in exolocomotion apply to (soft-goods) space suit legs. For example, space suit legs have high energy recovery and similar knee joint stiffness. In addition, video analysis of walk-run or walk-lope transitions by space-suited astronauts on the Lunar surface suggests that these transitions occur at Froude numbers as low as $Fr = 0.3$ (C. Carr, unpublished data). In these cases, loping or running is preferred at $Fr = 0.3$ presumably due to very low walking energy recovery.

Major differences between the exoskeleton and space suits include the much higher mass, impaired hip, ankle, and upper body mobility, and the presence of longitudinal pressure forces; these and other differences between space suits and the lower-body exoskeleton are reviewed and summarized in Chapter 4.

Space suits are likely to improve recovery during locomotion, but to do so in an

unbalanced way with respect to walking and running: while running energy recovery may be enhanced, the impaired hip and ankle mobility may greatly impair energy recovery during walking. This is precisely what the meta-analysis and regressions of Chapter 3 showed: a differential effect of the space suit on walking and running, with reduced gravity running S values not very high above unsuited values, but with walking S values comparatively higher across all gravity levels.

5.4.3 The Tuned Space Suit

The current study has an important implication for future space suit design: it provides a new start to answering the question: What is the optimal space suit joint torque? One of the mantras of space suit design for more than the last forty years has been to 'eliminate joint-torques,' based on the assumption that the best joint-torque is no joint torque. However, as Figure 5-11 illustrates, this is not necessarily the case when one considers lowering the metabolic cost of locomotion as an objective.

Consider an ideal space suit with lower legs whose stiffness can be adjusted from zero to beyond the value achieved in the Exoskeleton condition. With zero 'suit' (or exoskeleton) leg stiffness, the unsuited specific resistance is achieved. As the stiffness increases, some energy is stored in and released by the high-recovery exoskeleton or suit leg, slightly improving overall recovery and lowering S. Stiffness must decline because the observed S in the ExoControl condition is lower than the unsuited S. At some stiffness level, a minimum is achieved, but the available constraints make it impossible to determine whether the optimal stiffness is smaller or larger in magnitude than the effective stiffness of the ExoControl exoskeleton legs. For this reason, two representative gray curves are shown in Figure 5-11. It is likely the optimal stiffness is greater than the ExoControl exoskeleton leg stiffness (solid gray curve), based on subjective feel and the $\sim$8-fold difference in stiffness between the ExoControl condition and the Exoskeleton condition. As stiffness increases further, S must increase because under the Exoskeleton condition the exoskeleton legs are approximately eight times more stiff than under the ExoControl condition, and the observed S under the Exoskeleton condition is larger than the ExoControl condition. As the stiffness increases

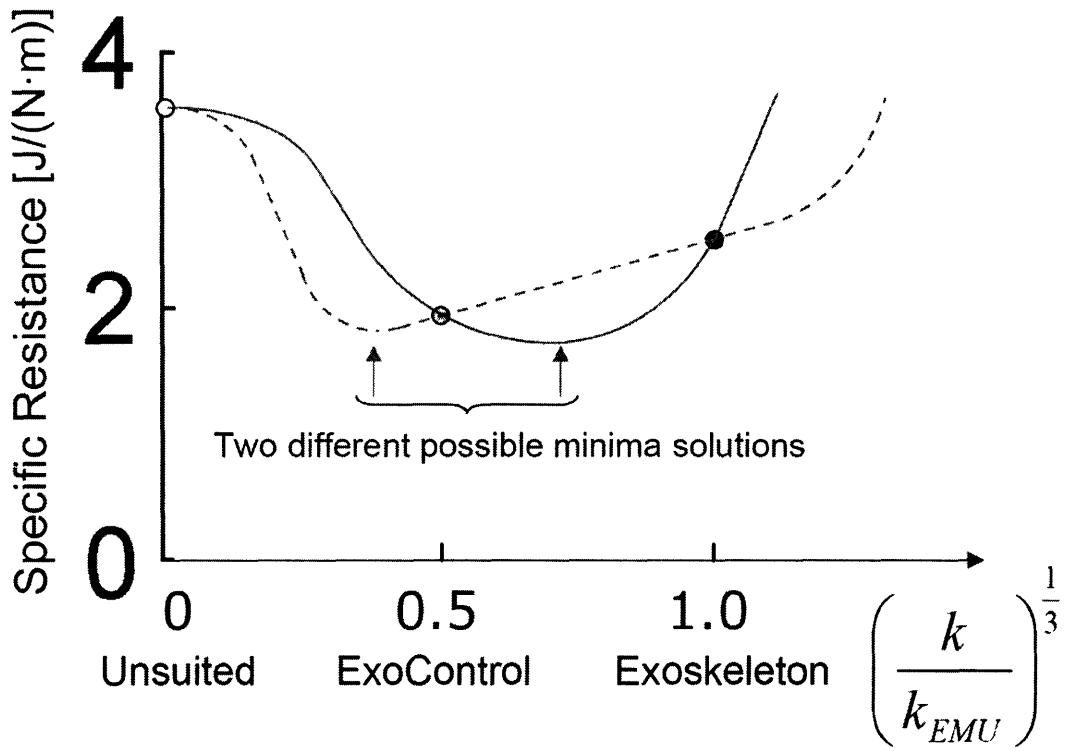

Figure 5-11: The 'Tuned Space Suit' concept, demonstrated using mean specific resistance values (averaged across Fr and subject) observed in the Lunar ($G = 0.165$) condition, plotted as a function of the EMU relative stiffness k/k_{EMU}. Unsuited specific resistance was observed to be higher than both exoskeleton configurations, with the ExoControl specific resistance lower than the Exoskeleton specific resistance. This implies that an exoskeleton leg stiffness exists, below the leg stiffness of the Exoskeleton configuration, which has minimum specific resistance. See text for a detailed explanation.

further, the greater stiffness of the suit or exoskeleton legs will disrupt normal kinematics more and more, until recovery and/or biomechanical advantage is impaired, resulting in a higher specific resistance. The extent to which the ideal stiffness would change with the G-level is unknown.

How would one go about creating a Tuned Space Suit? Modifying the thickness of the exoskeleton fiberglass bars and making additional measurements of specific resistance is one possibility. Another is to address the general problem of how springs in parallel with the legs change leg stiffness, k_{leg}, what changes this implies to regulation of effective total leg stiffness, $k_{eff} = k_{leg} + k_{suit}$, and how these changes might effect

the metabolic cost of locomotion.

Human leg stiffness, based on a mass-spring model of running [Blickhan, 1989, McMahon and Cheng, 1990], changes little with velocity [McMahon and Cheng, 1990], but does accommodate changes in surface stiffness [Ferris and Farley, 1997, Farley et al., 1998]. Ferris and Farley [1997] found that humans maintained similar vertical center of mass displacement despite a > 1000 fold change in surface stiffness k_{surf}.

What happens if regulation of k_{leg} is intentionally disrupted? McMahon et al. [1987] had subjects run with their knees bent ('Groucho' style, something they wouldn't normally do on their own), thereby reducing their leg stiffness to 82% of normal. This incurred a oxygen consumption penalty of up to 50% above 'normal' running, presumably because the lower leg stiffness led to larger oscillations of the center of mass ($\dot{W}_{in}$ increased, resulting in a higher $\dot{Q}_m - \dot{Q}_b$ for the same E_{musc} and η).

Like Ferris and Farley [1997], Kerdok et al. [2002] found that effective leg stiffness, k_{eff}, was the same despite variations in the surface stiffness. As surface stiffness decreased, leg stiffness increased, resulting in a similar effective leg stiffness ($1/k_{eff} = 1/k_{leg} + 1/k_{surf}$, because the leg and surface are in series). Over the range of k_{surf} tested (75.4-946 kN/m) Kerdok et al. [2002] found a drop in metabolic rate of 12% as k_{surf} was decreased.

Constant k_{eff} in the McMahon and Cheng [1990] running model implies similar magnitude oscillations of the center of mass (similar W_{in} per step), suggesting that the metabolic cost reduction found by Kerdok et al. [2002] results from increased recovery (η); Kerdok et al. [2002] computed energy delivery by the compliant surface, and found that for every watt delivered by the surface, the metabolic rate decreased by 1.8W. This same calculation could be performed for exoskeleton legs using data from trials for which kinematic data are available.

It is not known how humans modify leg stiffness in response to springs in parallel with the legs; however, to maintain the same center of mass motion, one would expect the response to be a reduction in k_{leg} that results in the 'normal' k_{eff} at the current G level. Donelan and Kram [2000] reported leg stiffness values for 2-5 m/s running: Earth-gravity stiffness values of 8-10 kN/m had declined to approximately 5.0-6.5

kN/m in $G = 0.25$. Because the EMU-like exoskeleton springs have stiffnesses in the range of several kN/m, they could be expected to have a significant effect on k_{leg}. Studying changes in k_{leg} in response to springs in parallel with the legs might lead to a better understanding of human leg stiffness regulation, in addition to determining whether it is feasible or desirable to build a tuned space suit.

McMahon et al. [1987] and Kerdok et al. [2002] have connected regulation of leg stiffness to the metabolic cost of locomotion, but the definitive theoretical and experimental link between leg stiffness, recovery, and metabolic cost has yet to be made. While such a link is beyond the scope of this work, further discussion about recovery and its impact beyond the exoskeleton experiment is in order.

5.4.4 The Role of Recovery in Gait Switching

Donelan and Kram [2000], in their study of dynamic similarity in reduced gravity running, concluded that a single unifying hypothesis for the effects of size, velocity, and gravity on both walking and running gaits will not be successful. However, the current work illustrates the linkage between the Froude number and the recovery in walking, a (tenuous, perhaps) linkage between recovery and the gait transition, and has demonstrated that basic assumptions regarding center of mass motion, running recovery, and muscle efficiency can produce specific resistance estimates that closely approximate measured values. The Froude number incorporates the effects of size and velocity, whereas gravity is represented both in the Froude number and in the calculation of positive work done by the locomotion muscles.

Recovery could provide the connection between walking and running that predicts the run-walk transition (Warning: some speculative material follows).

Why would recovery be a useful trigger for the run-walk transition? Because it relates net metabolic costs to center of mass kinematics and muscle efficiency, a gait transition occurring at the same value of recovery for two gait styles would trigger, in most cases, a gait transition to the gait style with the lower energetic cost.

How could one identify whether recovery triggers the run-walk transition or another gait transition? If the $\dot{W}_{in}$ term changed between gait styles (if, for example,

center of mass kinematics changed significantly), the gait transition might result in a discontinuous change in energetic cost, but a continuous change in recovery. Observing such a discontinuous change (in the cost of transport, for example) at the point of equal recovery might support the concept of recovery as a trigger.

A second method for assessing whether recovery triggers the run-walk transition would be to make computations of the recovery at the run-walk transition using existing data, or by making new measurements on animals (including humans). For example, Riskin and Hermanson [2005] reported that members of the species *Desmodus rotundus* (the common vampire bat) exhibit a 'unique bounding gait in which the forelimbs instead of the hindlimbs are recruited for force production as the wings are more powerful than the legs...[a gait] different from any gait previously described.' These bats transition from walking to running at a velocity of ≈ 0.43 m/s; for their size, the vampire bats have long forelimbs of approximate length 6.5 cm (measured from video data of Riskin and Hermanson [2005]), giving a transition Froude number of 0.29. Figure 5-12 illustrates how the equal-recovery at transition hypothesis can explain the differences in transition Froude numbers between humans and the *Desmodus rotundus*. The *rotundus* gait is extraordinarily similar to a gait style known for over 30 years: it is the direct quadrupedal analog of the loping gait performed by space-suited astronauts on the Moon, who also had a walk-lope transition Froude number of ~ 0.3.

More evaluation is required to see whether this finding generalizes; this generalization will depend upon an improved understanding of what conditions affect energy recovery in running for an individual and within and between species.

5.4.5 Summary and Conclusions

In Chapter 2, I developed a clear framework for sources of metabolic cost that permits analysis of both work output tasks and locomotion, and clearly differentiates between muscle efficiency and energy recovery (Chapter 2). This framework was used in Chapter 2 to compute the net energy expended in moving the space suit, which illustrated the benefits of mechanical counter-pressure space suits relative to

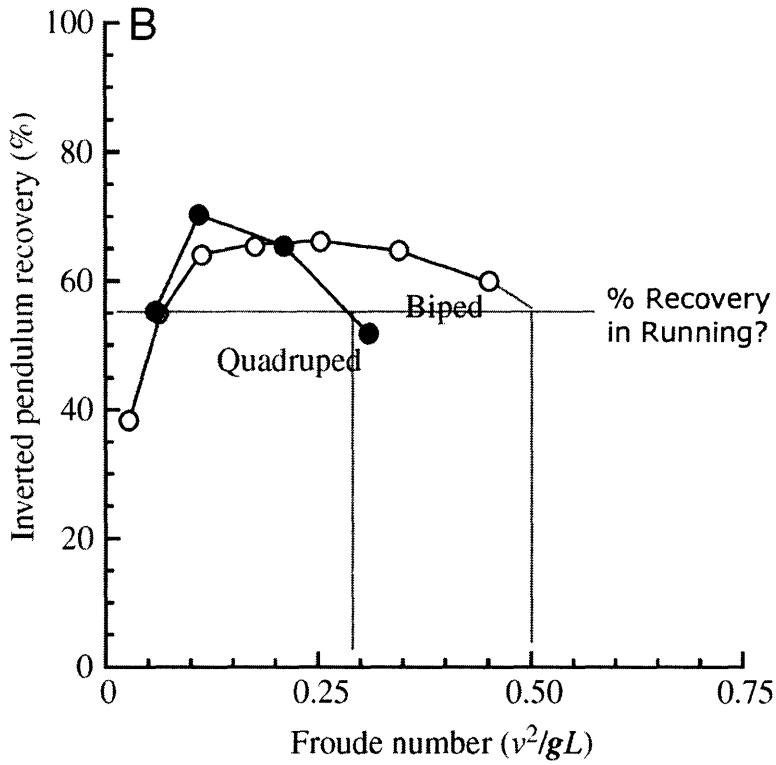

Figure 5-12: Percent recovery for a biped (humans) and quadruped (dogs) versus Froude number for a range of walking speeds. Percent recovery decreases more precipitously at faster speeds for the quadruped compared with the biped at similar Froude numbers. Quadruped data are from Griffin et al. [2004b], and biped data are for adults walking in normal gravity from Griffin et al. [1999]. Caption and figure from Griffin et al. [2004a]. The dotted horizontal line indicates human running energy recovery value computed by C. Carr from Kaneko [1990]. Running energy recovery, a function of elastic energy storage, may be similar across different species as demonstrated by the success and wide applicability of the mass-spring running model. The vertical lines represent the theoretical run-walk transition Froude numbers under the hypothesis that transition occurs at equal recovery values. Griffin et al. [2004b] do not report the Froude number at the run-walk transition for the quadrupeds (dogs) that they studied, but the horses studied in Griffin et al. [2004a] had a run-walk transition Froude number of 0.35. The vampire bats studied by Riskin and Hermanson [2005], quadrupeds that walk and run with a loping-style gait (see Chapter 2 for a definition of loping), transition from walking to running at $Fr = 0.29$.

gas pressure suits for work output and locomotion, at least in *in earth gravity.* That framework was used in this chapter to successfully estimate the specific resistance during unsuited locomotion, across gait forms and across G-levels, with no statistical differences between the observed values and the model predictions.

In Chapter 3, I transformed data from prior studies of unsuited and space-suited locomotion energetics into a common form and performed a regression analysis. The results hinted that space suit legs may act as springs, and that 'fast' ($Fr > 1$) running in space suits, at least in significantly reduced gravity conditions, has a lower cost of transport $[J/(kg \cdot m]$ than walking or slow running. This result has been confirmed by the results of the exolocomotion experiment described in this chapter: Exoskeleton legs caused a significant reduction in cost of transport and specific resistance ($J/(N \cdot m)$) relative to unsuited conditions, with this effect most pronounced under reduced gravity conditions.

In Chapter 4, I described the construction and characterization of the lower-body exoskeleton used in the exolocomotion experiment. Stiffness measurements revealed that proper exoskeleton spring selection results in equivalent knee joint-torques equivalent in form and magnitude to the EMU. Furthermore, the exoskeleton leg joint-torque comparison proves that space suit legs act as springs: if physical springs induce space-suit-knee-like joint-torques, then space suit knees–by definition–act like springs.

I hypothesized that exolocomotion would elevate the net energy recovery in both walking and running. The results of the exolocomotion experiment demonstrate that this is the case, even if the net energy recovery values in Figure 5-10 are overestimates. The second hypothesis relates to exoskeleton energetics: as hypothesized, the exoskeleton conditions decreased cost of transport and specific resistance in reduced gravity; the exoskeleton conditions increased cost of transport in Earth-gravity running. The third hypothesis was tested by examining how the relationship between the Froude number and energy recovery changed as a function of exoskeleton condition and G: because of significant declines in unsuited walking energy recovery in significantly reduced gravity ($G \leq 0.5$), the high exoskeleton energy recovery affected

walking proportionally more than running as compared to the unsuited conditions. As predicted, the Froude number at transition was reduced in the exoskeleton conditions as compared to the unsuited conditions.

Results of the exolocomotion experiment have two main implications for space-suited locomotion: First, they demonstrate that spring-like space suit legs may be beneficial in reducing metabolic cost during space-suited locomotion. Second, they raise the possibility that the optimal space-suit leg stiffness, with respect to minimizing the metabolic cost of locomotion, is non-zero: a space suit, tuned to the right stiffness, might achieve a local minima in the cost of transport. Finally, the excellent agreement of the $1g$ observations and model, along with the observed changes in the Froude number, support a linkage between recovery and the run-walk transition; further data are needed in order to determine whether transition occurs at equal recovery, or whether other factors such as the non-dimensional cadence are also involved.

The major contributions of the dissertation include:

1. A model that predicts metabolic cost in non-dimensional form for unsuited locomotion across running and walking and across gravity levels (Chapters 2 and 5),

2. An assessment of historical data that reveals the effect of pressure suits on work output and the metabolic cost of locomotion (Chapters 2 and 3),

3. A method of simulating a space suit using a lower-body exoskeleton, and methods for designing and characterizing the exoskeleton (Chapter 4),

4. An explanation for the differences in the energetic costs of walking and running in space suits (Chapters 2-5),

5. Evidence that there is an optimal space suit leg stiffness, perhaps an optimal space suit leg stiffness for a given gravity environment (Chapter 5),

6. Evidence, mostly indirect, that energy recovery plays a role in gait switching (Chapters 2 and 5).

Many roads lie ahead for interested souls: The current course of investigation could be greatly enhanced by high quality kinematics and kinetics data. Furthermore, there is much room to explore the interrelationships between spring stiffness, recovery, metabolic cost, and the run-walk transition – for example, one could extend the existing model to estimate the metabolic cost of exoskeleton locomotion based on kinematics measurements–. The general problem of how springs in parallel with the legs modify leg stiffness remains unsolved, and relates to whether the 'Tuned Space Suit' concept is viable and whether it is desirable from a cost-benefit standpoint: How sensitive is the metabolic cost to the optimal stiffness? Does the optimum change with gravity? It is not known how running energy recovery changes as a function of Froude number and gravity. One final question: Does the equal-recovery hypothesis for the run-walk transition hold, or does it require a more complicated formulation?

We shall see.

Appendix A

Hill Muscle Model

This appendix describes the implementation of the Hill Muscle Model, including a rough calculation of the approximate gravity dependence of muscle efficiency.

A.1 Model Derivation

In the same year in which he received the Nobel Prize "for his discovery relating to the production of heat in the muscle"[1], A.V. Hill demonstrated that muscles are most efficient for a particular range of the muscle velocity of shortening, v [Hill, 1922]. Hill later related the tension (force) produced by muscle undergoing an isotonic contraction, T, to the velocity of shortening [Hill, 1938] as:

$$(T + a) \cdot (T + b) = (T_0 + a) \cdot b, \tag{A.1}$$

where T_0 is isometric muscle tension, and a and b are constants. Geometrically, this equation represents a rectangular hyperbola with asymptotes of $T = -a$ and $T = -b$ [McMahon, 1984]. With no load ($T = 0$) the maximum shortening velocity v_{max} is achieved. Rewriting Equation A.1 in terms of normalized velocity v/v_{max} and normalized tension T/T_0 gives:

[1] See http://www.nobel.se/medicine/laureates/1922/.

$$\frac{v}{v_{max}} = \frac{1 - T/T_0}{1 + (T/T_0) \cdot k^{-1}}, \tag{A.2}$$

where $k = a/T_0 = b/v_{max}$. Equations A.1 and A.2 apply to nearly all types of muscles in non-insects, including skeletal, cardiac, and smooth muscle [McMahon, 1984]. In addition, $0.15 < k \leq 0.25$ for most vertebrate muscles [McMahon, 1984], although Alexander [2003] recommends $k = 0.25$ as a good average value for vertebrate muscles. The molecular basis for this widespread applicability has recently come to light: the load-dependence of the myosin stroke relative to its actin fiber is the primary molecular determinant of the mechanical performance and efficiency of skeletal muscle [Reconditi et al., 2004].

Because muscles share a common architecture within and across organisms and species, but differ in the types and proportions of protein isoforms upon which the common architecture depends, it seems reasonable that Equations A.1 and A.2 are so widely applicable. Van Leeuwen and Spoor [1992] expressed Equation A.2 in a different form and developed a related expression that takes into account the possibility of negative shortening velocities (muscle lengthening, or eccentric motion):

$$\frac{T}{T_0} = \begin{cases} \frac{v_{max} - v}{v_{max} + Gv} & \text{for} 0 \leq v \leq v_{max} \\ 1.8 - 0.8 \cdot \left[\frac{v_{max} + v}{v_{max} - rGv}\right] & \text{for} -v_{max} < v < 0 \end{cases} \tag{A.3}$$

where $G = 1/k$, and $r = 7.56$ is a factor that reflects the mechanics of eccentric motion.

For an isotonic contraction of a muscle in which all muscle fibers are oriented uniformly, so that the velocity of shortening and the tension are collinear, mechanical power output, $\dot{W}$, can be computed as

$$\dot{W} = \frac{d}{dt} \int \vec{T} \cdot \vec{dl} = T \frac{d}{dt} \int dl = T \frac{dl}{dt} = Tv = \frac{v(bT_0 - av}{v + b}, \tag{A.4}$$

where l is muscle length and t is time. In order to evaluate how the efficiency of muscle is linked to the parameters of the Hill equation (Equation A.1), Alexander [1997] defined muscle efficiency as the ratio of mechanical power to metabolic power

consumption of a fully activated muscle, P_{metab}, assuming adenosine tri-phosphate (ATP) as the energy source. The efficiency of production of ATP from aerobic respiration and foodstuffs, η_{ATP}, is only about 50% efficient [Alexander, 2003], so that the net efficiency from the rate of enthalpy change to muscular work is given by

$$E_{musc} = \eta_{ATP} \frac{\dot{W}}{P_{metab}}. \tag{A.5}$$

Alexander [1997] expressed P_{metab} as:

$$P_{metab} = T_0 v_{max} \Phi(v/v_{max}), \tag{A.6}$$

and then derived empirical expressions for Φ based on the data of Ma and Zahalak [1991]:

$$\Phi(v/v_{max}) = \begin{cases} 0.23 - 0.16 \cdot e^{\left(-8 \cdot \frac{v}{v_{max}}\right)} & \text{for} 0 \leq v \leq v_{max} \\ 0.01 - 0.11 \cdot \frac{v}{v_{max}} + 0.06 \cdot e^{\left(23 \cdot \frac{v}{v_{max}}\right)} & \text{for} -v_{max} < v < 0. \end{cases} \tag{A.7}$$

Using Equations A.4 and A.6, Equation A.5 can be rewritten as

$$E_{musc} = \eta_{ATP} \cdot \frac{T}{T_0} \cdot \frac{v}{v_{max}} \cdot \Phi(v/v_{max}). \tag{A.8}$$

Using $G = 4$ ($k = 0.25$) and $r = 7.56$ gives maximum $E_{musc} = 0.225$ for $v/v_{max} = 0.227$ and maximum normalized power $\dot{W}/(T_0 v_{max}) = 0.096$ for $v/v_{max} = 0.311$. The hill muscle model as computed using these parameters is shown in Figure A-1. The peak efficiency and peak power values are best visualized in a plot restricted to positive contraction velocities, as illustrated in Figure 2-1.

A.2 Gravitational Dependence of Muscle Efficiency

I have developed a speculative procedure to estimate the approximate dependence of muscle efficiency E_{musc} on gravity. The basic assumption of the derivation is that muscles operate at near peak efficiency under $G = 1$ conditions. This is a reasonable

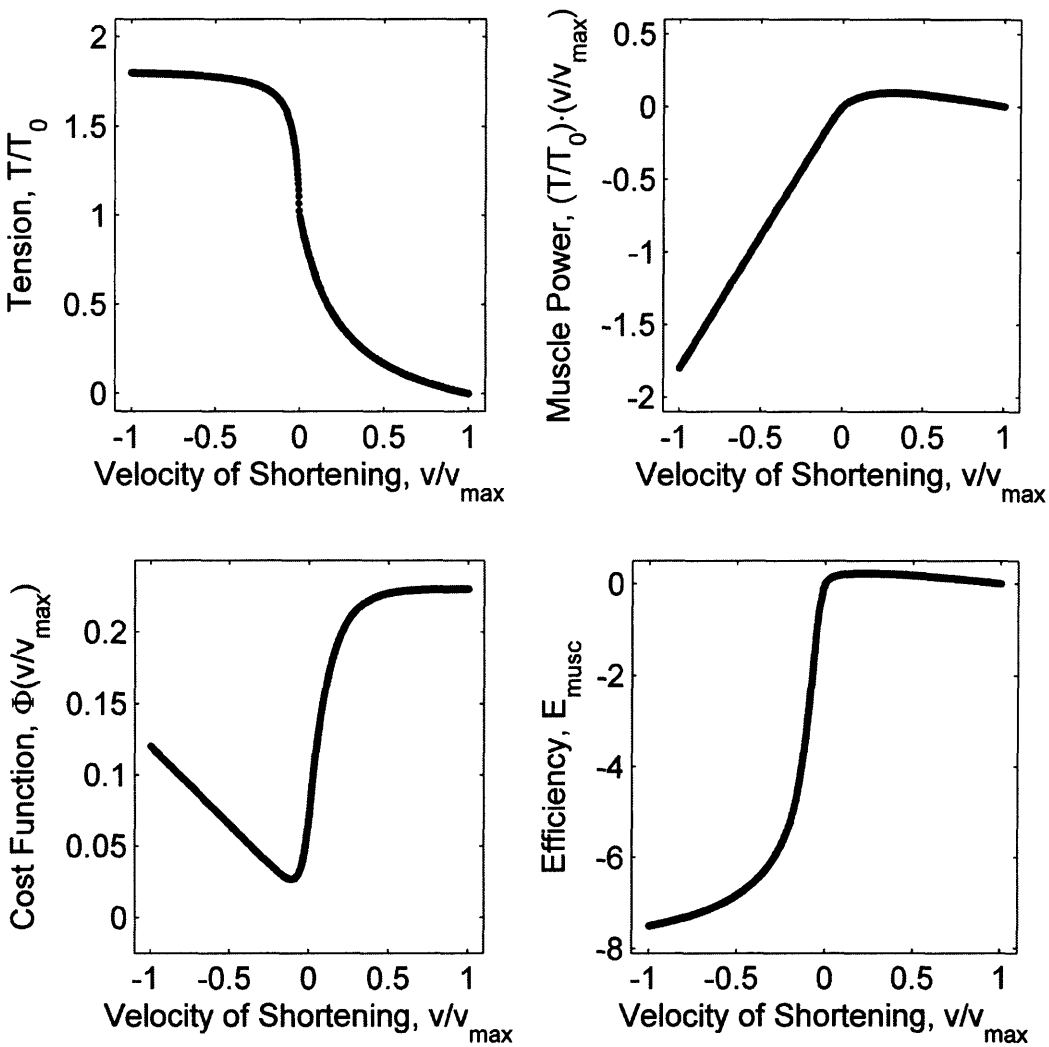

Figure A-1: Parameters of the Hill muscle model as a function of v/v_{max}, the ratio of muscle contraction velocity to maximum muscle contraction velocity. T/T_0 is the ratio of muscle tension to isometric tension, Φ is a cost function describing cellular energetics, and E_{musc} is the muscle efficiency.

assumption, as illustrated by the agreement to within 2-3% between the maximum muscular efficiency observed during slope walking [Margaria, 1976] or cycling [Whitt and Wilson, 1982] and the peak efficiency predicted by the above-implemented Hill Muscle Model.

To simulate the effects of reduced gravity on the muscle, the T/T_0 value at the $G = 1$ peak efficiency condition can be scaled so that the new 'reduced gravity' tension ratio is

$$\frac{T\prime}{T_0} = G \cdot \left(\frac{T}{T_0}\right)_{1G,E_{Peak}} . \tag{A.9}$$

From $T\prime/T_0$ a new v/v_{max} can be estimated using Equation A.2, allowing E_{musc} to be computed as a function of G (Figure A-2).

Why might the muscle efficiency vary with G but not vary substantially with velocity?[2] McMahon and others have shown that leg stiffness, but not vertical stiffness [McMahon and Cheng, 1990] is relatively constant as a function of velocity. Leg stiffness is related to contraction velocity, and therefore muscle efficiency can be maintained across a wide range of velocities.

[2]Assuming that velocity is not too small.

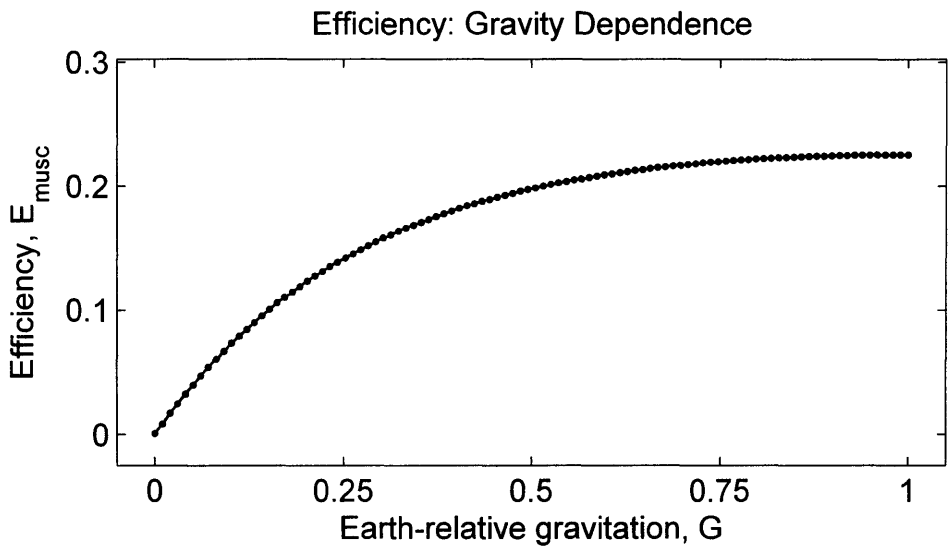

Figure A-2: Approximate gravitational dependency of muscle efficiency derived from the Hill Model.

Appendix B

Treadmill Velocity Measurement System

This appendix summarizes the design, construction, and testing of the treadmill velocity measurement system.

B.1 Electronics Design

The treadmill (Trotter CXT^{Plus}, Cybex Corporation, Medway, MA), used in the Chapter 5 experiment, displays velocity to a resolution of 0.1 MPH on its graphic display. Velocity is an important parameter in the Chapter 5 experiment. Because of poor velocity resolution and unknown accuracy I designed a system to measure the actual treadmill velocity.

The concept for this improvement is to sense the rotation of the rear treadmill roller. Counting rotations of the roller per unit time provides an easy way to accurately estimate the treadmill velocity. One argument against this solution is the possibility of slippage of the treadmill belt against the rear roller. While this is possible, slippage against the treadmill roller is more likely at the front roller, where the belt is driven. The rear roller motion results from the friction of the belt - only fast velocity changes in the belt are likely to cause slippage in the rear.

The implementation developed here is based on the OPB700 (combination IR

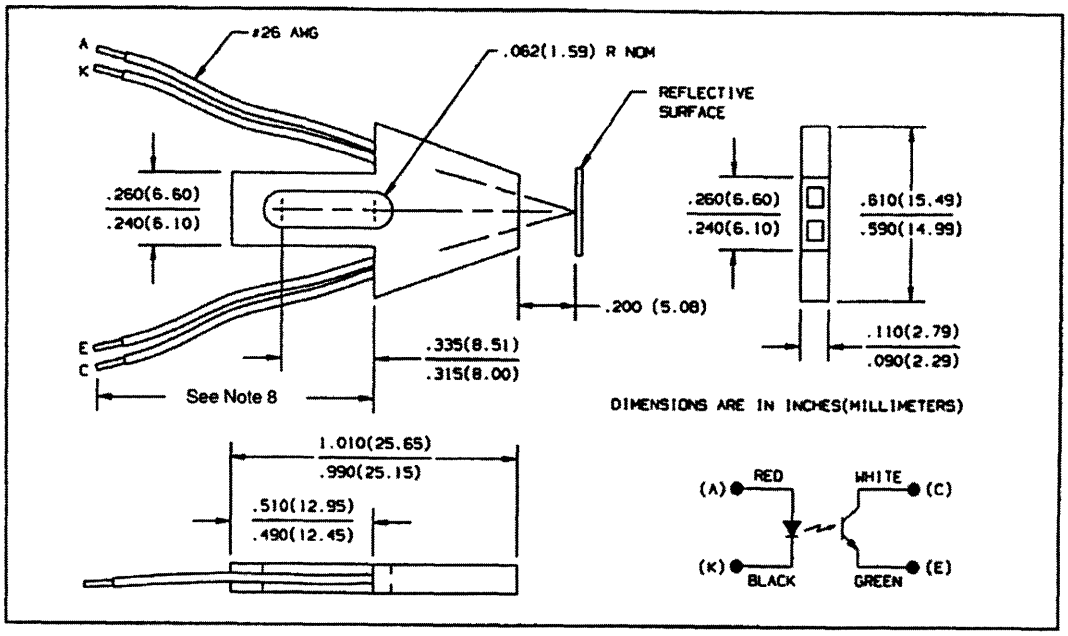

Figure B-1: OPB700 Sensor Mechanical Details (Product Bulletin OPB700, June 1996, Optek Corporation, Carrollton, Texas).

LED and phototransistor sensor), from Optek Technology, Carrollton, Texas, shown in Figure B-1.

A fixed axle-mounted sensor was used in conjunction with a reflective patch on the roller drum to count roller rotations. The same sensor could be used to identify a reflective patch placed directly on the belt; this would provide the most direct means of measuring velocity and would avoid the slippage problem mentioned above, but the reflective surface would be exposed and could be easily damaged. Also, because detections of the surface patch would be infrequent, this solution might require either careful timing measurements or long data collection periods in order to obtain good velocity estimates. The roller revolution detection approach is much simpler, and less prone to wear and tear.

For convenience, a 7805 +5V regulator was selected; a much smaller, more efficient regulator could certainly be used instead, as much less than the 1 Amp capability of the 7805 is required for use of the OPB700.

The diode forward current i_f of the OPB700 must be limited to < 100 mA; I

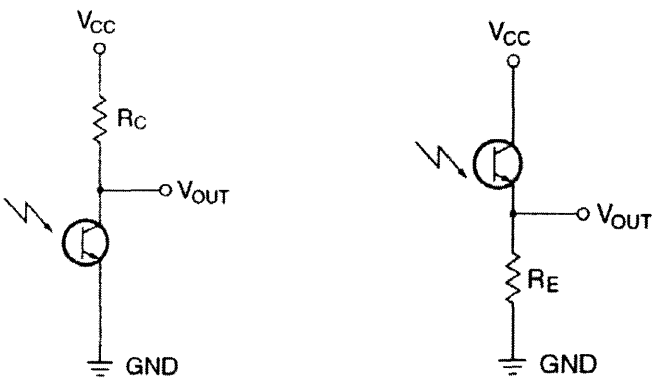

Figure B-2: From Fairchild Semiconductor Application Note AN-3005.

have chosen 40 mA as the product bulletin provides device operating curves at this condition. The desired bias resistance can be calculated as $R = (V_S - V_F)/i_f$, where V_F is the diode forward voltage (from the product bulletin) and $V_S = 5V$ is the supply voltage. For $i_f = 40$ mA we have $R = 82.5\Omega$. The nearest standard resistor value is 82Ω; power dissipation at this resistance would be $i_f^2 R = 0.16W$, so a $1/4W$ resistor can be selected (for example: bulk, $1/4W$, 5%, 5 pack, Digikey # $82QBK\text{-}ND$ is \$0.28).

The phototransistor can be used in two different configurations: common-emitter amplifier (CEA, Figure B-2 left) or common-collector amplifier (CCA, Figure B-2 right):

The CEA configuration generates an output that transitions from high to low when light is detected; the CCA output transitions from low to high when light is detected. The CCA configuration provides an active-high signal.

For each configuration, two modes of operation are possible: active or switch mode. In active mode, the output is proportional to detected photon flux up to some saturation level where the output no longer increases with increased flux. In switch mode the phototransistor is either "off" (cut-off) or "on" (saturated) depending upon the photon flux. I designed for the switch mode so that I could count pulses and use pulses per unit time to estimate the treadmill velocity.

The application note provides the following limits on the load resistance ($R_L = R_E$

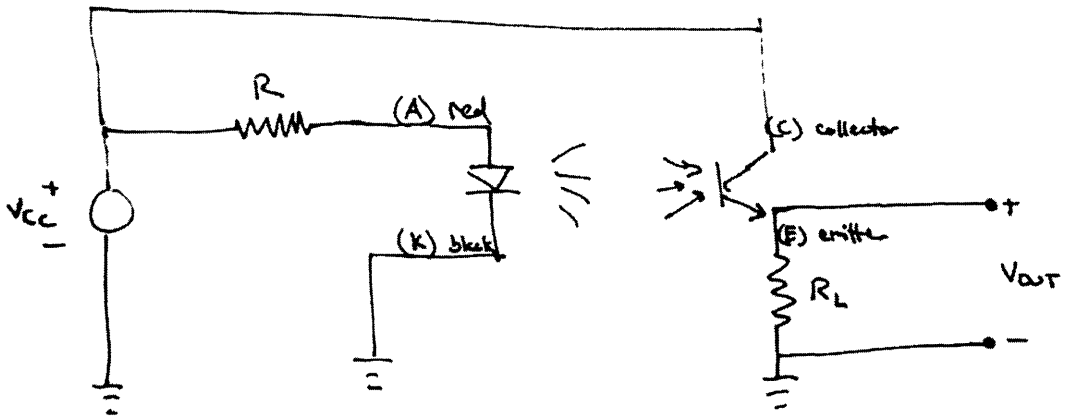

Figure B-3: Sketch of treadmill velocity measurement system circuit.

in our case since we are using the CCA configuration):

Active Mode: $V_{CC} > R_L \cdot I_{CC}$

Switch Mode: $V_{CC} < R_L \cdot I_{CC}$

We have $V_{CC} = 5.0V$, and, from the OPB700 product bulletin, $16\mu A$ for $V_{CE} = 5.0V$, $d = 0.02$ inches, assuming worst case minimum to $+2\sigma$. The switch mode condition requires $R_L > 31.3k\Omega$ for $I_{CC} = 160\mu A$ or $R_L > 313k\Omega$ for $I_{CC} = 16\mu A$.

Practically speaking, since the collector current depends upon the incident photon flux, which is dependent upon the forward diode current, distance to target, and target reflectivity, the load resistor will be a potentiometer that can be adjusted to ensure the output voltage will be several volts in the "on" state. A very conservative upper bound of the power dissipation for the potentiometer would be $I_{CC}^2 R_L = (160\mu A)^2 \cdot 313k\Omega = 8mW$ (assuming highest current and highest resistance). If the sensor is well-positioned then a $50k\Omega$ potentiometer ($4LG54BK\text{-}ND$, Digikey, $0.3W$ max, \$0.44 each) should be sufficient.

The overall circuit looks like the sketch in Figure B-3:

The voltage output of this circuit was sampled and digitized at 1 kHz using an analog and digital i/o module (PMD-1608FS, Measurement Computing, Middleboro, MA).

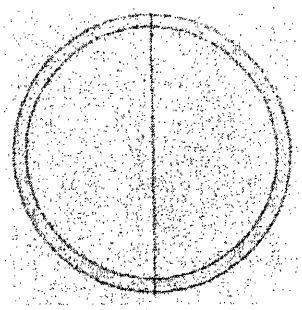

Circle Template

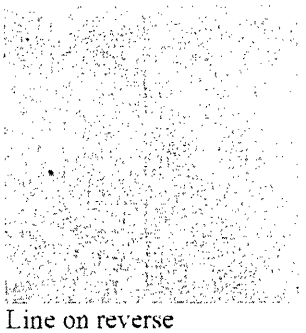

Line on reverse

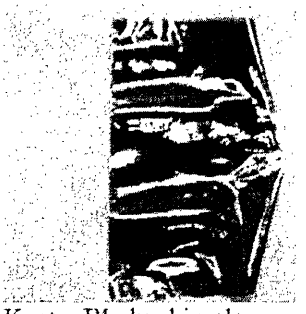

Kapton™ glued in place

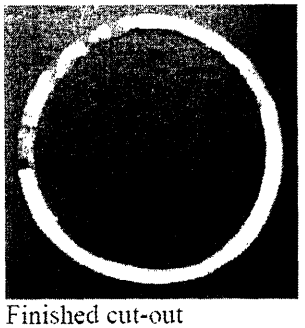

Finished cut-out

Cut-out in place on rear roller

Figure B-4: Reflective Layer Prototype

B.2 Mechanical Design

Reflective Layer

I first created a template of the right size to sit on a detent of the moving section of the roller (outer circle 2.26 in, inner circle 2.05 in, center line allowing 50% duty cycle). I built a test ring to do a fit check (Figure B-4): first I applied glue to a sheet of paper, applied copper-coated Kapton®with non-reflective side down to one half of sheet (Kapton®can be cut on paper cutter to get a nice straight edge). I cut the pattern out and mounted the ring on the movable detent of the roller. The white part can be colored black or one can start with black paper or other material to minimize reflectivity of the non-copper area.

To make a more robust ring, I cut out a ring using the water jet cutter from 1/8" thick Aluminum sheet, and attached the copper-coated Kapton®to one side of the ring (Figure B-5. The bare-aluminum side was later colored black using a permanent marker. For final mounting of the ring, I cleaned the ring and roller detent surface

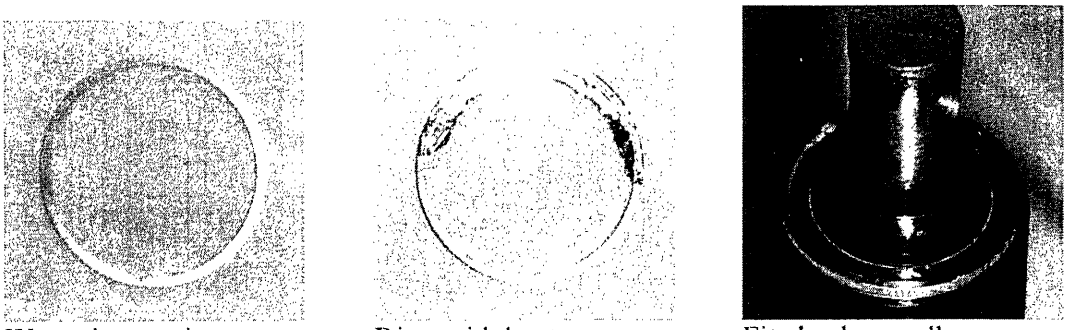

Water-jet cut ring | Ring with kapton | Fit check on roller

Figure B-5: Reflective Ring

using acetone and used silicone rubber sealant to bond the ring to the roller.

Sensor Mounting

The sensor was mounted on an additional shaft collar (McMaster-Carr, part # 6436K73). This two-sided Aluminum shaft collar fits on the 1 in shaft of the roller; a small hole was drilled and tapped to permit mounting of the OPB700AL sensor on the fixed portion of the shaft (Figure B-6). In a pinch one could just use thick rubber band to mount sensor, but the tapped screw hole with lock-tite®provides a more reliable mounting.

This shaft collar has an OD of 1.75 in, leaving 3/8 in thickness for drilling and tapping of a screw hole. To make a #4-40 tapped hole, I used a #43 drill for tapping, and tapped holes on two sides of the shaft collar to create two sensor placement options. A single screw permits distance adjustments of the sensor forward/backward to optimize photon flux to the phototransistor.

Figure B-7 shows the sensor mounted in-place on the rear treadmill roller.

B.3 System Evaluation

An initial test of the sensor was conducted at 1.0 MPH and 8.0 MPH, the velocity limits of the treadmill. Five seconds of data was collected at each speed, to ensure that the velocity could be determined even over this short time interval. The DC

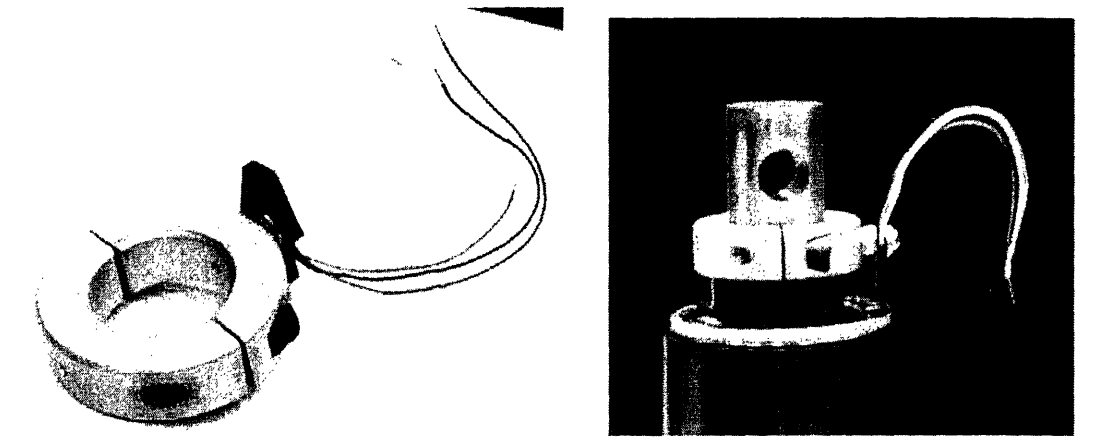

Shaft collar with tapped holes & sensor

Shaft collar in place on roller

Figure B-6: Mounting of the Sensor

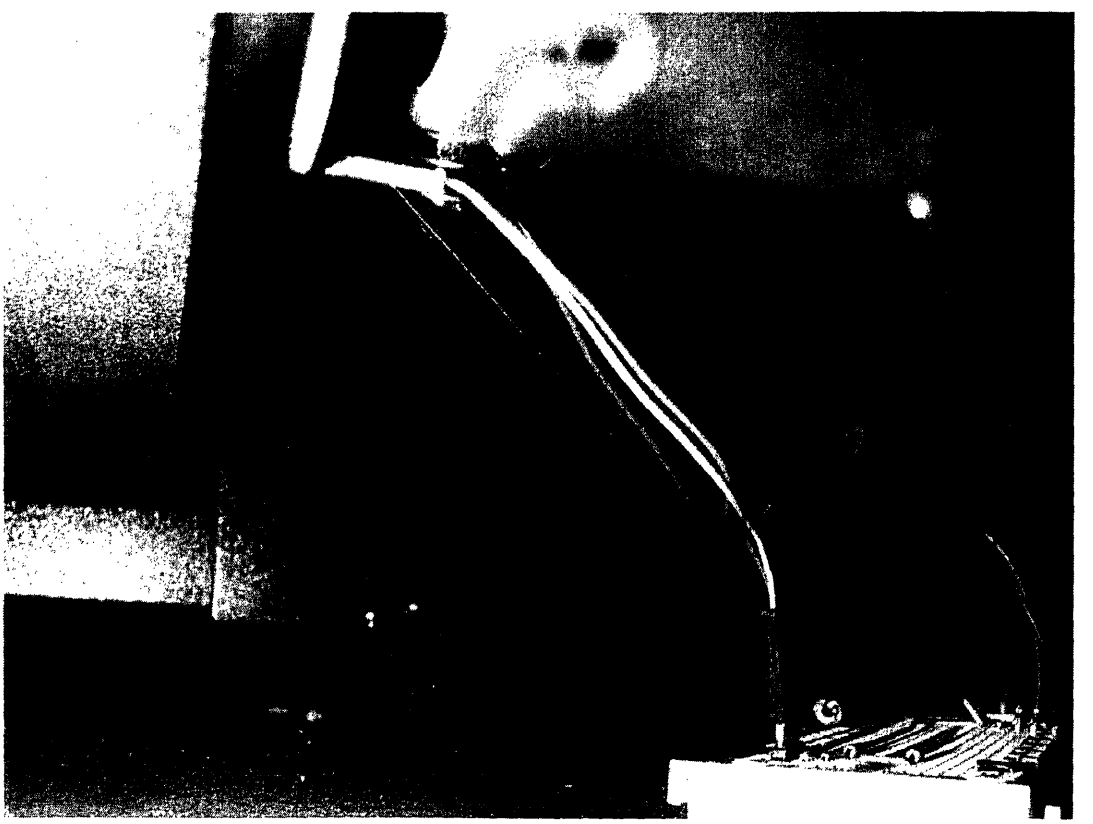

Figure B-7: Sensor mounted in-place on the rear treadmill roller.

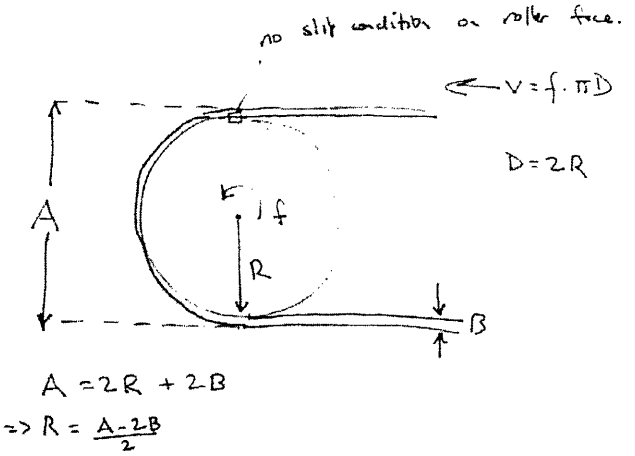

Figure B-8: Rear-roller geometry

component of the data was removed, and an FFT used to extract the peak frequency, which represents the frequency of rotation of the roller. To estimate the velocity, I computed the velocity as a function of the roller diameter and made some measurements, illustrated in Figure B-8, using a micrometer: I measured $A = 2.650$ in and $B = 0.080$ in, so that $R = 1.245$ in.

Results showed that the treadmill 1.0 mph indication is quite good (Figure B-9), and the 8.0 mph indication less so (Figure B-10); if the initial measurement is considered accurate, the 8.0 MPH indication would represent about 1.7% error.

The FFT results are cleaner for higher speed operations; at low velocities, harmonics of the fundamental frequency are present.

Next, a full calibration of the treadmill indicated velocity curve was performed. To select a given indicated velocity, I used the minimum number of "increase velocity button" clicks to obtain the indicated velocity. A given velocity was also set by starting at a prior velocity below the final desired indicated velocity. This same procedure was used throughout the Chapter 5 experiment to ensure that velocities were set in a consistent manner. I tested the indicated velocity over the full treadmill range from 1 MPH to 8 MPH in indicated increments of 0.1 MPH.

The indicated versus actual (estimated) velocity curve is shown in Figure B-11. The estimate of the treadmill roller diameter was then modified from 2.490 in to

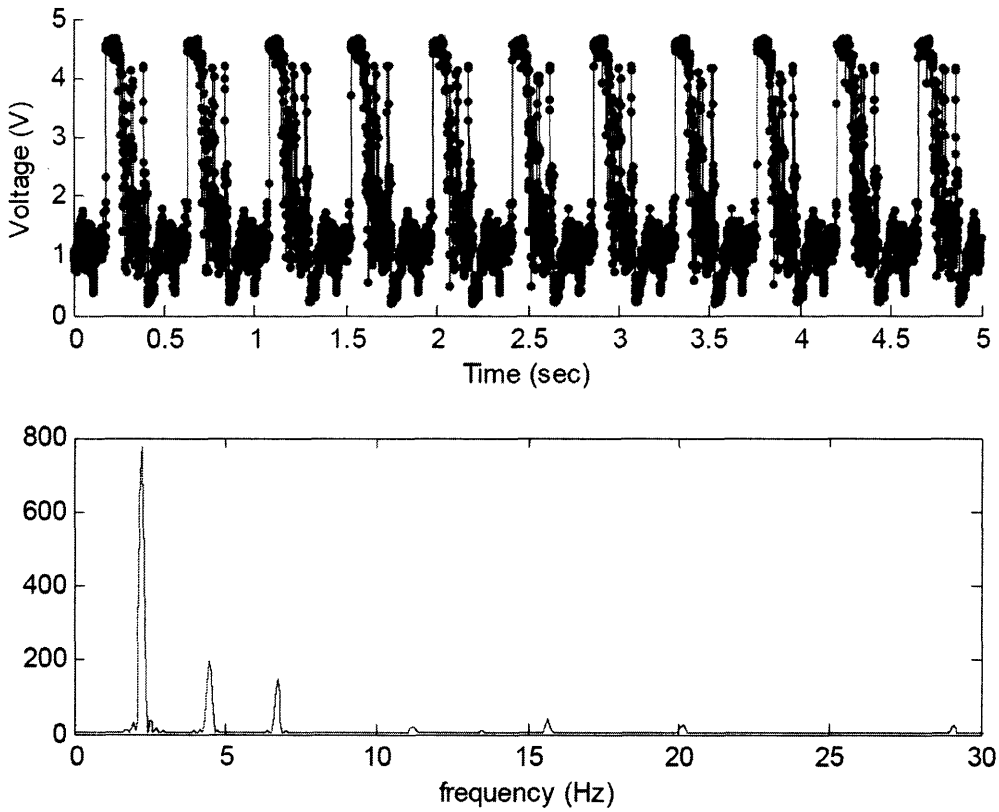

Figure B-9: Results for 1.0 MPH Indicated: $f_{peak} = 2.258$ Hz, $v_{estimated} = 1.004$ MPH.

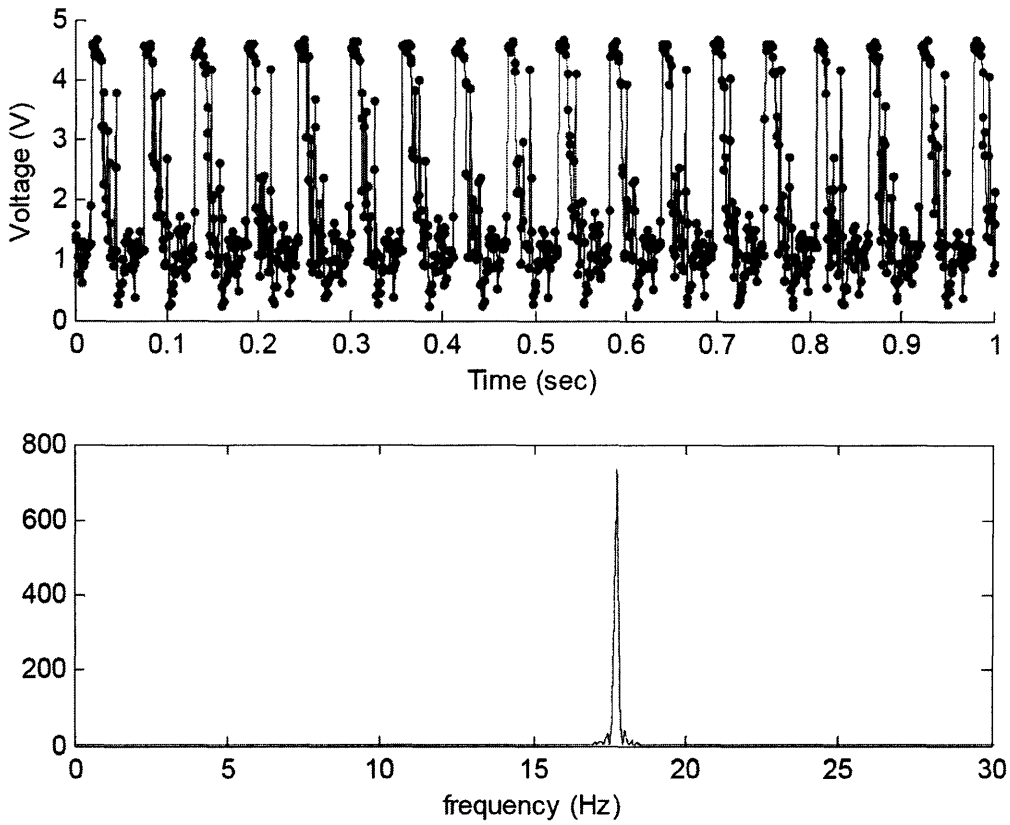

Figure B-10: Results for 8.0 MPH Indicated: f_{peak} = 17.700 Hz, $v_{estimated}$ = 7.867 MPH.

2.535 in to minimize the average error between the indicated and actual (estimated) velocity (this correction assumes that on average the treadmill indicated velocity is correct). Using the revised roller diameter, percent error for the indicated velocity was computed as

$$P_{error}\% = \frac{(v_{actual} - v_{indicated})}{v_{actual}} \cdot 100,$$

with

$$v_{actual} = f \cdot \pi \cdot D,$$

where f is the measured roller revolution frequency and D is the roller diameter. The RMS of the errors shown in Figure B-12 is 0.83%.

The run walk transition ($Fr = 0.5$) for a person in $1G$ with leg length 0.91 m transitions between walking and running at about 2.1 m/s or about 4.7 MPH. $Fr = 0.25$ (optimal walking) occurs at about 3.3 MPH. Errors between these values range from about -1% to $+1\%$. The percent error fluctuates from $< 2\%$ to $\approx 2\%$ for low velocities, such as those that might be encountered in low-Fr activity in reduced gravity.

In the final calibration used in analyzing all experiment velocity data, the minimum-bias roller diameter estimate was $D = 2.532$ inches, which achieved an excellent goodness of fit between indicated and actual (estimated) velocity (adjusted $R^2 = 0.9998$).

B.4 Bill of Materials

Spare copper-coated Kapton®was used, but similar material could be purchased from Dupont. Small proto-boards, miscellaneous wires, and 9V batteries are available from RadioShack. In practice, the 9V battery connection was replaced with 5V power provided by the data acquisition board. This prevented a low battery situation from causing failure of the velocity measurement system. Other materials required to make two complete systems are listed in Table B.1.

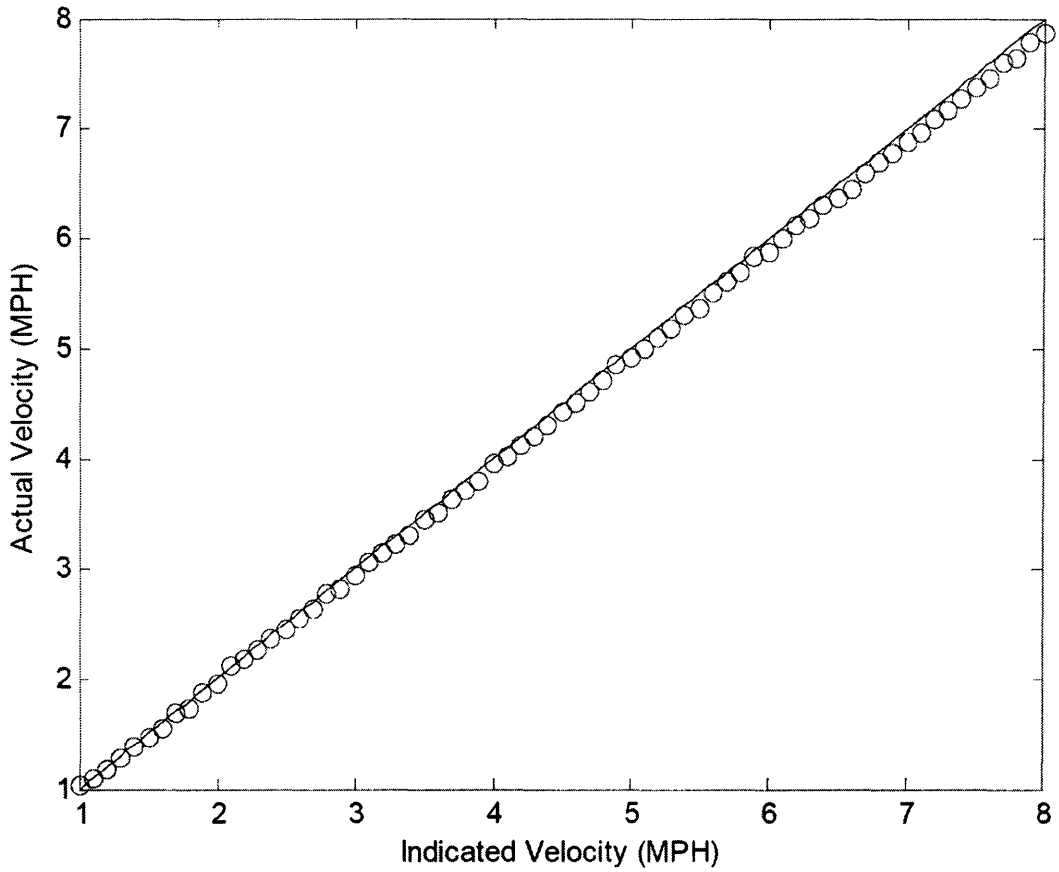

Figure B-11: Actual versus Indicated Treadmill Velocity

Table B.1: Velocity Measurement System Bill Of Materials

Part #	Description	Quantity	Cost	Vendor
6436K73	Al. 1 in. shaft collar	2	$4.71 each	McMaster-Carr
94690A107	#4-40 x 9/32 in	pack of 100	$4.54	McMaster-Carr
82QBK-ND	82Ω resistors	5 pack	$0.28	Digikey
365-1010-ND	OBP700 sensor	2	$9.90 each	Digikey
4LG54BK-ND	50$k\Omega$ Trim Pot	2	$0.44 each	Digikey
296-11108-1-ND	7805 5V Regulator	2	$0.52 each	Digikey
229K-ND	9V battery strap	2	$1.45 each	Digikey

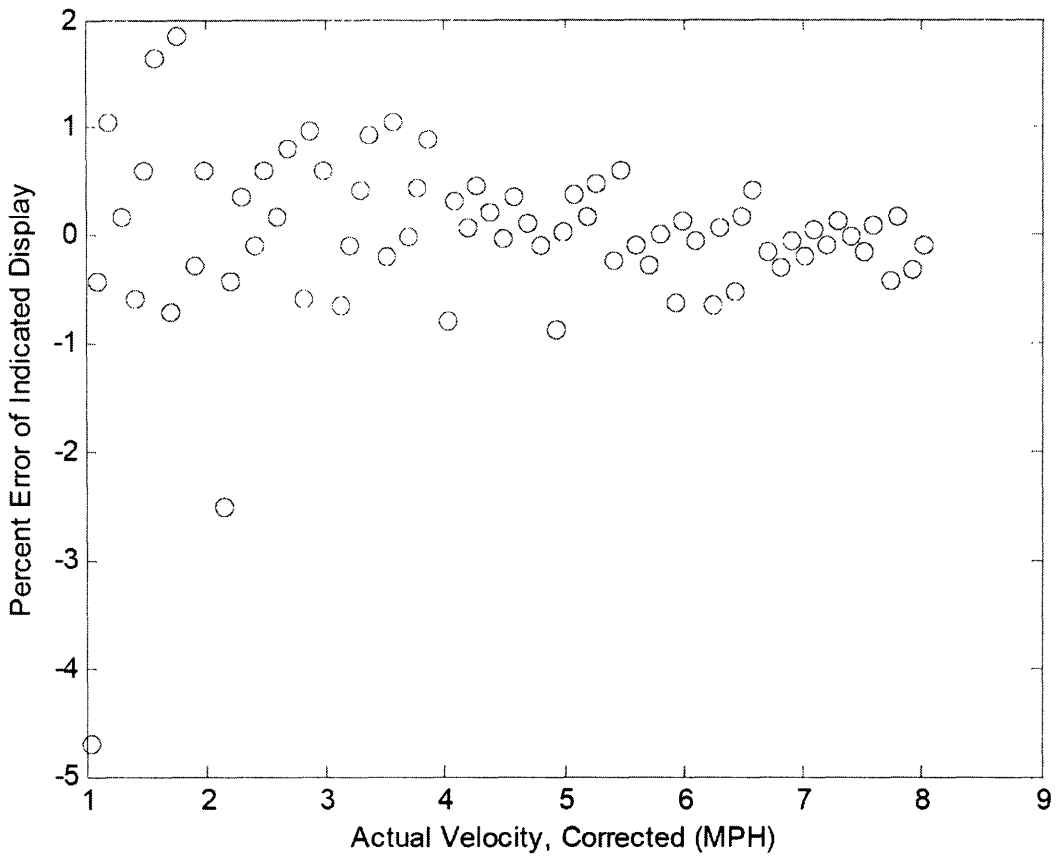

Figure B-12: Indicated treadmill velocity errors, computed after correcting the rear treadmill roller diameter estimate to achieve a mean error of zero.

Bibliography

R. M. Alexander. Optimization and gaits in the locomotion of vertebrates. *Physiol Rev*, 69(4):1199–227, 1989.

R.M. Alexander. Optimum muscle design for oscillatory movements. *J Theor Biol*, 184(3):253–259, 1997.

R.M. Alexander. *Principles of Animal Locomotion.* Princeton University Press, Princeton, New Jersey, 2003.

J. F. Annis and P. Webb. Development of the Space Activity Suit. Contractor Report CR-1892, National Aeronautics and Space Adminitration, 1971.

Arnold S. Barer, Isaak P. Abramov, Anatoly Yu Stoklitsky, and Sergei N. Filipenkov. Essential aspects of space suit operating pressure trade-off. In *24th International Conference on Environmental Systems and 5th European Symposium on Space Environmental Control Systems*, Friedrichshafen, Germany, 1994. Society of Automotive Engineers, Inc., Warrendale, Pennsylvania, USA. SAE 941330.

K. Bethke, C.E. Carr, B.M. Pitts, and D.J. Newman. Bio-suit development: Viable options for mechanical counter pressure? In *34th International Conference on Environmental Systems*, Colorado Springs, Colorado, USA, 2004. Society of Automotive Engineers, Inc., Warrendale, Pennsylvania, USA.

A. A. Biewener, C. T. Farley, T. J. Roberts, and M. Temaner. Muscle mechanical advantage of human walking and running: implications for energy cost. *J Appl Physiol*, 97(6):2266–74, 2004.

R. Billeter, H. Oetliker, and H. Hoppeler. Structural basis of muscle performance. *Adv Vet Sci Comp Med*, 38A:57–124, 1994.

R. Blickhan. The spring-mass model for running and hopping. *J Biomech*, 22(11-12): 1217–27, 1989.

G.W. Bush. U.S. space policy speech, 2004. NASA Headquarters, Washington DC, January 14, 2004.

C.E. Carr. *Distributed Architectures for Mars Surface Exploration.* S.M., Massachusetts Institute of Technology, 2001.

C.E. Carr, D.J. Newman, and K.V. Hodges. Geologic traverse planning for planetary eva. In *33rd International Conference on Environmental Systems (ICES)*, Vancouver, British Columbia, Canada, 2003. Society of Automotive Engineers, Inc., Warrendale, Pennsylvania, USA. SAE paper 2003-01-2416.

G. A. Cavagna, P. Franzetti, and T. Fuchimoto. The mechanics of walking in children. *J Physiol*, 343:323–39, 1983.

P. R. Cavanagh and R. Kram. Stride length in distance running: velocity, body dimensions, and added mass effects. *Med Sci Sports Exerc*, 21(4):467–79, 1989.

K. E. Conley. Cellular energetics during exercise. *Adv Vet Sci Comp Med*, 38A:1–39, 1994.

P. Danaher, K. Tanaka, and A. R. Hargens. Mechanical counter-pressure vs. gas-pressurized spacesuit gloves: grip and sensitivity. *Aviat Space Environ Med*, 76(4): 381–4, 2005.

B. L. Davis and P. R. Cavanagh. Simulating reduced gravity: a review of biomechanical issues pertaining to human locomotion. *Aviat Space Environ Med*, 64(6): 557–66, 1993.

M. H. Dickinson, C. T. Farley, R. J. Full, M. A. Koehl, R. Kram, and S. Lehman. How animals move: an integrative view. *Science*, 288(5463):100–6, 2000.

S. Dionne. AX-5, Mk III, and Shuttle Space Suit Comparison Test Summary. Technical report, National Aeronautics and Space Administration, August 1991. EVA Technical Document 91-SAE/SD-004.

J. M. Donelan and R. Kram. Exploring dynamic similarity in human running using simulated reduced gravity. *J Exp Biol*, 203(Pt 16):2405–15, 2000.

L. B. Du, X. H. Gao, H. Liu, and T. Q. Li. [a robot measurement system for spacesuit joint torque]. *Space Med Med Eng (Beijing)*, 16(3):187–92, 2003.

C. T. Farley and T. A. McMahon. Energetics of walking and running: insights from simulated reduced-gravity experiments. *J Appl Physiol*, 73(6):2709–12, 1992.

C. T. Farley, R. Blickhan, J. Saito, and C. R. Taylor. Hopping frequency in humans: a test of how springs set stride frequency in bouncing gaits. *J Appl Physiol*, 71(6): 2127–32, 1991.

C. T. Farley, H. H. Houdijk, C. Van Strien, and M. Louie. Mechanism of leg stiffness adjustment for hopping on surfaces of different stiffnesses. *J Appl Physiol*, 85(3): 1044–55, 1998.

D. P. Ferris and C. T. Farley. Interaction of leg stiffness and surfaces stiffness during human hopping. *J Appl Physiol*, 82(1):15–22; discussion 13–4, 1997.

R. H. Fitts, D. R. Riley, and J. J. Widrick. Functional and structural adaptations of skeletal muscle to microgravity. *J Exp Biol*, 204(Pt 18):3201–8, 2001.

E. L. Fox, R. L. Bartels, E. C. Chaloupka, J. E. Klinzing, and J. Hoche. Oxygen cost during exercise in simulated subgravity environments. *Aviat Space Environ Med*, 46(3):300–3, 1975.

A.L. Frazer, B.M. Pitts, P.B. Schmidt, J.A. Hoffman, and D.J. Newman. Astronaut performance: Implications for future spacesuit design. In *53rd International Astronautical Congress*, Houston, Texas, 2002.

G. Gabrielli and T.H. von Karman. What Price Speed? *Mechanical Engineering*, pages 775–781, 1950.

L. J. Gonzalez, J. C. Maida, E. H. Miles, S. L. Rajulu, and A. K. Pandya. Work and fatigue characteristics of unsuited and suited humans during isolated isokinetic joint motions. *Ergonomics*, 45(7):484–500, 2002.

T. M. Griffin, N. A. Tolani, and R. Kram. Walking in simulated reduced gravity: mechanical energy fluctuations and exchange. *J Appl Physiol*, 86(1):383–90, 1999.

T. M. Griffin, T. J. Roberts, and R. Kram. Metabolic cost of generating muscular force in human walking: insights from load-carrying and speed experiments. *J Appl Physiol*, 95(1):172–83, 2003.

T. M. Griffin, R. Kram, S. J. Wickler, and D. F. Hoyt. Biomechanical and energetic determinants of the walk-trot transition in horses. *J Exp Biol*, 207(Pt 24):4215–23, 2004a.

T. M. Griffin, R. P. Main, and C. T. Farley. Biomechanics of quadrupedal walking: how do four-legged animals achieve inverted pendulum-like movements? *J Exp Biol*, 207(Pt 20):3545–58, 2004b.

J. E. Haaland. Use of simple physiological measurements in obtaining relative energy expenditure and workloads during a simulated lunar surface mission. *Aerosp Med*, 39(2):153–8, 1968.

T. J. Harrington, 3rd Edwards, D. K., and E. C. Wortz. Metabolic rates in pressurized pressure suits. *Aerosp Med*, 36:825–30, 1965.

G.L. Harris. *The Origins and Technology of the Advanced Extravehicular Space Suit*, volume 24 of *AAS History Series*. American Astronautical Society, San Diego, California, 2001.

A.V. Hill. The maximum work and mechanical efficiency of human muscles, and their most economical speed. *J Physiology*, 56:19–41, 1922.

P. W. Hochachka. Solving the common problem: matching ATP synthesis to ATP demand during exercise. *Adv Vet Sci Comp Med*, 38A:41–56, 1994.

A.S. Iberall. Fundamental considerations of the design of mobile pressure suits. Technical report, National Bureau of Standards, United States Department of Commerce, April 3, 1951. Report 6.2/3508.

A.S. Iberall. The experimental design of a mobile pressure suit. *Journal of Basic Engineering*, pages 251–264, 1970.

Y. P. Ivanenko, R. Grasso, V. Macellari, and F. Lacquaniti. Control of foot trajectory in human locomotion: role of ground contact forces in simulated reduced gravity. *J Neurophysiol*, 87(6):3070–89, 2002.

R.S. Johnston, L.F. Dietlein, and C.A. Berry, editors. *Biomedical Results of Apollo (SP-368)*. National Aeronautics and Space Administration, Lyndon B. Johnson Space Center, Houston, Texas, 1975.

E.M. Jones. Apollo lunar surface journal, 2004. Accessed Aug-Sep, 2004 (http://www.hq.nasa.gov/alsj/).

E.M. Jones. Apollo lunar surface journal, 2005. Accessed February 18, 2005 (http://www.hq.nasa.gov/alsj/).

M. Kaneko. Mechanics and energetics in running with special reference to efficiency. *J Biomech*, 23 Suppl 1:57–63, 1990.

A. E. Kerdok, A. A. Biewener, T. A. McMahon, P. G. Weyand, and H. M. Herr. Energetics and mechanics of human running on surfaces of different stiffnesses. *J Appl Physiol*, 92(2):469–78, 2002.

R. Kram, A. Domingo, and D. P. Ferris. Effect of reduced gravity on the preferred walk-run transition speed. *J Exp Biol*, 200(Pt 4):821–6, 1997.

J.F. Kubis, J.T. Elrod, R. Rusnak, J.E. Barnes, and S.C. Saxon. Apollo 16 time and motion study (n73-16825). Technical report, National Aeronautics and Space Administration, July, 1972 1972.

C. R. Lee and C. T. Farley. Determinants of the center of mass trajectory in human walking and running. *J Exp Biol*, 201(Pt 21):2935–44, 1998.

S. M. Lee, P. A. Bishop, S. M. Schneider, and M. C. Greenisen. Simulated shuttle egress: comparison of two space shuttle protective garments. *Aviat Space Environ Med*, 72(2):110–4, 2001.

Y. Li, W. Wang, R. H. Crompton, and M. M. Gunther. Free vertical moments and transverse forces in human walking and their role in relation to arm-swing. *J Exp Biol*, 204(Pt 1):47–58, 2001.

S. P. Ma and G. I. Zahalak. A distribution-moment model of energetics in skeletal muscle. *J Biomech*, 24(1):21–35, 1991.

R. Margaria. *Biomechanics and Energetics of Muscular Exercise.* Clarendon Press, Oxford, England, 1976.

R. L. Marsh, D. J. Ellerby, J. A. Carr, H. T. Henry, and C. I. Buchanan. Partitioning the energetics of walking and running: swinging the limbs is expensive. *Science*, 303(5654):80–3, 2004.

T. A. McMahon and G. C. Cheng. The mechanics of running: how does stiffness couple with speed? *J Biomech*, 23 Suppl 1:65–78, 1990.

T. A. McMahon, G. Valiant, and E. C. Frederick. Groucho running. *J Appl Physiol*, 62(6):2326–37, 1987.

T.A. McMahon. *Muscles, Reflexes, and Locomotion.* Princeton University Press, Princeton, New Jersey, 1984.

V. Menendez, M. Diener, and J.M. Baez. Performance of EVA suit soft flat pattern mobility joints. In *24th International Conference on Environmental Systems and 5th European Symposium on Space Environmental Control Systems*, Friedrichshafen, Germany, 1994. Society of Automotive Engineers, Inc., Warrendale, Pennsylvania, USA. SAE paper 941331.

A. E. Minetti. The biomechanics of skipping gaits: a third locomotion paradigm? *Proc Biol Sci*, 265(1402):1227–35, 1998.

A. E. Minetti. Walking on other planets. *Nature*, 409(6819):467, 469, 2001.

S. Mochon and T. A. McMahon. Ballistic walking. *J Biomech*, 13(1):49–57, 1980.

S. P. Mohanty, S. S. Babu, and N. S. Nair. The use of arm span as a predictor of height: A study of South Indian women. *J Orthop Surg (Hong Kong)*, 9(1):19–23, 2001.

D.A. Morgan, R.P. Wilmington, A.K. Pandya, J.C. Maida, and K.J. Demel. Comparison of Extravehicular Mobility Unit (EMU) Suited and Unsuited Isolated Joint Strength Measurements (NASA TP-3613). Technical report, National Aeronautics and Space Administration, June, 1996.

NASA. Man-System Integration Standards (NASA-STD-3000), Rev. B. Technical report, National Aeronautics and Space Administration, July, 1995.

D. J. Newman, H. L. Alexander, and B. W. Webbon. Energetics and mechanics for partial gravity locomotion. *Aviat Space Environ Med*, 65(9):815–23, 1994.

D.J. Newman, P.B. Schmidt, D.B. Rahn, N. Badler, and D. Metaxas. Modeling the extravehicular mobility unit (EMU) space suit: Physiological implications for extravehicular activity (EVA). In *30th International Conference on Environmental Systems (ICES) and 7th European Symposium on Space Environmental Control Systems*, Toulouse, France, 2000. Society of Automotive Engineers, Inc., Warrendale, Pennsylvania, USA. SAE paper 2000-01-2257.

OED. Oxford English Dictionary, 2004. URL: http://www.oed.com/. Accessed Fall 2004.

J. F. Patton, T. E. Bidwell, M. M. Murphy, R. P. Mello, and M. E. Harp. Energy cost of wearing chemical protective clothing during progressive treadmill walking. *Aviat Space Environ Med*, 66(3):238–42, 1995.

H. Pontzer. A new model predicting locomotor cost from limb length via force production. *J Exp Biol*, 208(Pt 8):1513–24, 2005.

D.S. Portree and R.C. Treviño. Walking to Olympus: An EVA chronology. Technical report, National Aeronautics and Space Administration, Washington D.C., October 1997. Monographs in Aerospace History Series #7.

E. J. Prescott and E. C. Wortz. Metabolic costs of upper torso exercises vs torque maneuvers under reduced-gravity conditions. *Aerosp Med*, 37(10):1046–9, 1966.

D.M. Ray. *Partial Gravity Simulation Using a Pneumatic Actuator with Closed Loop Mechanical Amplification.* S.M. thesis, University of Houston, 1993.

M. Reconditi, M. Linari, L. Lucii, A. Stewart, Y. B. Sun, P. Boesecke, T. Narayanan, R. F. Fischetti, T. Irving, G. Piazzesi, M. Irving, and V. Lombardi. The myosin motor in muscle generates a smaller and slower working stroke at higher load. *Nature*, 428(6982):578–81, 2004.

D. K. Riskin and J. W. Hermanson. Biomechanics: independent evolution of running in vampire bats. *Nature*, 434(7031):292, 2005.

T.J. Roberts. Moving on land: optimizing for minimum cost. In E.R. Weibel, C.R. Taylor, and L. Bolis, editors, *Principles of Animal Design.* Cambridge University Press, Cambridge, England, 1998.

W. G. Robertson and E. C. Wortz. Effect of lunar gravity on metabolic rates. *Aerosp Med*, 39(8):799–805, 1968.

E.M. Roth. Bioenergetics of Space Suits for Lunar Exploration (SP-84). Technical report, National Aeronautics and Space Administration, 1966.

F. Saibene and A. E. Minetti. Biomechanical and physiological aspects of legged locomotion in humans. *Eur J Appl Physiol*, 88(4-5):297–316, 2003.

W. G. Sanborn and E. C. Wortz. Metabolic rates during lunar gravity simulation. *Aerosp Med*, 38(4):380–2, 1967.

W. R. Santee, W. F. Allison, L. A. Blanchard, and M. G. Small. A proposed model for load carriage on sloped terrain. *Aviat Space Environ Med*, 72(6):562–6, 2001.

P. Schmidt. *An Investigation of Space Suit Mobility with Applications to EVA Operations*. Doctoral dissertation, Massachusetts Institute of Technology, 2001.

P.B. Schmidt, D.J. Newman, and E. Hodgson. Modeling spacesuitmobility: Applications to design and operations. In *31st International Conference on Environmental Systems*, Orlando, Florida, USA, 2001. Society of Automotive Engineers, Inc., Warrendale, Pennsylvania, USA. SAE paper 2001-01-2162.

T.J. Snow. EVA Console Handbook (JSC-20597). Technical report, NASA Lyndon B. Johnson Space Center, September, 2000.

W. E. Springer, T. L. Stephens, and I. Streimer. The metabolic cost of performing a specific exercise in a low-friction environment. *Aeromed Acta*, 34:486–8, 1963.

R. W. Stauffer, M. McCarter, J. L. Campbell, and Jr. Wheeler, L. F. Comparison of metabolic responses of United States Military Academy men and women in acute military load bearing. *Aviat Space Environ Med*, 58(11):1047–56, 1987.

J. A. Stolwijk. Thermal loads in lunar ambulation. *Aerosp Med*, 41(11):1266–8, 1970.

R.W. Stone. Man's motor performance including acquisition of adaptation effects in reduced gravity environments. In *Man in Space Symposium*, Moscow, Russia, 1971. Unknown publisher.

I. Streimer, D. P. Turner, C. A. Tardiff, and T. L. Stephens. An Investigation of the Effects of Pressure Suit Wearing on Work Output Characteristics. *Aerosp Med*, 35: 747–51, 1964.

K. Tanaka, J. Waldie, G. C. Steinbach, P. Webb, D. Tourbier, J. Knudsen, C. W. Jarvis, and A. R. Hargens. Skin microvascular flow during hypobaric exposure with and without a mechanical counter-pressure space suit glove. *Aviat Space Environ Med*, 73(11):1074–8, 2002.

K. Tanaka, R. Limberg, P. Webb, M. Reddig, C. W. Jarvis, and A. R. Hargens. Mechanical counter pressure on the arm counteracts adverse effects of hypobaric exposures. *Aviat Space Environ Med*, 74(8):827–32, 2003.

G. J. van Ingen Schenau and P. R. Cavanagh. Power equations in endurance sports. *J Biomech*, 23(9):865–81, 1990.

J. L. Van Leeuwen and C. W. Spoor. Modelling mechanically stable muscle architectures. *Philos Trans R Soc Lond B Biol Sci*, 336(1277):275–92, 1992.

J.M. Waligora. The Use of a Model of Human Thermoregulation During the Apollo and Skylab Programs (N76-11172). Technical report, NASA Lyndon B. Johnson Space Center, 1976.

P. Webb. Closed breathing-ventilating systems using recirculated oxygen. *J Aviat Med*, 30(4):273–9, 1959.

B. Webbon, L. Montgomery, L. Miller, and B. Williams. A comparison of three liquid-ventilation cooling garments during treadmill exercise. *Aviat Space Environ Med*, 52(7):408–15, 1981.

P. G. Weyand, D. B. Sternlight, M. J. Bellizzi, and S. Wright. Faster top running speeds are achieved with greater ground forces not more rapid leg movements. *J Appl Physiol*, 89(5):1991–9, 2000.

F.R. Whitt and D.G. Wilson. *Bicycling Science.* The MIT Press, Cambridge, Massachusetts, 1982.

L. A. Wickman and B. Luna. Locomotion while load-carrying in reduced gravities. *Aviat Space Environ Med*, 67(10):940–6, 1996.

E. C. Wortz. Effects of reduced gravity environments on human performance. *Aerosp Med*, 39(9):963–5, 1968.

E. C. Wortz and E. J. Prescott. Effects of subgravity traction simulation on the energy costs of walking. *Aerosp Med*, 37(12):1217–22, 1966.

S. Wright and P. G. Weyand. The application of ground force explains the energetic cost of running backward and forward. *J Exp Biol*, 204(Pt 10):1805–15, 2001.

R. Wu. *Human Readaptation to Normal Gravity Following Short-Term Simulated Martian Gravity Exposure and the Effectiveness of Countermeasures.* S.m. thesis, Massachusetts Institute of Technology, 1999.

F. Yang and X. G. Yuan. [a dynamic model of the extravehicular (correction of extravehicuar) activity space suit]. *Space Med Med Eng (Beijing)*, 15(6):453–4, 2002.